

Fused Filament Fabrication of Polycarbonate Components in a Simulated On-Orbit Environment

By

Marshall Harrington Quinn
4513002

in partial fulfillment of the requirements to obtain the degree of

Master of Science
in Aerospace Engineering

at the Delft University of Technology
to be defended publicly on May 24th, 2018 at 9:30 a.m.

Supervisor:	Dr. ir. J. Guo	TU Delft:
Thesis Committee:	Ir. B. Zandbergen	TU Delft (Chair)
	Dr. U. Lafont	European Space Agency
	J.A. Versteegh	Ultimaker BV
	Dr. C. Rans	TU Delft

Acknowledgments

I would like to thank my supervisor Dr. Guo for his assistance over the course of my research. His experience helped me stay on track and when I had a question he was always able to give me a well thought out and helpful answer. I would like to sincerely thank Johan Versteegh for being an invaluable source of knowledge regarding FFF and the Ultimaker printer. Troubleshooting the, many, problems I encountered would have taken much longer without Johan's knowledge and assistance. I would also like to thank Dr. Lafont for his help with structuring my research and running some tests. A thank you as well to Sevket Uladag, Gertjan Mulder and Berthil Grashof for helping me with my testing. In addition to the individuals who assisted my I would like to thank Ultimaker BV for providing me with the printer on which my research was based and who gave me license to modify it as much as I needed and break a few things in the process.

Aside from my academic support I would like to thank my family. It has been a long road to this thesis with many ups and downs and they were always there to support and encourage me. This entire degree and experience of living abroad wouldn't have been possible without the financial support of my amazing parents. I would also like to say a special thank you to my girlfriend Kate for helping me schedule, occasionally waking me up when I slept through my alarm and for always being supportive of me.

Finally, I would like to say a thank you to all my friends, particularly those I have met here in Delft. I came to Delft not just to study, but also for the experience of living abroad, and you have helped to make that experience as amazing as it was. I won't forget it any time soon.

Abstract

This thesis aimed to investigate the use of Fused Filament Fabrication (FFF) to fabricate structural components from polycarbonate in an on-orbit environment. The ability of an FFF printer to survive in a simulated on-orbit environment and function correctly was investigated first. Next the dimensional accuracy of components fabricated in a simulated on-orbit environment were evaluated. Finally, the mechanical properties of components fabricated in a simulated on-orbit environment were evaluated. Additionally, the thermal and outgassing behaviour of polycarbonate fabricated with FFF in a simulated on-orbit environment was investigated.

These investigations were carried out by placing a commercially available FFF printer in a simulated on-orbit environment. Aspects of the on-orbit environment with long term effects, such as atomic oxygen (ATOX) and ultraviolet (UV) radiation were ignored as their effects on the FFF process itself would be minimal. The microgravity aspect was also ignored as FFF had already been proven to work in a microgravity environment and due to the difficulty of testing in microgravity. The simulated on-orbit environment was chosen to solely be a vacuum environment. The printer was placed in the vacuum environment and several tests were performed to determine functionality of heaters, servos and control. This was followed by fabrication of components of increasing complexity in vacuum to evaluate printer and FFF process functionality. Several test components were then fabricated for flexural, tensile and compressive testing. These test components were evaluated for dimensional and mass accuracy and were qualitatively analyzed. Following this analysis, the three mechanical tests were carried out according to ASTM standards. The dimensional and mechanical property analysis involved printing two sub-sets of each component, one in normal atmospheric conditions and one in the vacuum environment and comparing the two sub-sets.

It was found that that the FFF process can be successfully carried out in a vacuum environment. The printhead could be accurately positioned, the heaters functioned properly and filament was correctly extruded with minimal modifications required. Unexpected clogging of the nozzle was observed in the vacuum environment, likely due to premature softening of the filament caused by inadequate cooling. This was addressed by replacing the nozzle with one which better isolated the filament from the heated nozzle. Test components with small cross-sectional areas had very poor quality, likely due to printing on soft preceding layers caused by the lack of convective cooling in vacuum. Dimensional analysis of components showed that there were often significantly different dimensions depending on the environment they were printed in however there was little practical difference. In the tensile and compressive tests, the components printed in vacuum had a significantly higher strength than the components printed in atmosphere. In the tensile test the vacuum components also fractured at a higher strain.

In conclusion it was found to be possible to use the FFF process in a vacuum environment to fabricate dimensionally accurate polycarbonate components with a variety of geometries. While there were issues with thermal control, these issues can be solved with currently available technology. This research sets the basis for FFF to be implemented on-orbit to fabricate useful spacecraft components. FFF in an on-orbit environment could be used for maintenance and repair of satellites or to manufacture entire space systems. Manufacturing on-orbit reduces launch requirements as raw material can be packaged very efficiently and components do not need to be designed to withstand the forces of launch.

Table of Contents

Acknowledgments	3
Abstract	5
List of Figures	12
List of Tables	15
List of Abbreviations.....	17
1 Introduction	19
1.1 General Introduction.....	19
1.2 Research Questions.....	19
1.2.1 Primary Research Question	19
1.2.2 Secondary Research Questions	20
1.3 Research Objectives	20
1.4 Structure of Thesis Report.....	21
2 Background Information	23
2.1 Fused Filament Fabrication	23
2.2 On-Orbit Environment.....	26
2.2.1 Pressure On-Orbit.....	26
2.2.2 Thermal Environment On-Orbit	26
2.2.3 Other Aspects of the On-Orbit Environment	26
2.3 On-Orbit Manufacturing.....	27
2.4 State of the Art of FFF On-Orbit.....	28
2.4.1 Additive Manufacturing Facility and 3D Printing in Zero g Demonstrator	28
2.4.2 Portable on Orbit Printer 3D	28
2.5 Technical Issues with FFF On-Orbit	29
2.5.1 Outgassing.....	29
2.5.2 Thermal Environment.....	30
2.5.3 Microgravity	31
2.5.4 Quality Control and Maintenance	31
3 Experimental Setup	33
3.1 Experimental Setup Requirements	33
3.2 Experimental Environment.....	33
3.2.1 Vacuum	34
3.2.2 Temperature	38
3.2.3 Gravity	38
3.2.4 Other Factors	39
3.2.5 Final Experimental Environment.....	39

3.3	Experimental Printer	39
3.4	Material Choice.....	41
3.5	Concerns Related to FFF Printing in the Vacuum Chamber	44
3.5.1	Outgassing.....	44
3.5.2	UFP Generation	46
3.6	Printer Modifications	49
3.6.1	Outgassing Reduction	49
3.6.2	Removal of Printhead Fans	52
3.6.3	Wiring	53
4	Experimental Setup Validation and Testing	57
4.1	Printhead Heating and Cooling.....	57
4.2	Buildplate Heating and Cooling	58
4.3	Validation of New Wiring	59
4.4	Estimation of Decreased Cooling in Vacuum.....	61
4.5	Analysis of Expected Problems Related to FFF in Vacuum.....	62
4.5.1	Reduced Cooling of Printed Component	62
4.5.2	Heater Temperature Control	64
4.5.3	Servo Motor Overheating	65
4.5.4	Outgassing of Component While Printing	66
5	Performance of FFF in Vacuum	67
5.1	Printer Functionality.....	67
5.1.1	Heater Performance.....	67
5.1.2	Servo Performance.....	69
5.2	Issues with Printed Component.....	71
5.2.1	Reduced Cooling.....	72
5.2.2	Bubbling of Upper Layers.....	78
5.3	Issues with the FFF Process	80
5.3.1	Nozzle Clogging	80
5.3.2	Outgassing Test	85
6	Mechanical Property (MP) Series Components	89
6.1	Overview.....	89
6.2	Flexural Component.....	90
6.3	Tensile Component	90
6.4	Compressive Component	92
6.5	Control of Variables While Fabricating MP Series Components.....	92
6.5.1	Controlled Variables	92
6.5.2	Uncontrolled Variables	93

6.6	MP Series Cura Profile	94
7	Quality of Components Printed in a Vacuum Environment	95
7.1	Dimensional Analysis.....	95
7.1.1	Procedure.....	95
7.1.2	Flexural Components.....	95
7.1.3	Tensile Components	97
7.1.4	Compressive Components	99
7.2	Mass Analysis.....	100
7.2.1	Procedure.....	100
7.2.2	Flexural Components.....	101
7.2.3	Tensile Components	102
7.2.4	Compressive Components	102
7.3	Qualitative Analysis.....	103
7.3.1	Procedure.....	103
7.3.2	General Defects and Observations.....	103
7.3.3	Flexural Component Defects.....	105
7.3.4	Tensile Components Defects	106
7.3.5	Compressive Components Defects.....	107
7.3.6	Qualitative Analysis Conclusions.....	107
8	Mechanical Properties of Polycarbonate Fabricated Using FFF in a Vacuum Environment	109
8.1	Flexural Test.....	109
8.1.1	Flexural Testing Components.....	109
8.1.2	Flexural Testing Procedure	109
8.1.3	Results and Analysis	112
8.2	Tensile Test.....	114
8.2.1	Tensile Testing Components	115
8.2.2	Tensile Testing Procedure.....	116
8.2.3	Results and Analysis	118
8.3	Compressive Test	125
8.3.1	Compressive Testing Components	125
8.3.2	Compressive Testing Procedure.....	126
8.3.3	Results and Analysis	127
9	Conclusions and Recommendations.....	132
9.1	Conclusions.....	132
9.2	Recommendations	133
9.2.1	Future Research	134
9.2.2	Roadmap to Implementation On-Orbit	135

Bibliography	136
Appendices.....	140
Appendix A – vacuubrand MD-1 Specifications	140
Appendix B – Ultimaker 2+ Specification.....	141
Appendix C – Connector Pinouts.....	142
Appendix D – MATLAB Script for Servo Cooling.....	144
Appendix E – MATLAB Script for FFF Thread Cooling.....	145
Appendix F – FTIR Analysis of Outgassing Windows	147
Appendix G– “Solid No Brim” Cura Profile.....	148

List of Figures

Figure 1: A schematic of an extrusion based additive manufacturing process, such as FFF	23
Figure 2: Two desktop 3D printers, a Builder Premium Medium with a metal structure on the left [13] and an Ultimaker Original+ with a wood structure on the right [14].....	24
Figure 3: The printhead of an Ultimaker 2+ showing the nozzle in yellow at the bottom, the X and Y gantry rods, the connecting structure, buildplate and the Bowden tube at the top.....	25
Figure 4: The AMF showing the print volume and a printed plastic component [11]	28
Figure 5: The POP3D printer aboard the ISS [8].....	29
Figure 6: Sample O20, a very difficult to print on Earth component which was printed by the 3DP on-orbit [7]	31
Figure 7: Heraeus VT 6130 M vacutherm in the cleanroom	34
Figure 8: The vacuubrand MD-1 vacuum pump used for testing	35
Figure 9: Vacuum chamber pressure over time.....	36
Figure 10: The DN16 vacuum flange connection on the read of the vacuum chamber.....	37
Figure 11: 1/4" (6 mm) vacuum tubing and DN16/DN 6 adapter	37
Figure 12: The MakerBot Replicator+ [41].....	39
Figure 13: An unmodified Ultimaker 2+ FFF 3D printer [42]	40
Figure 14: A side wall of the UM2+ printer before (left) and after (right) material removal	50
Figure 15: The filament spool holder (left) and the filament spool (right).....	51
Figure 16: A servo motor (left) and a filament feed gear (right) showing green/grey lubricant	52
Figure 17: The regulating fan (centre) and cooling fans (left and right) of the UM2+, removed from the printhead	52
Figure 18: The four Dsub connectors inside the vacuum camber	53
Figure 19: the Dsub connectors on the rewired power supply.....	54
Figure 20: The main board (left) and display board (right) of the UM2+ printer	54
Figure 21: Four Dsub connectors for connecting the PCBs to the exterior of the vacuum chamber ..	55
Figure 22: Four Dsub connectors for connecting the printer to the interior of the vacuum chamber	56
Figure 23: The heating curve of the printhead, with and without fan	57
Figure 24: The cooling curve of the printhead, with and without fan	58
Figure 25: The heating curve of the buildplate.....	59
Figure 26: The cooling curve of the buildplate	59
Figure 27: Cooling rate of a component with and without convective heat transfer	62
Figure 28: Convective heat transfer of a component.....	62
Figure 29: Cooling of a segment of an extruded polymer thread	64
Figure 30: (L) PP-01-04-A and (R) PP-02-01-A.....	70
Figure 31: (L-R) PP-01-01-V, PP-01-05-V and PP-01-11-V.....	72
Figure 32: PP-01-05-V showing a counter clockwise twist	72
Figure 33: Results of the DSC test including T_g	73
Figure 34: Temperature of the 8x8x0.2 layer over time.....	74
Figure 35: 8x8x5 mm COMSOL component temperature in a 0 Pa environment at (L-R) 0s, 10s, 20s, 30s, 40s, 50s, 60s.....	75
Figure 36: Average temperature of the top surface of the 8x8x5 component over time.....	76
Figure 37: Convective flux from a polycarbonate component	77
Figure 38: Radiative flux from a polycarbonate component	78
Figure 39: Bubble on top surface of component printed in vacuum	79

Figure 40: Results of the TGA testing	80
Figure 41: (L) PP-01-01-V and (R) PP-01-02-V	81
Figure 42: Expanded section and ring on filament when printing PP-01-01-V and PP-01-02-V	82
Figure 43: Expanded section and ring of the second clog	83
Figure 44: Expanded section and ring of the third clog	84
Figure 45: Stock printhead (L) and PEEK rated printhead (R)	85
Figure 46: FTIR window #169 in position in the vacuum chamber	86
Figure 47: MP-01, a modified ASTM D790 flexural testing component	90
Figure 48: Geometry of an ASTM D638 component with Type I highlighted in yellow [70]	91
Figure 49: MP-02, a modified Type I ASTM D638 tensile testing component	91
Figure 50: MP-03, a ASTM D695 compressive testing component	92
Figure 51: The Mettler Toledo Classic analytical balance used for mass analysis	101
Figure 52: Tail on the bottom layer of MP-01 (L) and MP-02 (R) components	104
Figure 53: Damage resulting from tail removal	104
Figure 54: Bulge on an MP-01 component	105
Figure 55: Top (L) and bottom (R) surfaces of an MP-02 component	105
Figure 56: Roughness on the upper surface on an MP-01 component	106
Figure 57: Defect on bottom layer, end of MP-02 component	107
Figure 58: The seam on an MP-03 component	107
Figure 59: The three-point bending apparatus used for the flexural test	110
Figure 60: Force/deformation curves of the flexural test	112
Figure 61: The yield zones of MP-01-03-A and MP-01-08-V	114
Figure 62: MP-01-02-A and MP-01-07-V after flexural testing	114
Figure 63: MP-02-01-V to MP-02-05-V (left to right)	115
Figure 64: MP-02-06-A to MP-02-10-A (left to right)	116
Figure 65: Flexural testing set-up	117
Figure 66: Fouling of top extensometer grip	118
Figure 67: Stress/strain curves of the tensile components	119
Figure 68: MP-02-01-V to MP-02-05-V (left to right) after testing	122
Figure 69: L-R, The fracture zones of MP-02-01-V (top), MP-02-03-V (top and bottom)	123
Figure 70: MP-02-06-A to MP-02-10-A (left to right) after testing	123
Figure 71: L-R, fracture zones of MP-02-06-A (top), MP-02-07-A (top) and MP-02-08-A (bottom) ..	124
Figure 72: The pattern of the pneumatic grips on MP-02-01-V	124
Figure 73: The buildplate layout for the MP-03 components	125
Figure 74: Compressive test set-up	126
Figure 75: Force/deformation of components tested to 20mm compressive deformation	128
Figure 76: A MP-03 component deforming under high compressive load	128
Figure 77: Force/deformation of components tested to 5mm compressive deformation	129
Figure 78: MP-03-03-V and MP-03-06-A after compressive testing	130
Figure 79: MP-03-01-V and MP-03-10-A after compressive testing	131
Figure 80: A roadmap to a feasible FFF printer for use on-orbit	135

List of Tables

Table 1: Pressure at LEO	35
Table 2: Compatibility of investigated materials with the UM2+ printer	42
Table 3: Vacuum properties of investigated materials.....	44
Table 4: The processing temperatures for a UM2+ for the final four polymers of interest	44
Table 5: Ultimaker 2+ parts, materials and outgassing evaluation	45
Table 6: Outgassing data of two polycarbonate 3D printing filaments.....	46
Table 7: ISO cleanroom particulate limits by particle size [60]	48
Table 8: The temperature holding of the UM2+ printhead at 260 °C.....	58
Table 9: Event times during outgassing test (FTIR window #169)	87
Table 10: Contaminants recorded in the vacuum chamber while printing (#169) and not printing (#170).....	88
Table 11: Dimensions of flexural components.....	96
Table 12: Volumes of flexural components	97
Table 13: Dimensions of tensile components	98
Table 14: Dimensions of compressive components	99
Table 15: Volumes of compressive components	100
Table 16: Mass of the flexural test components.....	101
Table 17: Mass of tensile test components	102
Table 18: Mass of the compressive test components	103
Table 19: Results of flexural testing	113
Table 20: Tensile testing results.....	120
Table 21: Modulus of elasticity of the tensile components.....	121
Table 22: Compressive testing results.....	129

List of Abbreviations

3DP.....	3D Printing in Zero g Demonstrator
ABS.....	Acrylonitrile Butadiene Styrene
AMF.....	Additive Manufacturing Facility
ASTM.....	American Society for Testing and Materials
CAD.....	Computer Aided Design
COTS.....	Commercial Off the Shelf
CPE.....	Copolyester
DASML.....	Delft Aerospace Structures & Materials Laboratory
DSC.....	Differential Scanning Calorimetry
ESA.....	European Space Agency
ESTEC.....	European Space Research and Technology Centre
ESAMM.....	Extended Structure Additive Manufacturing Machine
FFF.....	Fused Filament Fabrication
FTIR.....	Fourier-Transform Infrared Spectroscopy
ISPR.....	International Standard Payload Rack
ISO.....	International Standards Organization
ISS.....	International Space Station
LEO.....	Low Earth Orbit
MIS.....	Made in Space
NASA.....	National Aeronautics and Space Administration
OOM.....	On-Orbit Manufacturing
PC.....	Polycarbonate
PEEK.....	Polyether Ether Ketone
PEI.....	Polyether Imide
PLA.....	Polylactic acid
POP3D.....	Portable on Orbit Printer 3D
R3DO.....	Plastic Recycling System for Creating 3D Printer Feedstock On-Orbit
TGA.....	Thermogravimetric Analysis
TUI.....	Tethers Unlimited Inc
UM2+.....	Ultimaker 2+

1 Introduction

This first chapter introduces the concept of OOM and the current use of FFF printers in space. This chapter also introduces the research questions and research objectives of the thesis work. The structure of the thesis report is discussed. This chapter is intended to outline the main goals of the research and make it clear what is being investigated.

1.1 General Introduction

There is currently a large amount of interest in the concept of on-orbit manufacturing (OOM) being shown by both governmental agencies and companies. The SpiderFAB concept by Tethers Unlimited (TUI) [1], the Extended Structure Additive Manufacturing Machine (ESAMM) [2] and Archinaut [3] concepts of Made in Space (MIS) and the work being done by Magna Parva [4] are the first research into the manufacture of very large structures on-orbit around Earth. These concepts are very similar to a NASA proposal for OOM from 1987 [5] as they intend to use a pultrusion process to create very long, constant cross section structural elements from composite materials.

There are also three on-orbit implementations of Fused Filament Fabrication (FFF), a common 3D printing process, which are the 3D Printing in Zero g Demonstrator (3DP) [6] and Additive Manufacturing Facility (AMF) [7] made by MIS and NASA and the ESA funded "Portable on Orbit Printer 3D" (POP3D) [8]. These printers have been hosted aboard the International Space Station (ISS). The FFF process can fabricate complex geometries from a wide variety of thermoplastics and could supplement the high throughput and relative inflexibility of the pultrusion based concepts.

The three FFF printers mentioned above have been shown to function correctly in a microgravity environment due to their use on-orbit and during testing in parabolic flight which is capable of replicating the zero g environment for short, consecutive periods of time [8], [9]. The use of these printers on-board the ISS has proven that it is possible to print polymer based components on-orbit in a microgravity environment including functional components which have been used to facilitate experiments on board the station [10] and satellite structural components [11]. While these printers have been very successful in laying the groundwork for FFF printing on-orbit they have several limitations including the size of the printers, the potential for contamination of the air inside the ISS and their location aboard the ISS in low Earth orbit (LEO). This limits the printers aboard the ISS to only fabricating small components for use within the ISS and prevents them from being used to help manufacture large scale space infrastructure. To produce larger components, remove the issue of air contamination and allow FFF to be used anywhere in space, the process must be tested and proven to work in an on-orbit environment.

1.2 Research Questions

The research questions are the key drivers that the thesis research intends to answer. All research and testing carried out over the course of the thesis was done to help answer these questions. The research questions themselves are composed of a single top-level research question which is the ultimate question that the research intends to answer which is further broken down into three sub-questions. These sub-questions break the top-level research question down into smaller, more manageable parts and are structured such that once all sub-questions are answered an answer to the top-level research question can be determined.

1.2.1 Primary Research Question

Prior to beginning work on the thesis an in-depth literature study was conducted to determine the state of the art of OOM and the use of FFF on-orbit. After determining the state of the art, the current limitations of the FFF process on-orbit were identified. Finally, a research question was

formulated which aimed to address some of the limitations of the FFF process. The primary research question is presented below.

“Can Fused Filament Fabrication (FFF) be carried out in a vacuum environment representative of Low Earth Orbit (LEO) and fabricate polymer-based components that are representative of components used for space systems?”

The primary research question is the driving question for the thesis work. The primary research question was formulated by considering the research needed to expand on the concept of FFF on-orbit, the availability of equipment for testing and according to personal interest.

1.2.2 Secondary Research Questions

As the primary research question is a very high-level question it must be broken down into smaller, more manageable sub-questions. These secondary research questions are presented below. Each of the secondary research questions could be further broken down to create a large set of small, simple questions.

“Can an FFF printer function in an environment representative of the on-orbit environment?”

The first secondary research question is needed to prove that testing of the FFF process can be carried out with the equipment and time available. Answering this question will also show if the subsystems of an FFF printer, including the heaters, positioning and filament feed system can function in a simulated on-orbit environment. This question ensures the printer will function in the vacuum environment before fabrication of evaluation components takes place. If the printer itself cannot function properly in a vacuum environment, then any further research into the FFF process itself is impossible. Modifications to the printer used in this research can be used to inform the design of a dedicated vacuum qualified printer used in a real on-orbit implementation of FFF.

“Can an FFF printer accurately fabricate components in a vacuum environment representative of the on-orbit environment?”

To design an engineering component, regardless of place of manufacture, it must be known what geometries can be fabricated. The precision of the fabrication process and the possible tolerances must also be known to the designer. The second secondary research question above aims to address this by determining the accuracy of the FFF process in a simulated on-orbit environment compared to the accuracy possible on-Earth with normal pressure, temperature and gravity.

“How do the mechanical properties of FFF polymer-based components change when fabricated in a vacuum environment representative of the on-orbit environment?”

When designing a component, the mechanical properties of the material it is fabricated from must be known. Depending on the application a variety of material properties must be known to design a component that will perform to specification. While the material properties of most polymers are known, including many thermoplastics which are fabricated using FFF, the material properties of thermoplastics fabricated using FFF in an on-orbit environment have not been determined. This secondary research question is designed to address this and allow for components to be safely designed for fabrication using FFF on-orbit.

1.3 Research Objectives

The purpose of the thesis research is to show that satellite components can be fabricated using FFF in a representative LEO environment. This will be done by characterizing the effects of the on-orbit environment on an FFF printer, the FFF process and thermoplastic components fabricated with FFF.

Proving this concept would set the basis for spacecraft components to be fabricated using FFF on-orbit, outside of the atmosphere of a space station. The FFF process could be applied to spacecraft of all shapes and sizes and could also be used to fabricate components on the surface of celestial bodies. This allows for fabrication of components larger than can be accommodated aboard the ISS and eliminates the need to design the printer to prevent contamination of the space station or other contained human habitat.

Firstly, it must be proven that an FFF printer can function correctly and extrude thermoplastic filament at the same rates and temperatures that are possible in an atmosphere. For the purposes of this report atmospheric conditions are assumed to be a pressure of 1 atm (101.325 kPa) and a temperature of approximately 25 °C. Operations carried out “in atmosphere” are carried out in the above-mentioned pressure and temperature conditions unless otherwise noted. “Atmosphere components” are components fabricated in the above noted pressure and temperature. The print head must be able to maintain a variety of temperatures (within a normal operational range) and the print head must extrude at the same rate in vacuum and in atmosphere. It should also be shown that the print head does not jam or otherwise malfunction when operating in a vacuum environment. The printer must also accurately position the printhead and move at the translational rates required for printing. This may include showing proof of concept that FFF printing can fabricate polymer-based components in a simulated on-orbit environment. The survival of the electronics of a FFF printer in a vacuum is outside of the scope of testing. This is because the goal of this research is to investigate the FFF process itself. Space rated electronics would be designed and manufactured to run the printer in a real implementation.

The second step of the research is to determine the accuracy with which an FFF printer can fabricate polymer-based components in a simulated on-orbit environment. To evaluate this several parameters of components fabricated in a simulated on-orbit environment need to be recorded, analyzed and compared with components fabricated in atmosphere. These parameters could include, but not limited to: the dimensional accuracy, mass, volume and density of the fabricated components. Components fabricated in vacuum must also be free of defects such as voids, delaminations or cracks. All components printed in vacuum will be compared against components with the same geometry printed in atmosphere which were fabricated using the same printer and settings.

Finally, the mechanical properties of thermoplastic printed using FFF in vacuum will also be assessed. In this report the mechanical properties of the printed components are of interest. These mechanical properties could include yield and ultimate tensile strength, Young’s modulus, Poisson’s ratio, surface roughness, material hardness and density and will be determined according to the appropriate testing standards. The values of the mechanical properties of the vacuum fabricated components will be compared against components printed in atmosphere from the same material with the same printer and settings and against polymer fabricated using traditional, non-3D printing, methods.

1.4 Structure of Thesis Report

This thesis report details all the work done throughout the research project. As seen above, Chapter 1 introduces the work including a short background on OOM. The research questions, sub-questions and objectives are also presented in this section. Chapter 2 then follows and presents the required background information to understand the thesis work and to provide context for the decisions that are made throughout. This background information includes information on the FFF process, the on-

orbit environment and OOM. It also discusses the current state of the art of FFF and the technical issues associated with conducting FFF in an on-orbit environment.

Chapter 3 begins to discuss the thesis work itself with the experimental setup being determined. First the components of the experimental setup are discussed followed by the appropriate equipment being sourced. First the experimental environment is discussed and specified. Equipment is then sourced including a vacuum chamber, FFF printer and vacuum pump. The polymer material to be used for testing is also selected at this point. After the experimental apparatus is specified some concerns related to printing in the vacuum chamber are addressed and the modifications needed to utilize the printer in the vacuum chamber are laid out. Chapter 4 then deals with the validation of the experimental setup to ensure it can accurately simulate the experimental environment and everything works correctly prior to tests beginning in a vacuum environment. This chapter also includes analysis of some expected problems related to FFF in a vacuum environment.

Chapter 5 is the start of actual testing with the performance of the printer being assessed in the vacuum environment and preliminary tests being carried out. First the printer is validated with each subsystem being evaluated for performance in a vacuum. Several test components were also printed in this chapter and several issues with the FFF process were identified, analyzed and solved. Chapter 6 defines the MP series of test components which were used for the dimensional analysis as well as the mechanical property testing. Chapter 7 details the dimensional analysis of the MP series of components and compares components printed in a vacuum environment with those printed in atmosphere as well as to the nominal geometry. This analysis includes analysis of the spatial dimensions and mass as well as a qualitative analysis. Chapter 8 discusses the mechanical testing and gives the results of the mechanical testing. The test components, procedure and results of the three tests carried out: flexural, tensile and compressive are discussed in this chapter. The results are analyzed, and any interesting findings are noted. Finally, Chapter 9 presents the conclusions of the thesis research and gives recommendations for future work.

2 Background Information

This chapter presents the background information required to understand the thesis work and the concepts used within it. The background information also helps to provide context for the decisions made in the research. This chapter begins with an overview of the FFF process and the on-orbit environment. Following presentation of information on the process and environment the concept of OOM is presented and defined. A detailed state of the art of FFF on-orbit is then presented and the technical issues which are associated with conducting FFF in an on-orbit environment are discussed.

2.1 Fused Filament Fabrication

Fused Filament Fabrication (FFF) is also known as Fused Deposition Modelling (FDM) and is a type of additive manufacturing that is capable of fabricating components from polymer-based feedstock. FFF is the most common technology used in polymer-based 3D printers. FFF belongs to the category of “extrusion based processes” within additive manufacturing, where the feedstock is supplied as a solid which is partially melted and extruded onto the work surface, building up the component in layers as shown in Figure 1 [12]. In the FFF process the feedstock is supplied as a long, thin filament of thermoplastic, generally stored as a large spool of material.

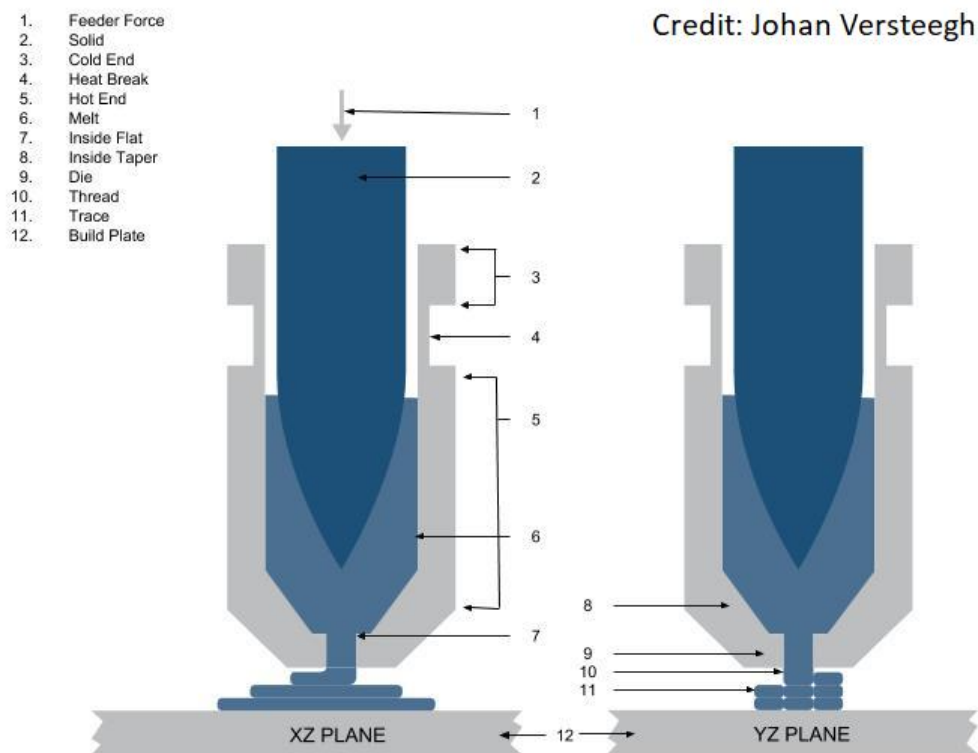


Figure 1: A schematic of an extrusion based additive manufacturing process, such as FFF

A FFF printer consists of several main subsystems including the structure, printhead, buildplate, positioning system and electronics. The purpose of the structure is to keep all the parts of the printer accurately located and to provide a rigid platform for the printing process. As there are multiple moving parts in an FFF printer the structure must be rigid to ensure the printhead can be accurately located and material can be deposited in the correct locations. FFF printer structures are commonly made of strong polymers (such as acrylic), metal, composite “sandwich” materials or even wood. FFF printer structures are usually a cube or rectangular prism in shape but can be of any geometry which can support the other parts of the printer and providing the necessary rigidity. FFF

printer structures are usually composed of sheet or plate material, rods and fasteners to hold the structural parts together.

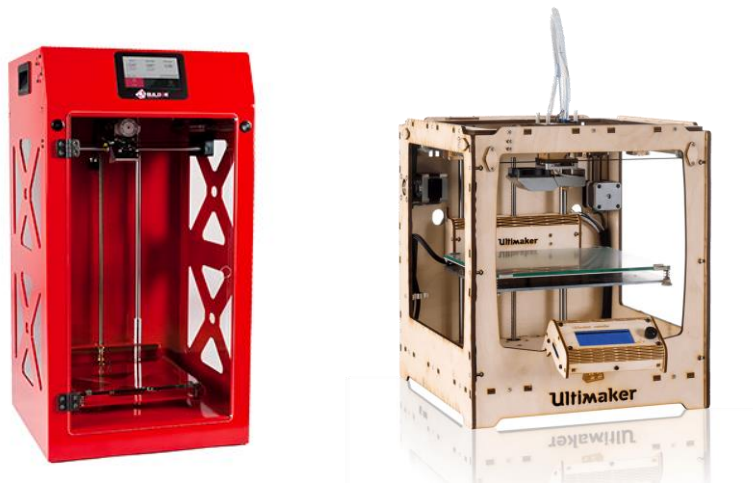


Figure 2: Two desktop 3D printers, a Builder Premium Medium with a metal structure on the left [13] and an Ultimaker Original+ with a wood structure on the right [14]

The printhead is the part of an FFF printer which heats the thermoplastic filament to the appropriate processing temperature and extrudes the molten plastic through a nozzle, or die, onto the buildplate or preceding layers of plastic. A portion of the printhead of an FFF printer, and its constituent parts and sections, is shown in Figure 1. The hot end of the printhead includes a heater for heating the hot end and melting the filament. The heater can be monitored and controlled by the printer electronics using a thermistor or thermocouple. The hot end also includes a nozzle/die to extrude the melted material. The nozzle of the printer consists of a small metal chamber which has a small hole in the bottom for the plastic to be extruded out of. The hole in the nozzle is most often less than a millimetre in diameter with smaller holes giving better surface finish and accuracy at the cost of longer printing time. The filament is pushed out of the nozzle by the feeder force provided by the filament feed system

The cold end includes a structure for connecting to the positioning system and sometimes a set of fans for cooling the extruded material. The printhead can be attached to the positioning system in a variety of ways depending on the layout of the printer. Often the printhead sits on a gantry that allows it to be moved in the X and Y axes along linear bearings as seen in Figure 3. The movement of the printhead along the gantry is controlled by servo motors. The cold end of the printhead is thermally isolated from the hot end by a thermal break. The printing filament in the cold end should be solid during printing while the material in the hot end should be melted and malleable.

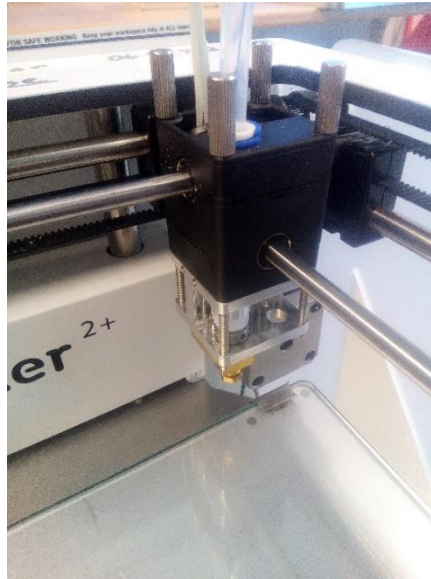


Figure 3: The printhead of an Ultimaker 2+ showing the nozzle in yellow at the bottom, the X and Y gantry rods, the connecting structure, buildplate and the Bowden tube at the top

The buildplate is the surface of the printer that the printhead extrudes the first layer of the component on. The buildplate is often made of glass as it is a smooth and easily cleanable material. The buildplate can be heated to aid adhesion of the initial layer of extruded thermoplastic to the buildplate. The heating of the buildplate can also help to control the internal stresses in the printed component which occur as it cools. The buildplate temperature can be set in a certain range of temperatures, restricted by the printer, and is monitored and controlled by the electronics by means of a thermistor or thermocouple, like the printhead heater. The glass sheet at the bottom of Figure 3 is the buildplate of an Ultimaker 2+.

The filament feed system feeds the filament from where it is stored on its spool into the printhead for extrusion. The filament feed system forwards the filament by gripping it with a toothed wheel whose rotation is controlled by a servo motor. The toothed wheel is pressed firmly into the filament, often with a simple spring, to maintain a firm contact as it moves. There are two main layouts for the filament feed system: direct and Bowden tube. In the direct feed system, the toothed wheel and servo motor are mounted directly on the printhead while in the Bowden tube layout the wheel and motor are located away from the printhead and the filament is delivered to the nozzle by means of a long tube. The Bowden tube layout has the advantage of less weight on the printhead reducing the motion artifact that are created during printhead acceleration at the cost of greater complexity and difficulty in printing flexible filaments [15].

FFF printers can print a wide variety of thermoplastics depending on the printer and the intended application of the fabricated component. The most commonly used plastics in the FFF process are acrylonitrile butadiene styrene (ABS) and polylactic acid (PLA) [16]. These polymers are commonly used because of their ease of printing and low cost. Higher performance engineering plastics are also printed using FFF such as acrylic, nylon and polycarbonate (PC). These higher performance engineering plastics are used when greater strength, operational temperature or other traits are required for a particular application. The main drawbacks of these higher performance plastics are higher processing temperature, difficulty adhering to buildplate and greater cost of filament. There are also FFF printers which can print extremely high performance plastics as polyether ether ketone (PEEK) or polyether imide (PEI) [17]. These thermoplastics have extremely high strengths, high stiffness and are very dimensionally stable. These plastics are used only for very demanding

applications in industries such as aerospace or defense due to their cost and processing temperatures which often require specialized printer. Modern FFF printers are available in a wide range of sizes ranging from small printers that can fit on a desktop to large industrial printers the size of a refrigerator or larger. Common consumer FFF printers are capable of achieving resolutions in the range of 12.5 microns in the X and Y directions and 2.5 microns in the Z direction [16].

2.2 On-Orbit Environment

The environment on-orbit is a very different gravitational, pressure and thermal environment compared to Earth. While the gravitational constant in much of the orbital space around Earth is not much weaker than the gravitational constant on the Earth's surface, objects in orbit experience constant freefall and therefore function in an environment of effective microgravity [18]. This microgravity environment can make many common processes much more difficult, or even completely impossible to implement on-orbit.

2.2.1 Pressure On-Orbit

The pressure environment on-orbit is characterized by a vacuum in the ultra high vacuum (UHV) range [19]. The pressure experienced in space around the Earth can vary from an absolute pressure of around 10^{-4} Pa at low earth orbit (LEO) [20] to a pressure approaching 10^{-14} Pa in interplanetary space. [20]. The pressure within satellites can be slightly higher than the ambient pressure with satellites in LEO sometimes experiencing internal pressures of up to 1.3×10^{-3} Pa [21]. The low pressure on-orbit can cause outgassing of spacecraft materials. Outgassing is where materials release absorbed water vapour and volatile organic molecules when exposed to a low-pressure environment. The rate of outgassing is higher for more volatile materials or when materials are heated [22].

2.2.2 Thermal Environment On-Orbit

The thermal environment experienced on-orbit differs greatly from that on the surface of Earth. The temperature experienced by a satellite in LEO varies greatly depending on the geometry of the satellite, the heat generation of sub-systems, the orbit and the thermal control sub-system of the satellite. As the orbital space around Earth is fairly close to the Earth on a solar system scale, a satellite on-orbit experiences a flux from the Sun approximately equal to that experienced by Earth, 1367 W/m^2 [23]. A satellite on-orbit is also subject to blackbody radiation from the Earth and radiation from the Sun reflected onto the satellite by the Earth. A satellite on-orbit also has heat generated by internal sub-systems or components. Due to the very low vacuum present on-orbit heat can only be dissipated by radiation. Conduction and convection through air are not possible modes of heat transfer. A satellite in LEO will also periodically pass through eclipse behind the Earth leading to large temperature variations. While the thermal control subsystem can mitigate these variations the average satellite temperature will likely be significantly cooler during eclipse and warmer when directly exposed to the Sun.

2.2.3 Other Aspects of the On-Orbit Environment

While the atmosphere at the altitude of LEO is much less dense than at sea level there are still particles to be considered. The atmosphere at LEO is composed of un-ionized particles and is approximately 80% atomic oxygen (ATOX) and 20% nitrogen [21]. Collisions with ATOX can cause degradation of polymers resulting in increase of surface roughness, loss of mass and changes in thermal and mechanical properties [24]. ATOX can also create a phenomenon called "spacecraft glow" where ATOX resistant materials glow when subjected to ATOX flux, leading to interference with optical equipment [24].

The Earth receives 1367 W/m^2 of radiation from the sun with approximately 8% in the 100-400 nm range [21]. As there is no ozone layer between the satellite and the Sun all the UV radiation is incident on the satellite. UV radiation in this range can attack polymeric materials resulting in changes ranging decreased surface finish and loss of mass to degradation of chemical bonds and polymer embitterment. The effects of UV radiation attack on polymers is broadly similar to the effects of ATOX attack on polymers and can result in changed mechanical and thermal properties of the polymer material [24] [25].

Satellites in orbit around the Earth are also exposed to high levels of high energy ionizing radiation from radiation belts, cosmic rays and particles ejected from the Sun. This radiation can cause degradation of satellite components and materials in a similar manner to ATOX and UV radiation depending on the component material and the energy level of the radiation. [21]

The orbital environment also has many small particles that may collide with a satellite. These particles, naturally occurring micrometeoroids and manmade orbital debris, can cause significant damage to spacecraft due to their extremely high velocities.

2.3 On-Orbit Manufacturing

On-orbit manufacturing (OOM), in the general sense, is the process of manufacturing space systems, subsystems or components while on-orbit around a celestial body. OOM consists of three stages; fabrication, assembly and integration [26]. In the fabrication stage, basic components are fabricated from their raw materials. The fabrication process is not restricted to any specific component or process. Types of spacecraft components which could be fabricated on-orbit include structural components [1], functional components (e.g. solar cells, solar sails, optics), electronics [27] and propellant [28]. As FFF is a fabrication process this report focuses almost exclusively on the fabrication stage of OOM. Following fabrication is the assembly stage where the components are assembled together to form a completed space system. On-orbit assembly has been carried out before with the International Space Station (ISS) [29] and the Mir space stations [30] using a combination of robotic arms and astronauts to manipulate and assemble space station modules [31]. The third and final stage of OOM is the integration stage where the assembled system, subsystem or component is functionally integrated to allow all subsystems to function, operationalizing the spacecraft [26]. The assembly and integration stages of OOM can utilize components fabricated on-orbit, on-ground or a combination of the two.

OOM occurs on-orbit around a celestial body, an environment distinguished from the environment on the surface of a celestial body by persistent effective microgravity and usually by a lack of, or minimal presence of an atmosphere. Skomorohov et. al. define “the term “in-orbit” refers to the part of orbital space around Earth up to geostationary Earth orbit (GEO) as place of manufacture” [26]. Based on the definition of Skomorohov et. al. a final definition of OOM was formulated below:

“On-orbit manufacturing is an activity which involves the fabrication of components from raw material, and optionally the assembly and integration of components into a larger space system, which occurs on-orbit around a celestial body”

This definition will be used for the entirety of this report. This definition does not restrict OOM to a specific process, material, origin of the material or final manufactured system. The selection of the orbital space around Earth as being the location to be considered as “on-orbit” is because the orbital space around Earth is the easiest to access and has the most potential customers for on-orbit servicing, maintenance or manufacturing missions using OOM. A more inclusive definition of “on-orbit” would include manufacturing done on-orbit around any celestial body or in deep space such

as interplanetary or even interstellar space. These locations have the same aspects of the orbital space around Earth, effective microgravity and hard vacuum, and OOM implementations that are designed for the orbital space around Earth could also function in these environments.

2.4 State of the Art of FFF On-Orbit

This section presents the state of the art of FFF on-orbit. At the time of writing FFF has not been carried out on-orbit outside of the ISS and therefore only printers which have functioned aboard a space station are discussed.

2.4.1 Additive Manufacturing Facility and 3D Printing in Zero g Demonstrator

The first 3D printer in space was the “3D Printing in Zero g Demonstrator (3DP)” developed by Made in Space (MIS) which was a precursor to the Additive Manufacturing Facility (AMF). The main function of the 3DP was providing a testbed for experiments regarding 3D printing in space [6]. The 3DP produced a variety of items used for research into 3D printing including a functional ratchet wrench, a multitool and a faceplate for the printhead of the printer itself. The 3DP used ABS, a common thermoplastic to print components using the FFF process. These components were transported back to Earth from the ISS and compared to the same components printed on Earth using the same model printer. [7] The 3DP also produced components which were used for ISS operations and experiments. An example of this is a buckle which was used on the exercise equipment aboard the station. [10]

The AMF is a commercial FFF 3D printer that followed the 3DP and was also developed by MIS. It is shown in Figure 4. The AMF is currently in space aboard ISS and will be operational until the station is decommissioned. The AMF is a small 3D printer with a print volume of 100mm x 100mm x 140mm and is designed to fit in an International Standard Payload Rack (ISPR). The AMF is capable of printing ABS, HDPE and PEI+PC thermoplastics with a resolution of 0.15mm in the X and Y directions and 75 microns in the Z direction. [11] This wider variety of polymers when compared to the 3DP or the POP3D below give the AMF more flexibility and allow it to fabricate components for a wider range of applications.



Figure 4: The AMF showing the print volume and a printed plastic component [11]

2.4.2 Portable on Orbit Printer 3D

The other example of an FFF printer being used on-orbit is the “Portable on Orbit Printer 3D” (POP3D). The POP3D is a project of the Italian Space Agency and was built under contract by ThalesAlenia Space and can be seen below in Figure 5. The POP3D is a small 3D printer with a print

volume of 50mm x 50mm x 45mm that uses the FFF process to print PLA polymer components. The purpose of the POP3D was to fabricate a single component on-orbit to characterize the performance of FFF printing on-orbit. In early 2016 the POP3D, aboard the ISS, printed a Y-shaped pipe joiner that had previously been printed on ground. The POP3D, together with the printed component was then transported back to Earth and the component was tested to see how FFF printing on-orbit compared to the same printing on Earth. [8] The results of this testing were not available at the time of writing.

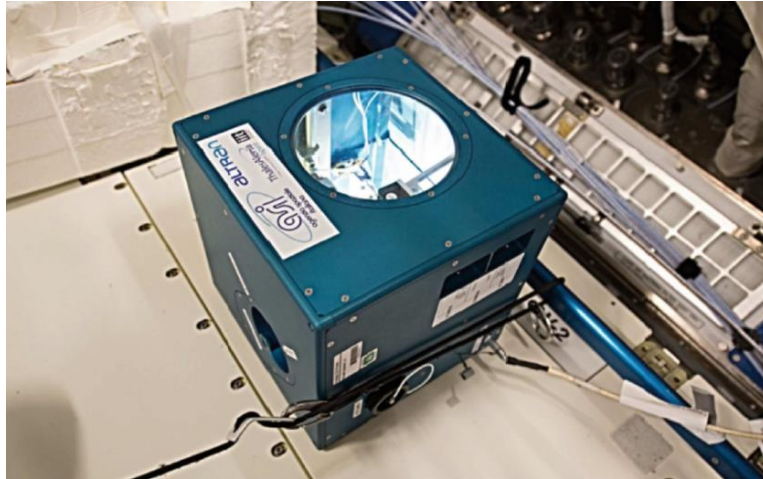


Figure 5: The POP3D printer aboard the ISS [8]

2.5 Technical Issues with FFF On-Orbit

In this section the main technical issues associated with using the FFF process in an on-orbit environment are discussed. As FFF has not yet been carried out in an on-orbit environment these technical issues are only predicted issues and are not an exhaustive list. It is possible that some of these predicted issues will not be a problem and that there will be unforeseen technical issues. The technical issues discussed include outgassing, the thermal environment, the microgravity environment and quality control.

2.5.1 Outgassing

The vacuum environment on-orbit causes outgassing of the polymers used in the FFF process. Outgassing is defined by ESA as “release of gaseous species from a specimen under high vacuum conditions” [32]. Polymers can absorb a wide variety of gases which will be desorbed through the outgassing phenomenon when exposed to vacuum. Polymers can also absorb water vapour from the air which will also be outgassed when exposed to a vacuum environment. [22] This is particularly problematic for hygroscopic materials such as nylon, ABS or polycarbonate (PC) which tend to readily absorb water from the surroundings. The level of outgassing depends on the chemical makeup of the polymer, the pressure of the vacuum the polymer is exposed to and the temperature [22].

All the polymer parts of an FFF printer as well as the printing filament itself will outgas and give off volatile compounds and water vapour when exposed to the vacuum environment on-orbit. The main parameters for measuring outgassing are Total Mass Loss (TML), Recovered Mass Loss (RML), Collected Volatile Condensable Material (CVCM) and Water Vapour Recovered (WVR). These values can be obtained by testing the material according to ECSS-Q-ST-70-02C or to the equivalent NASA standard. In this test the materials are brought to a pressure of 10^{-3} Pa and are then heated to 125 °C for 24 hours. Nearby to the heated samples is a collection plate which is maintained at 25 °C to collect outgassed material.

TML is defined by ESA as the “total mass loss of material outgassed from a specimen that is maintained at a specific constant temperature and operating pressure for a specified time” [32]. CVCM is the “quantity of outgassed matter from a test specimen that condenses on a collector maintained at a specific temperature for a specific time” [32] and shows the amount of outgassed material which will condense and buildup on cool nearby surfaces. WVR is the “mass of the water vapour regained by the specimen after the optional reconditioning step” [32] and shows the amount of outgassed material which is water vapour. RML is equal to the TML minus the WVR [33] and will therefore always be lower than the TML value. RML is an important parameter because water vapour is not considered a contaminant in many applications. TML, CVCM, and RML are expressed as percentages of the original sample mass. WVR is expressed as a percentage and “is calculated from the differences in the specimen mass determined after the test for TML and CVCM and again after exposure to atmospheric conditions and 65 % relative humidity at room temperature (22 ± 3) °C” [32]. The ESA recommendations for material selection for a spacecraft are an RML <1% and a CVCM <0.1% [34].

The material choice for both the construction of an on-orbit FFF printer and the printed filament itself should have a low TML, CVCM and have a WVR that is a large proportion of the TML. Choosing materials with low outgassing characteristics would decrease the risk of contamination of delicate sensors or optics nearby the FFF printer. The increased outgassing with increased temperature means that temperatures during fabrication should be kept as low as possible. Polymer filament and components could also be baked out in a heated vacuum environment prior to flight to remove absorbed gas and kept in a dry environment to prevent water vapour absorption. Even if everything possible is done to reduce outgassing it cannot be eliminated entirely and must be accounted for in the design process.

2.5.2 Thermal Environment

If the OOM process is not contained within a pressurized space station, the on-orbit environment presents a challenging thermal environment as the fabrication process must function in a hard vacuum. The vacuum in the UHV range means that thermal energy produced during fabrication can only be dissipated by radiation or conduction through the spacecraft structure. This could make temperature regulation of the fabrication process difficult and would require a complex thermal regulation system. The thermal system may require large radiators, to adequately dissipate thermal energy from high temperature processes which otherwise would have been dissipated by conduction or convection. This could add significant launch volume reducing the efficiency of OOM as well as introducing additional complexity.

An OOM system in orbit may also experience periodic variations in temperature due to the Sun exposure and eclipse cycles as it orbits. The large temperature fluctuations caused by this cycle may be a problem if the fabrication process can only occur in a certain temperature range. These challenging thermal conditions may influence the heating or cooling rates of the material as it is fabricated. Incorrect heating or cooling could cause the final component to fall short of specifications relating to strength, stiffness or surface finish. Changes in differential cooling after fabrication could also lead to warping or bending of components.

Because of this difficult thermal environment, the thermal regulation of any implementation of FFF on-orbit in vacuum must be very carefully designed and tested. The thermal control of both the printhead and buildplate of the printer must be designed to accommodate the lack of convective cooling and the wide range of ambient temperatures. The thermal regulation of the build volume as the polymer component is cooling must also be carefully controlled or the component must be

tested to determine if it is dimensionally accurate under the expected cooling regime. Changes in length of the printer structure could also occur with the temperature fluctuations throughout the satellites orbit and the effects of these changing dimensions on the coordinate system used by the printhead must also be considered.

2.5.3 Microgravity

Gravity is often used to help position material or equipment, sort material or to keep material and waste out of the way. The FFF process does not rely on gravity to function and is therefore a good choice for on-orbit additive manufacturing. This is shown by the success of the 3DP [9], AMF and POP3D [8] printers. Problems potentially facing FFF relating to microgravity include adhesion of the fabricated component to the buildplate, waste material control and feedstock control. Printing on the ISS with the 3DP has shown that adhesion of ABS to the print bed is not a problem in microgravity, with instances of “super-adhesion” being recorded [9]. The environment surrounding the build volume would have to be carefully controlled to ensure waste material does not damage equipment. In a free-floating implementation, one that is not aboard a space station, the layout of the fabrication machinery must be designed very carefully as there is no ground to rigidly fix equipment to. A proper coordinate and control system for all fabrication equipment must therefore be established.

Although microgravity creates some fabrication challenges it also presents several benefits. Without effective gravity, components will not slump as they are being fabricated. This is particularly helpful when considering long components or components with large overhangs such as Sample Number 020 printed by the 3DP and shown in Figure 6 below. Lack of effective gravity also allows for more flexibility when designing the manufacturing area, eliminating the requirement for equipment to be fixed to a certain ground plane. This could enable a more efficient use of space as the manufacturing facility could be laid out in three dimensions. Lack of effective gravity also allows for simpler, longer and less strong fabrication machinery to be used as the equipment does not need to support its own weight.

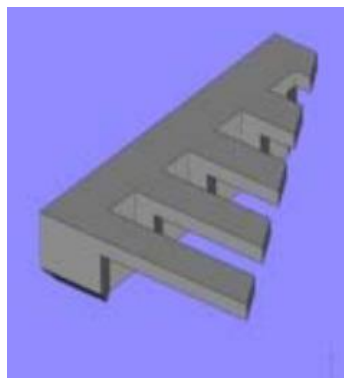


Figure 6: Sample 020, a very difficult to print on Earth component which was printed by the 3DP on-orbit [7]

2.5.4 Quality Control and Maintenance

The isolation of the OOM facility on-orbit means that the system must be very self sufficient. This means that the quality control of the system must be either monitored remotely or automated. The quality control system must identify a wide variety of deficiencies in a wide variety of fabricated components. To do this the quality control system must be very flexible. The flexibility needed makes using physical tools to measure or test the fabricated components difficult as many tools or measurement devices would be required to address all possible quality deficiencies. The ability of OOM to fabricate components with complex geometry and large sizes also makes quality control

difficult. Quality control systems based on imaging and machine vision were proposed for the SpiderFAB architecture [1] and have been researched specifically for on-orbit 3D printing [35], [36]

Any components which are identified as deficient must either be repaired or disposed of. Repair on-orbit is very difficult as the OOM facility only has limited stores of material and only has a specific set of abilities. Repair operations may require functionality not present in the OOM facility. Designing the OOM facility for every possible repair scenario or upgrading the facility as each repair scenario occurred would be incredibly difficult and costly. If a component cannot be repaired there must be a system in place to dispose of the component in manner which does not interfere with the OOM process or create space debris. The high cost of transporting material to orbit means every discarded component wastes large amounts of money. It may then be beneficial to design the OOM system with a greater focus on producing components correctly the first time rather than relying on repair or discarding components which do not meet specification. A system for recycling waste material into usable filament may also be useful, similar to the R3DO system being developed by MIS [37].

3 Experimental Setup

This chapter details the development of the experimental apparatus that was used to investigate the performance of an FFF printer in a vacuum environment. This includes sourcing of the equipment including the FFF printer, vacuum pump and vacuum chamber. Background research into the use of the equipment, the associated risks and mitigation strategies to reduce risk is also presented. The modifications to the FFF printer to allow it to function in the vacuum chamber are also presented.

3.1 Experimental Setup Requirements

The experimental setup needs to fulfill several requirements to make it suitable for the research. As the research questions are very broad there are many ways to approach the task of answering them. The best method of approaching the research question must therefore be determined based on many factors. A series of requirements therefore need to be set out to determine which each option should fulfill. The option which fulfills the most requirements is most likely to yield results that are useful in answer the research questions.

The purpose of this research is to examine the effect a simulated on-orbit environment has on the FFF process and components fabricated by the process. As such the experimental setup must be able to replicate the on-orbit environment to some extent. This could include the pressure, thermal and/or microgravity environments. It could also include other aspect of the on-orbit environment such as ATOX, UV radiation and micrometeoroids. As these are difficult to simulate the experimental setup should focus on the aspects which are most relevant to the FFF process itself, the vacuum and thermal environment. While microgravity is also very important, the FFF process has already been demonstrated in a microgravity environment.

The next key aspect of the experimental setup is the FFF printer itself. The printer must be a proven design as creating a custom printer is beyond the scope of the thesis. The printer must reliably fabricate a variety of geometries in a normal atmosphere. The printer needs to fit within the volume which is used to simulate the on-orbit environment. This is a key consideration because the FFF process must be carried out in this environment for meaningful results to be observed. The printer should be easily modified, and spare parts should be readily available as it is expected that a printer will not function properly in a simulated on-orbit environment in “off the shelf” configuration. The printer should also be capable of printing with a variety of polymers, particularly higher strength engineering polymers.

There are also several practical concerns that must be addressed. The equipment for the experimental setup needs to be readily accessible to a MSc student. Use of the equipment should not require an overly large time or financial budget. As research into FFF in a simulated on-orbit environment is in the very early stages and unforeseen problems may occur the experimental setup should be chosen such that damage is unlikely and any potential risks can be mitigated.

3.2 Experimental Environment

The first part of the experimental apparatus that needed to be specified was the experimental environment. As the goal of the thesis work is to investigate the performance of an FFF printer in a simulated LEO environment an appropriate environment must first be specified and a means of reproducing it must be found. The specification of the simulated LEO environment depended on the LEO environment as well as the availability of suitable equipment.

The vacuum chamber in the cleanroom on the 8th floor of the TU Delft Aerospace Engineering building was the first possibility identified for the simulated on-orbit environment. The vacuum

chamber would allow for the pressure environment to be easily created and maintained. The vacuum chamber was investigated and found to be a Heraeus VT 6130 M Vacutherm from Thermo Scientific which can be seen below in zzFigure 7. This chamber is available for use by aerospace MSc students and is conveniently located in the aerospace engineering building. This vacuum chamber is also capable of heating to 200 °C allowing it to simulate a variety of thermal environments if needed. Due to these advantages and the time constraints of the thesis it was decided to investigate if this vacuum chamber was suitable for testing. The simulated LEO environment would be specified to be created with this chamber. If it was deemed that the specification of the LEO environment varied too much from the actual LEO environment for it to provide a useful test only then would an alternate vacuum chamber be looked for. Other options included using a large environmental chamber at ESA or only enclosing the printhead in a simulated on-orbit environment. Time in a large environmental chamber would be prohibitively expensive and contamination due to the polymer filament and printer parts would be large concern. Only enclosing the printhead would not allow complete components to be fabricated as the printhead could not move relative to the buildplate. Because of these issues these options were discarded.



zzFigure 7: Heraeus VT 6130 M vacutherm in the cleanroom

3.2.1 Vacuum

There are a variety of values of pressure at LEO given by different sources which are compiled in Table 1. LEO was chosen as the area of interest in orbital space because most potential customer spacecraft are located there and it would be the easiest location to access for further testing. These pressures depend on the altitude of the satellite above the Earth's surface and whether the pressure is measured inside or outside the satellite. All of these pressures are in the high vacuum (HV) or UHV ranges [19].

Pressure at LEO	Reference
-----------------	-----------

Approximately 10^{-4} Pa ranging to a minimum value of 10^{-14} Pa in interplanetary space.	[20]
LEO vacuum is typically 10^{-9} to 10^{-11} (and 10^{-6} to 10^{-7} Torr inside satellites)	[21]
Pressure in space is defined as ultra-high vacuum of less than the order of 10^{-5} Torr. The magnitude of pressure is dependent on altitude and solar effect so as to be on the order of 10^{-5} Torr at an altitude of 200 km and 10^{-12} Torr at 6500 km	[24]

Table 1: Pressure at LEO

The Heraeus VT 6130 M is rated for a minimum vacuum pressure of $1 \cdot 10^{-2}$ mbar ($7.5 \cdot 10^{-3}$ Torr or 1 Pa) [38]. This is a significantly rougher vacuum than the roughest vacuum pressure at LEO by approximately four orders of magnitude. While this is not optimal, and a higher vacuum would be preferred, it is important to consider this pressure in the context of the research goals. The effects of the LEO environment on the FFF printer are where outgassing of polymer materials occurs and where convective cooling is extremely small or eliminated as a means of heat transfer from the printer or components.

After it was established that the Heraeus VT 6130 would be used for testing a suitable vacuum pump needed to be sourced to pull the vacuum in the chamber. When originally inspected, the chamber was plumbed to a vacuubrand RZ-6 vacuum pump. Concerns were raised by other researchers about whether the outgassing and ultra-fine particles (UFPs) generated during the FFF process could damage the pump. If the pump were to become damaged it could seriously delay their research as a replacement pump was sourced. Because of these concerns the RZ-6 pump could not be used for testing. The concerns of the outgassing and UFP generation damaging the vacuum pump are addressed later in this report in Section 3.5.



Figure 8: The vacuubrand MD-1 vacuum pump used for testing

Another vacuum pump was found, a vacuubrand MD-1, that was available for MSc students. As this pump was not in use there were no concerns related to damage or contamination. It was found that the Heraeus VT 6130 M has a valve that can isolate the chamber from the pump. This valve would be closed, and the pump turned off, during printing operations isolating pump from the FFF process and preventing damage. Additionally, the MD-1 is a dry pump, without oil, meaning that any particulate ingested into the pump will simply be blown out the exhaust and cannot buildup in any lubricant.

This pump can be seen in Figure 8. The specification of the MD-1 vacuum pump can be found in the MD-1 column of the technical data table in Appendix A – vacuubrand MD-1 Specifications. The absolute vacuum pressure achievable by the MD-1 pump is 1.1 Torr (1.5 mbar, 150 Pa). The MD-1 pump is therefore compatible with the VT 6130 M vacuum chamber and the pump is the limiting factor determining the absolute maximum vacuum pressure.

Although both the Heraeus VT 6130 M and vacuubrand MD-1 specifications were known it is possible the actual achievable pressure may be higher or lower. To determine the possible pressure the MD-1 vacuum pump was plumbed to the chamber and vacuum was drawn until it stabilized. The pressure was monitored over time and can be seen in Figure 9 below.

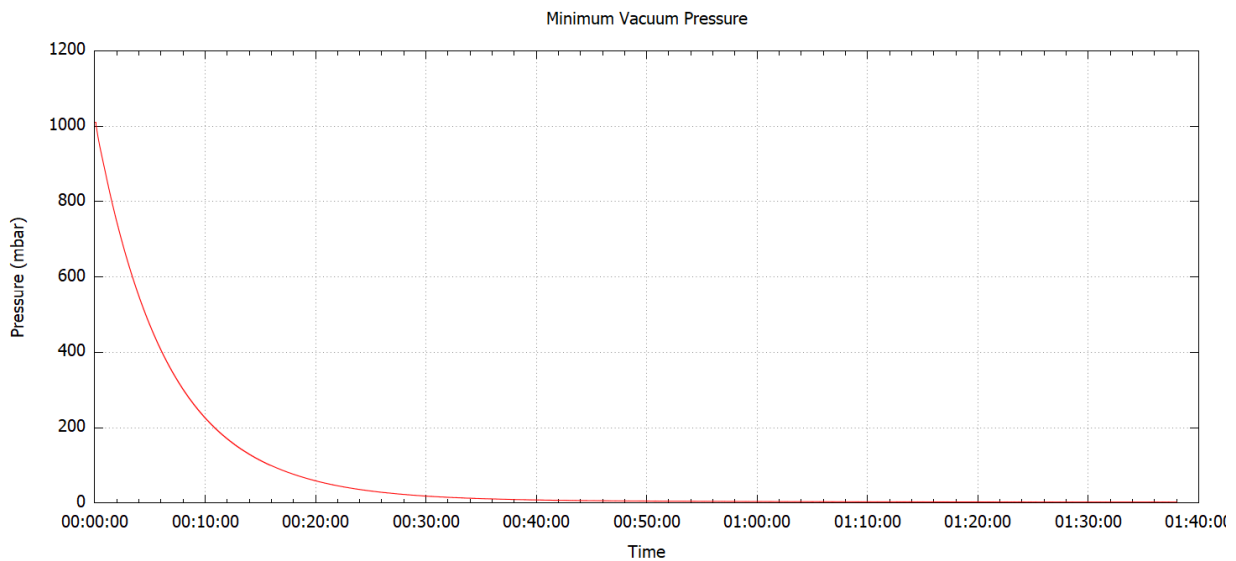


Figure 9: Vacuum chamber pressure over time

Figure 9 shows that the pressure in the vacuum chamber drops very quickly in the first 10 minutes with the rate of pressure drop decreasing between 10 and 30 minutes. After approximately 40 minutes the rate of pressure decrease becomes extremely small. After 1 hour and 45 minutes the pressure had stabilized at 2.66 mbar (266 Pa). This means that the experimental apparatus cannot achieve the rated pressure of 150 Pa. The length of pumping time is also an issue as the vacuum chamber needs to be available for use by all students and staff of the TU Delft SSE group. If a component is to be printed at the minimum possible pressure then the time needed to print a single component is the sum of the pump down time, the printing time and the cooling time. If a larger component with a print time of 2-3 hours is printed the cycle time to fabricate each component could reach six or more hours. This would require the usage of the vacuum chamber for the entire day, precluding its use by other researchers. If a series of components is to be fabricated, such as for mechanical testing, this could require the exclusive use of the vacuum chamber for weeks at a time. As this was not feasible a solution had to be found.

Using a higher pressure, with a lower pump-down time, would reduce the issue related to time constraints. This higher pressure needed to be selected as a balance between the pressure and pumping time. A pressure of 1000 Pa (10 mbar) can be reached with the MD-1 pump is approximately 35 minutes, where the rate of pressure drop begins dropping. This is one quarter the time required to reach the minimum pressure while still achieving a pressure only 1% of normal, atmospheric pressure of 1 atm (101325 Pa). As 1000 Pa seems to present the best balance of pressure and pump-down time it was selected as the experimental pressure. The level of convective

cooling occurring at this pressure compared to the convective cooling present in an atmosphere with pressure of 1 atm is investigated thoroughly in Section 5.2. Sourcing an alternate vacuum pump was considered however both the cost and delivery time of a new pump were unfeasible. Damage to a brand new, expensive pump by outgassed material or UFPs also presented a serious issue.

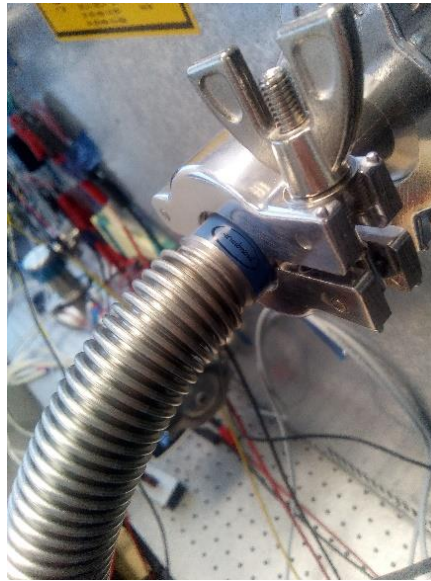


Figure 10: The DN16 vacuum flange connection on the read of the vacuum chamber

A method of plumbing the MD-1 pump to the VT 6130 M vacuum chamber was also required. The VT 6130 M vacuum chamber has a DN16 vacuum flange connection for attaching a vacuum pump [38], as seen in Figure 10, while the MD-1 pump has a DN6 barbed connection intended for tubing with an inner diameter (ID) of 1/4" (6 mm) [39]. An aluminum DN16 to DN6 adaptor and DN6 vacuum rated tubing were obtained from Dijkstra Verenigde. After delivery of these parts they were test fitted to the MD-1 pump and the VT 6130 M chamber and were found to fit properly. No hose clamps were required as Dijkstra specified that the vacuum within the tubing would pull it onto the barbed DN6 connectors.



Figure 11: 1/4" (6 mm) vacuum tubing and DN16/DN 6 adapter

3.2.2 Temperature

The temperature experienced by a satellite in LEO varies greatly depending on the geometry of the satellite, the geometry of the orbit, the heat generation of sub-systems and the thermal control sub-system of the satellite. Because of this variation and the ability of the thermal control subsystem to regulate the temperature a wide variety of temperatures could be expected. The temperature of the simulated LEO environment used for testing is more heavily influenced by other factors. These factors include the heating ability of the VT 6130 M vacuum chamber and the allowed ambient air temperatures for both the MD-1 vacuum pump and the Ultimaker 2+ FFF printer (the selection process of which is discussed in Section 3.3)

The VT 6130 M vacuotherm has built-in heaters for heating the internal volume and is rated for up to 200 °C [38]. The VT 6130 M does not have any built-in cooling capability and is therefore restricted to working in the temperature range between ambient room temperature and 200 °C. This is assuming that no cooling system can be fitted into the vacuum chamber. While this may be possible the purpose of this thesis is to investigate the FFF process in vacuum. Building an apparatus that can be retrofitted to cool the VT 6130 M would be a large project in and of itself. It was therefore decided that ambient room temperature (~25 °C) to 200 °C could provide an adequate range of temperatures for testing.

The next consideration regarding the temperature is the operational temperatures of the MD-1 vacuum pump and the Ultimaker 2+ FFF printer. The operational temperature of the MD-1 pump is 10 to 40 °C [39] while the operational temperature for the UM2+ printer is given as 15 to 32 °C [40]. As any effects of the ambient temperature on the printer or pump should be avoided if possible it was decided to use the 15 to 32 °C range of the UM2+ printer as the temperature range for testing. This is also prudent as it is the most conservative temperature range of any of the critical pieces of equipment. The final temperature decided for the testing was the ambient room temperature of the room where testing was being carried out. This is simplest option and eliminates any variables regarding the heating of the VT 6130 M. Room temperature was chosen instead of a temperature between room temperature and the 32 °C upper limit because the printhead and buildplate of the printer are very hot during printing and will therefore increase the temperature of the internal volume of the VT 6130 M. The temperatures can be monitored by recording with a thermocouple. If the temperature within the VT 6130 M exceeds the 32 °C upper limit it will be noted, and the fabricated components can be checked for any problems after fabrication.

3.2.3 Gravity

Although the gravitational environment on-orbit is an environment of persistent microgravity the testing will be carried out in normal gravitational conditions of approximately 1 g. This is because the FFF process has already been demonstrated to work in the microgravity environment on-orbit through the 3DP, AMF and POP3D. The purpose of this thesis is to investigate the FFF process in a simulated LEO vacuum environment. It is assumed that if the FFF process can be shown to work in a vacuum environment, in addition to its previous demonstration in a microgravity environment, then the FFF process can work correctly in a microgravity and vacuum environment simultaneously. Using a drop tower or parabolic flight to simulate microgravity would not be possible as these are only capable of producing short periods of effective microgravity. These short periods would not allow the FFF process to fabricate a complete component. If possible, the printer could be inverted during printing in the simulated on-orbit environment to show that the FFF process is independent of the direction of the gravity vector.

3.2.4 Other Factors

As noted above in Section 2.2 there are many other aspects of the on-orbit environment including atomic oxygen (ATOX), UV radiation, ionizing radiation, micrometeoroids and orbital debris. These factors can cause degradation of polymers however they only do so after prolonged exposure [21]. As this thesis is about the fabrication process, not the long-term performance or viability of polymer components in a space environment, these additional environmental aspects were deemed to be out of scope. In addition, creating an simulated environment for these aspects within the VT 6130 M vacuum chamber would be a very difficult project and would be prohibitive in both cost and time constraints. There is also a limited amount of space in the vacuum chamber, most of which is taken up by the 3D printer, making the use of additional equipment inside the vacuum chamber difficult.

3.2.5 Final Experimental Environment

In conclusion the experimental environment was chosen to be an environment with a pressure of 1000 Pa (10 mbar) with a temperature of 25 °C. No other aspects of the on-orbit environment were chosen to be simulated in the experimental environment however these would have to be addressed in further research into the FFF process in an on-orbit environment. The reference environment, against which components fabricated in the experimental environment will be compared, was defined as normal atmospheric pressure and temperature of 1 atm and 25 °C.

For the remainder of this report the experimental environment is referred to as the vacuum environment. References to “the vacuum environment” refer to the experimental environment stated above and references to a “vacuum component” refer to a component fabricated using FFF in the experimental environment. Procedures carried out “in vacuum” are carried out in the above mentioned experimental environment. The same is true for “atmosphere environment” which refer to the atmospheric reference environment above. “In atmosphere” refers to a process carried out in the atmospheric reference environment and an “atmosphere component” is a component fabricated using FFF in the atmospheric reference environment respectively.

3.3 Experimental Printer

To carry out testing a suitable 3D printer needed to be sourced. The most important consideration when sourcing the 3D printer was that it fit in the Heraeus VT 6130M vacuum chamber. The internal dimensions of the VT 6130 M are 495 x 489 x 529 mm (w x h x d) [38]. The first printer investigated was the MakerBot Replicator+ owned by the space systems engineering (SSE) group of the aerospace faculty. This printer can be seen below in Figure 12.



Figure 12: The MakerBot Replicator+ [41]

The MakerBot Replicator+ has external dimensions of 52.8 x 44.1 x 41.0 cm (depth, width, height) [41] and can therefore just fit in the VT 6130M vacuum chamber. Although using the MakerBot was feasible it has several drawbacks the most important of these is the reliability. After speaking with Dr. Guo and Sevket Uladag regarding the printer it was found to have a reputation as being unreliable and inaccurate. The issue of unreliability would be exacerbated by exposure to the vacuum environment and inaccuracy means that it would be hard to compare components printed in vacuum to those printed in atmosphere due to uncertainty regarding the root cause of any observed problems. The MakerBot is also only capable of printing in PLA and ABS thermoplastics, neither of which are very strong and are not normally used in the fabrication of engineered components. In addition to the problems with the performance of the MakerBot the large amount of polymer used in the printer structure presented the potential for high levels of outgassing when exposed to the vacuum environment. The integrated nature of printhead and direct filament feed system of the MakerBot would make modification of the printer for use in the vacuum environment difficult.

To find alternate printer, Dutch manufacturers of 3D printers were contacted to see if they were interested in supporting this thesis research. Dutch manufacturers were contacted first due to their proximity to TU Delft and therefore ease of meeting and shipping. Foreign manufacturers were considered and would be contacted if no Dutch manufacturer responded. Ultimaker BV replied and after a meeting with Bas van Deursen and Johan Versteegh it was agreed that Ultimaker would supply an Ultimaker 2+ (UM2+) printer, seen below in Figure 13, any Ultimaker brand polymer filament and any needed spare parts for the thesis work. The specifications of the UM2+ can be seen below in Appendix B – Ultimaker 2+ Specification.



Figure 13: An unmodified Ultimaker 2+ FFF 3D printer [42]

The UM2+ has external dimensions of 342 x 357 x 388 mm (w x d x h) and can fit in the Heraeus VT 6130 M vacuum chamber. The UM2+ also has many advantages over the MakerBot that was originally considered for the thesis work. The UM2+ is capable of printing in a wide variety of materials including materials such as polycarbonate (PC) and nylon [40], which are higher strength thermoplastics more suited to high performance structural components. The UM2+ is also extremely accurate with XYZ accuracy of 12.5, 12.5 and 2.5 microns respectively. The UM2+ has less plastic

incorporated in its structure. Having a dedicated printer for the thesis research also meant that modifications could be made to the printer without worrying about breaking the printer and interfering with other users. The UM2+ was chosen as the printer to be used for testing over the more advanced Ultimaker 3 as the Ultimaker 3 includes more advanced functions which would not be useful or would complicate operation in vacuum. The Ultimaker 3 also has a more integrated printhead making modifications more difficult compared to the UM2+.

In addition to the material support in the form of a test printer and spare parts, having the support of a 3D printer manufacturer was an invaluable resource. It was deciding in the meeting at Ultimaker that Johan Versteegh would act as an advisor for the thesis research. This advisor position would include providing help with setting up the printer, adhering to best practices for 3D printing and helping to troubleshoot hardware and software issues encountered over the course of the thesis work. This support in combination with the advantages of the UM2+ printer led to it being selected as the test printer for the thesis research.

3.4 Material Choice

Following selection of 3D printer, the material used for testing needed to be chosen. The main considerations taken when choosing the material to be used during testing were: likelihood of being used in a real on-orbit implementation of FFF, the vacuum properties and the compatibility of the material with the UM2+ printer. These areas are discussed in greater depth below.

To determine which materials are most likely to be used in a real on-orbit implementation of FFF significant background research was conducted. The SpiderFAB concept being developed by TUI aims to construct long beams from PEEK/carbon fibre composite [1]. The 1987 NASA proposal to use pultrusion on-orbit also investigated PEEK reinforced carbon fibre to manufacture large space stations [5]. ESA has also been investigating using PEEK to fabricate CubeSat structures on-ground which would then be conventionally launched to orbit. The lead researcher Dr. Ugo Lafont states that he is investigating using PEEK for CubeSat bodies because “PEEK is a thermoplastic with very good intrinsic properties in terms of strength, stability and temperature resistance, with a melting point up around 350 °C. PEEK is so robust that it can do comparable jobs to some metal parts.” [43]. This shows that PEEK can be used as a structural material for spacecraft, a key for on-orbit FFF. The same article also states that “the Materials’ Physics & Chemistry team is collaborating with ESA’s Directorate of Human Spaceflight and Robotic Exploration on a space-optimised PEEK printer for initial testing on ‘zero-g’ aircraft flights, then eventually at the service of astronauts on the International Space Station.” [43]. This shows that PEEK printing may be soon be tested in a microgravity environment and is being investigated for on-orbit use. PEEK is therefore an excellent candidate for testing.

Another material of interest is PEI. PEI is an excellent candidate polymer for printing because it has already been used on-orbit aboard the ISS as the AMF is able to print a PEI/PC blend [11]. PEI has also been investigated as a structural material for space going components including CubeSat structures [44] and a deployable composite boom [45]. The same NASA proposal as above also investigated the use of PEI to manufacture the theoretical space station alongside PEEK [5]. NASA has also published a paper about modifying a COTS printer to print high processing temperature and high strength thermoplastics such as PEI [46]. PEI is therefore a material of interest for testing.

In addition to general background research a meeting with Dr. Ugo Lafont, the lead researcher from [43], and Dr. Guo was held at ESTEC. During this meeting the material choice was discussed. Dr. Lafont suggested that four polymers were of particular interest for use in space for OOM: polyamide (Nylon) reinforced with carbon fibre, PEEK reinforced with carbon fibre, PEEK and PEI. This validated

the background research which suggested PEEK and PEI as being polymers of interest as well as adding two new polymers of interest.

A major consideration when choosing the polymer for testing was the compatibility of the plastic with the UM2+ printer. The testing in this thesis is restricted to using only the available 3D printer, a UM2+. While this printer can be modified to function with polymers it is not already compatible with this could require large investments of time and money to implement, which would delay the investigation into the real question of this research, the comparison of components printed in vacuum to those printed in atmosphere. Additionally, modifying the printer to print with non-compatible plastics would add an element of uncertainty to the printing process. This uncertainty would make it difficult to tell if defects in prints were due to the modifications, printing settings or the vacuum environment. A real implementation of FFF on-orbit would use a custom-built 3D printer with a series of plastics that it is engineered to work best with. Table 2 below shows the compatibility of the above four polymers of interest, as well as the polymers the UM2+ is already compatible with.

Material	Full Name	Compatible with UM2+	Modifications Required
PLA	Polylactic acid	Yes	None
ABS	Acrylonitrile butadiene styrene	Yes	None
CPE	Copolyester	Yes	None
PC	Polycarbonate	Yes	None
Nylon	Nylon	Yes	None
Nylon/CF	Polyamide (Nylon) reinforced with carbon fibre	Partially, non-reinforced Nylon is	Likely a more abrasion resistant nozzle
PEEK	Polyether ether ketone	No	All metal printhead and firmware modifications
PEEK/CF	PEEK reinforced with carbon fibre	No	All metal printhead and firmware modifications and likely a more abrasion resistant nozzle
PEI	Polyetherimide	No	All metal printhead and firmware modifications

Table 2: Compatibility of investigated materials with the UM2+ printer

In Table 2 the compatibility of each plastic with the UM2+ printer is shown along with any modifications that would be needed to allow the plastic to be used. The UM2+ is already engineered to be compatible with the first five plastics eliminating the need for any modifications [40]. The UM2+ is not rated to print PEEK and PEI due to the high processing temperatures required for these materials. PEEK requires a printhead temperature of 360 to 410 °C and a buildplate temperature of 120 °C [47] and PEI requires a printhead temperature of 350 to 380 °C and a buildplate temperature of 140 to 160 °C [48]. The UM2+ printer is rated for printhead temperatures of up to

260 °C and buildplate temperatures of up to 110 °C [40]. To print successfully at the processing temperatures required for PEEK and PEI the printhead of the UM2+ would have to be replaced with an all-metal printhead to avoid problems caused by the degradation or softening of the polymer components in the UM2+ printhead at the elevated temperatures. The firmware of the UM2+ would also have to be altered to allow these higher temperatures to be achieved. The buildplate or buildplate heater may also have to be replaced with higher performance parts. Extensive testing would have to be carried out to ensure the UM2+ functions correctly with the modifications. Because of these constraints it was decided that PEEK and PEI would be eliminated as potential materials for use during testing.

With PEEK and PEI eliminated carbon fibre reinforced Nylon is then considered. The UM2+ is rated to print Nylon but not Nylon with reinforcement, carbon fibre or otherwise. Printing a material with reinforcement would abrade the inside of the nozzle, gradually widening it and changing the performance of the printer. This would have to be accounted for over time by the printer or the nozzle would have to be replaced with a much more abrasion resistant material. As these options would require significant retrofitting and testing and would detract from the point of the research it was decided that reinforced Nylon would not be considered. This poses an interesting problem as the UM2+ is rated to print Nylon. Nylon would be a good material for testing as it is a constituent component of one of the materials suggested by Dr. Lafont. Although this is important there are other factors to consider such as the vacuum properties of the material and the similarity of the material processing parameters to the parameters required for printing PEEK and PEI.

All plastics will outgas and give off volatile compounds and water vapour when exposed to the vacuum environment as discussed above in Section 2.5.1. This is particularly true when the plastic is heated to a high temperature, such as during processing in the FFF process. If the FFF process is to be implemented on-orbit the plastic used must have very low outgassing properties. Low outgassing properties are also desired for testing to avoid damaging the vacuum chamber, the vacuum pump or other equipment or experiments in the vacuum chamber. This played an important role in the material selection as there were concerns raised regarding the potential for damage or contamination of the vacuum chamber and vacuum pump addressed below in Section 3.5. As noted before the ESA recommendations for material selection for a spacecraft are an RML <1% and a CVCM <0.1% [34].

Table 3 shows the vacuum properties of all the UM2+ compatible materials as well as PEEK and PEI for comparison. These properties given are the four main parameters for characterizing outgassing which were discussed in Section 2.5.1. Included is the exact name of material entry in the relevant data base and the reference from the database from which the data was sourced.

Material	TML (%)	CVCM (%)	WVR (%)	RML (%)	Database Entry Name	Source
PLA	0.56	0.01	0.33	0.23	PLA Plastic (MakerBot)	[49]
ABS	0.94	0.04	0.25	0.69	ABS Plastic, 3D Printed	[49]
CPE	1.89	0.11	0.00	1.89	Eccostock CPE polyethylene	[49]
PC	0.17	0.00	0.14	0.03	Stratasys Polycarbonate PC10 - Rapid Prototype Material	[49]

Nylon	1.14	0.01	0.29	0.85	Zytel 101L White Modified Nylon 66	[49]
PEEK	0.31	0.00	0.06	0.25	PEEK (PolyEtherEtherKetone)	[50]
PEI	0.40	0.00	0.06	0.34	Ultem® PEI (PolyEtherImide)	[50]

Table 3: Vacuum properties of investigated materials

It can be seen in Table 3 that polycarbonate clearly has the best outgassing properties with a TML of 0.17% and a CVCM of 0.00%. Nylon has average outgassing properties with a TML of 1.14% and CVCM of 0.01%. PLA and ABS have slightly better values than Nylon, but they are still significantly worse than PC. It is interesting to note the good vacuum properties of both PEEK and PEI, further reinforcing their suitability for use in the on-orbit environment. As CPE has worse vacuum properties than Nylon it is eliminated right away. The remaining four polymers are therefore: ABS, PLA, PC and Nylon. Nylon has the advantage of being the closest to one of the original four materials of interest while PC has the best vacuum properties. While Nylon seems promising PEEK and PEI are more promising materials for use in vacuum. The material with the closest processing conditions would provide the closest analogue to PEEK and PEI for studying how a FFF printer functions and a fabricated component behaves in a vacuum. As the processing temperatures of PEEK and PEI are very high this would be the polymer with the highest processing temperature of the remaining four.

Material	Printhead Temperature (°C)	Buildplate Temperature (°C)	Source
PLA	210	60	[51]
ABS	250	80	[52]
PC	260	110-115	[53]
Nylon	250	60	[54]

Table 4: The processing temperatures for a UM2+ for the final four polymers of interest

Table 4 shows the processing temperatures recommended by Ultimaker for the four remaining polymers of interest for a 0.4 mm nozzle diameter. PC has the highest processing temperature for both the printhead and the buildplate followed by ABS, Nylon and finally PLA. PC therefore provides the best analogue for the processing conditions of PEEK and PEI. Because of this and the extremely low outgassing properties of PC, it was selected as the material to be used. Specifically, black, Ultimaker brand, PC filament was supplied by Ultimaker for testing.

3.5 Concerns Related to FFF Printing in the Vacuum Chamber

After the experimental setup had been determined other users of the vacuum chamber expressed concern that the FFF process would damage the vacuum chamber or other equipment in it. There were two main concerns: the outgassing of polymer printer parts and filament, and the generation of UFPs by the FFF printing process. Prior to beginning testing, further research into the risks posed by the operation of the FFF printer in the vacuum chamber was required by both Dr. Gill and Dr. Guo. This included both the risks associated with the testing and mitigation strategies.

3.5.1 Outgassing

The first concern that needed to be addressed was the outgassing of printer parts and filament when exposed to vacuum. The potential for outgassing material to condense on and interfere with

equipment was a major concern. The outgassed material could also condense on the walls of the vacuum chamber, build up and then outgas again when vacuum was created for a different experiment. The outgassed material could also potentially harm the vacuum pump. The process of addressing and mitigating these risks is presented below.

First the components on the UM2+ that present to most concern for outgassing were identified, their material determined and the relevant vacuum properties were gathered. This information is shown in Table 5. Table 5 shows the printer part in question, its material, the vacuum properties of that material, whether the printer part is removable and if a replacement is possible. All outgassing data was retrieved from the NASA outgassing database [49].

Printer Part	Material	TML	CVCM	Removable	Replacement
Wiring Sheaths	Nylon	1.09-5.06	0.00	Yes	Kapton tape
Side Panels	Perspex (PMMA/Acrylic)	0.51-0.81	0.00-0.05	Some	Aluminum or other plastic
Top, bottom, front and back panels	Dibond (painted Al and LDPE sandwich)	0.52 (LDPE)	0.11 (LDPE)	No	Aluminum or other plastic
Bowden Tube	TFM (Teflon)	0.01	0	No	N/A
Printhead structure and sliders	ABS	0.37-1.13	0.00-0.16	Some	Aluminum or other plastic
Feed system gears	Nylon	1.09-5.06	0.00	No	Aluminum or other plastic
Build plate heater	Silicone	0.02-0.98	0.00-0.28	No	Space rated heater
PVC coated wire	PVC	15.49-21.46	9.10-10.03	No	FEP or other vacuum rated wiring

Table 5: Ultimaker 2+ parts, materials and outgassing evaluation

Most items on the printer are under or close to the ESA guidelines for outgassing even when using TML. The level of outgassing expected in the vacuum chamber during testing is expected to be significantly less than the values shown due to the relative pressure difference. The values of outgassing in Table 5 were obtained from an outgassing test similar to ECSS-Q-ST-70-02C during which the pressure is $1 \cdot 10^{-3}$ Pa [32]. The expected pressure during testing is 150 Pa resulting in a pressure difference of five orders of magnitude. Additionally the vacuum chamber will be at approximately room temperature during testing while the outgassing values are determined at a temperature of 125 °C, [32] further reducing outgassing of the printer compared to the nominal values. Because of these environmental differences it was assumed that printer parts with outgassing properties near the ESA recommendations would not pose any risk.

The nylon components and PVC coated wire are the two items which are well beyond the ESA guidelines. To mitigate this the nylon wire sheathes were removed and the gears can be replaced if they are judged to present an issue. The low mass of the gears means a correspondingly small amount of material will be released via outgassing. The PVC has high outgassing characteristics and it was thought that it might present an issue. Although PVC has high outgassing characteristics there is already PVC wiring in the vacuum chamber for a variety of experiments. The PhD students using the vacuum chamber were consulted and did not report any issues associated with outgassing from PVC coated wiring. This suggests that the relatively small amount of wire and extremely rough vacuum do not cause the wire to outgas at a problematic level. The use of small gauge wire, along with minimization of the total wire in the vacuum, means only a small mass of PVC was exposed to vacuum.

The print material itself was also of concern as it must be heated up to 260 °C during printing, increasing outgassing. PC was chosen to be the material used for testing in large part due to its extremely low outgassing properties. PC has a RML 33 times lower than ESA guidelines, shown in Table 6 below, and even if its outgassing characteristics increase many times over when heated it will still be well below the guideline.

Material	TML	CVCM	WVR	RML
Stratasys polycarbonate PC10 - Rapid prototype material	0.17	0.00	0.14	0.03
Stratasys polycarbonate PC10 -- Support material	0.10	0.00	0.07	0.03

Table 6: Outgassing data of two polycarbonate 3D printing filaments

Other potential contaminants include the lubrication on filament feed gears as well as the paint on the structure and servos. These are present on the printer with very small masses and will therefore outgas a correspondingly low amount. Outgassing evaluation for these materials is difficult due to the uncertainty of the exact lubricant or paint used and the lack of outgassing data available for these materials. It was decided that they did not pose an outgassing risk due to the extremely small mass and very rough vacuum. The bearings on the X, Y and Z axes do not have lubrication as the printer supplied by Ultimaker was previously modified with oil-less bearings.

During the meeting with Dr. Lafont the risk of outgassing to the vacuum chamber and vacuum pump was discussed and the ESA procedure for cleaning contamination from vacuum chambers was discussed. The procedure for cleaning the vacuum chambers at ESTEC consisted of two parts. The first part of the cleaning procedure is to thoroughly scrub the inside of the chamber with a cloth and a solvent, commonly isopropanol or acetone. Following the manual cleaning a vacuum is drawn in the chamber and any contaminants are baked out by heating the chamber to 80-100 °C. As the Heraeus VT 6130 M chamber is capable of heating to a temperature of 200 °C [38] this bake out procedure is possible with the available equipment. It is therefore possible to remove contaminants, if any are identified, from the walls of the vacuum chamber.

To quantify the level of outgassing a specialized collector plate could be put in the chamber during the bake out to collect any outgassing products. This plate could then be analyzed ex-situ using Fourier-transform infrared spectroscopy (FTIR) to identify the compositions and masses of outgassing products. Dr. Lafont also indicated that he would be willing to supply several collector plates and would assist in FTIR inspection if necessary. By using this method during the first few test prints, it will be possible to exactly quantify the outgassing risk of FFF in the vacuum chamber. This is discussed further in Section 5.3.2.

3.5.2 UFP Generation

The second contamination concern regarding 3D printing in the vacuum chamber was the generation of UFPs during the melting and extrusion of plastic during the FFF process. The FFF process generates significant amounts of UFPs regardless of the printer model or material used [55] at rates nearing $1 \cdot 10^{12}$ particles per minute [56]. The only information currently available for FFF with PC filament puts its UFP generation around $1 \cdot 10^{10}$ to $1 \cdot 10^{11}$ particles per minute [56]. These particles range in size from approximately 10 nm to 120 nm with no particles outside this size range being recorded [57]. There are a variety of concerns regarding the generation of UFPs in by the Ultimaker 2+ printer in the vacuum chamber, all of which will be addressed below.

3.5.2.1 UFPs Sticking to Chamber Walls

The first concern is that the UFPs generated will stick to the chamber walls and outgas when the chamber is pumped down in other experiments, possibly contaminating, damaging or interfering

with the experiments. Due to their extremely small size the UFPs generated will cool very quickly and solidify before striking the chamber walls. The relatively cool UFPs will have difficulty sticking to the room temperature walls, as PC does not stick to cool surfaces very readily. This is shown by the build plate temperature of 110 °C required for printing. The possibility of UFPs sticking to the chamber walls is therefore low.

The total mass of PC UFPs generated is estimated to be approximately 1×10^{-7} g/min if it is assumed that all particles produced are of the largest possible diameter, 120 nm. This means that for each hour of printing only 6×10^{-6} g of polycarbonate is released into the vacuum chamber. This extremely small mass of thermoplastic will not form any sort of noticeable buildup on the chamber walls even if all particles managed to stick to the walls. Even if a noticeable amount of PC UFPs became stuck to the walls of the vacuum chamber the outgassing would be negligible due to the extremely low outgassing properties of PC and the extremely small built up mass. Any buildup could also be easily cleaned off.

Although the mass of polycarbonate released in the form of UFPs is extremely small the potential of contamination was mitigated through good testing procedure. Before fabricating full size test components, the printer was placed in the vacuum chamber and printed a series of small components with gradually increasing print times. The print times began at roughly 10-15 minutes and ramped up in 10-15 minute increments until print times in the range of 1.5-2 hours, the print times for full sized components, are reached. Between each print run the vacuum chamber was vented and thoroughly inspected to ensure there is no buildup of polycarbonate. The inspection was conducted optically as well as by running a hand over the interior of the chamber to identify any buildup by feel. Only once the vacuum chamber had been inspected and found free of buildup at one print time was a longer print be permitted.

3.5.2.2 Damage to Vacuum Pump

The second concern involving the UFP generation was the possibility that the UFPs would be sucked into the vacuum pump and damage it. The manufacturer of the vacuum pump, vacuubrand, was contacted and asked whether particles in the 10 to 120 nm range would cause damage to the MD-1 diaphragm pump. The following was the response from vacuubrand, "As long as these small particulates are dry and do not polymerise inside the pump, they will blow out at exhaust of pump, you may take away the pumps exhaust silencer to allow particulates to blow out." The high processing temperature of the polycarbonate and vacuum environment in the chamber will cause all water vapour to be quickly outgassed from the plastic during processing. The polycarbonate particles are therefore very dry when aspirated into the pump. Polycarbonate itself is a very inert material and due to the lack of solvents or corrosive gases in the printing atmosphere the polycarbonate UFPs will not polymerize inside the vacuum pump. As stated above the mass of polycarbonate created by the FFF process is extremely small and would be unlikely to cause issues with the pump even if all the mass settled within the pump.

Although the UFPs generated by the printing process are expected to pass straight through the vacuum pump and not cause any damage the risk can be mitigated with good testing procedure. The pump will be isolated from the vacuum chamber during printing by means of the valve in the Heraeus VT 6130 M vacuum chamber. This means that the pump will not be running while the FFF process is generating UFPs. The chamber will be vented to ambient atmosphere after each print so there are not residual UFPs in the chamber when the pump is turned on for the next print. This prevents the chance of UFP ingestion by the vacuum pump.

Particulate filters cannot be used to protect the vacuum pump from UFP aspiration because there are no filters which can trap particles in the 10 to 120 nm size range. When contacted, Demaco NL offered a PolyPro Filter which can filter particles down to a size of 2 microns [58]. The minimum size of filterable particles was found to be 0.3 microns, three times the size of the largest particles generated during the 3D printing process [59].

3.5.2.3 Contamination of the Cleanroom

The potential for the UFPs generated by the FFF printing process to contaminate the cleanroom itself was also of concern. If large amounts of particulate are released into the cleanroom it is possible that the level of particulate could exceed limits set out by the ISO 14644-1 cleanroom standard. As the exhaust of the vacuum pump is open to the cleanroom all particles produced by the FFF process are vented to the cleanroom atmosphere. As noted above, studies of UFP generation by FFF printers show that the particles produced by these types of printers are exclusively in the 10 nm to 120 nm size range [57]. These studies showed no increase in particles outside this size range due to FFF printer operation [57]. This means the largest particles generated by the FFF process are 120 nm, or approximately 0.1 μm , in diameter. This places the UFPs generated by the FFF process in the smallest particle size that is measured when evaluating cleanrooms, as seen in Table 7.

CLASS	Number of Particles per Cubic Meter by Micrometer Size					
	0.1 micron	0.2 micron	0.3 micron	0.5 micron	1 micron	5 microns
ISO1	10	2				
ISO2	100	24	10	4		
ISO3	1,000	237	102	35	8	
ISO4	10,000	2,370	1,020	352	83	
ISO5	100,000	23,700	10,200	3,520	832	29
ISO6	1,000,000	237,000	102,000	35,200	8,320	293
ISO7				352,000	83,200	2,930
ISO8				3,520,000	832,000	29,300
ISO9				35,200,000	8,320,000	293,000

Table 7: ISO cleanroom particulate limits by particle size [60]

The cleanroom on the 8th floor of the Aerospace Engineering building is an ISO 8 standard cleanroom. The maximum number of particles allowed per cubic metre of air in a ISO 8 cleanroom can be seen in the second from bottom row of Table 7. For the ISO 8 class of cleanroom there is no limit given for the number of particles with the maximum diameter of 0.1 microns given. As there is no limit to the number of particles with a diameter of less than 0.1 micron (or 0.2 microns if there are slightly larger particles produced) the UFPs emitted by an FFF printer cannot compromise the cleanliness of the ISO 8 cleanroom.

Although an FFF printer cannot cause particles to exceed ISO limits in an ISO 8 cleanroom several steps can be taken to mitigate any potential effects of generated UFPs on the cleanroom environment. Several steps were taken to mitigate the risk of the UFPs on the cleanroom atmosphere. The exhaust stream of the vacuum pump was carefully considered to ensure it is pointing away from any sensitive equipment. Sensitive equipment was identified before any printing took place in the cleanroom. The exhaust stream was positioned to avoid the exhaust gas from being confined in a small volume, to avoid the potential buildup of very high levels of UFPs.

3.5.2.4 Health Concerns

The potential health implications of UFP inhalation were also of concern. Currently FFF printers are largely unregulated as evidenced by their wide distribution and use in residential settings however they must adhere to the relevant guidelines for air quality. Guidelines for air quality separate

pollution into types such as carbon monoxide, lead, nitrogen dioxide, ozone, PM2.5, PM10 and sulphur dioxide. The PM2.5 class of pollution is defined as “fine inhalable particles, with diameters that are generally 2.5 micrometers and smaller” [61]. As mentioned above the particulate generated by FFF printers is in the range of 10-120 nm (0.01-0.12 μm) putting it in the PM2.5 class of particulate pollution. The European limit for PM2.5 particle exposure is 25 $\mu\text{g}/\text{m}^3$ averaged over 1 year [62] while the American limit is 35 $\mu\text{g}/\text{m}^3$ averaged over 3 years [63]. To ensure a conservative measure is taken the stricter, European limit was used. The thesis advisor, Johan Versteegh from Ultimaker BV, was contacted to obtain values of PM2.5 concentration when printing with an Ultimaker 2+ with polycarbonate filament. Research conducted by Ultimaker BV showed that the Ultimaker 2+ printer with polycarbonate filament produced a concentration of 8660 particles/ cm^3 , which is approximately equal to around 21 $\mu\text{g}/\text{m}^3$, over the course of 3 days of printing. This means that the printer and filament combination used for the thesis is well within the European and American standards for PM2.5 particulate pollution.

Although the printer and filament combination is within the relevant limits of PM2.5 pollution further steps were taken to mitigate the effects of PM2.5 pollution. The printer was only used for a small number of hours throughout the day with gaps between each print run. This allowed time for the particles to disperse, preventing concentrations from reaching the 21 $\mu\text{g}/\text{m}^3$ level observed by Ultimaker, which was observed over a continuous 3-day print. The printer was not used overnight, creating a large block of time each day for particles to disperse. Suitable precautions were taken when opening the chamber door to prevent exposure to any high concentration of particles that may have accumulated.

3.6 Printer Modifications

This section discusses the modifications that were done to the UM2+ printer to allow it to function in the vacuum chamber. This includes removal of unnecessary components, reduction in polymer components to reduce outgassing and rewiring the printer to allow signals to pass in and out of the vacuum chamber.

3.6.1 Outgassing Reduction

Outgassing of the printer components and the filament was identified as a potential issue. To reduce the risk of outgassing contaminating the vacuum chamber a variety of modifications were made to the UM2+ printer to reduce the amount of outgassing when exposed to a vacuum environment.

3.6.1.1 Printer Structure Side Walls

The largest plastic parts on the UM2+ printer are the side walls which are constructed from Perspex, otherwise known as plexiglass, Polymethyl methacrylate (PMMA) or acrylic. While acrylic has reasonable outgassing properties the side walls have a large mass and would therefore outgas a large amount even with a TML of 0.51% [64]. As the side walls of the printer cannot be removed replacement options were investigated. Replacement was deemed to be too difficult as the bearings of the X and Y axes are seated in the side walls. Replacement of the side wall would therefore lead to uncertainty in the alignment of the printhead gantry which could impact the quality of printing. As replacement was unfeasible it was decided that the amount of plastic in the side walls would be reduced by cutting out the central parts of the side walls leaving the X and Y axis bearings and bolt holes undisturbed.

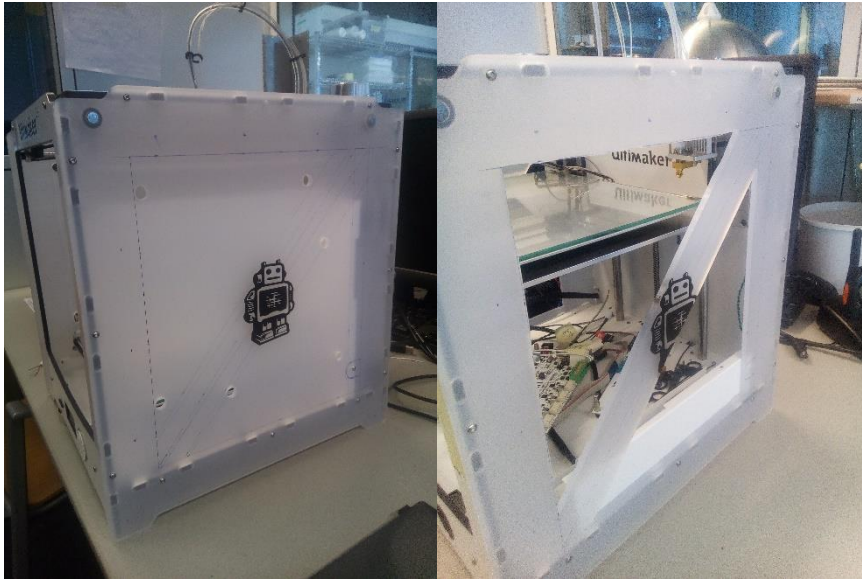


Figure 14: A side wall of the UM2+ printer before (left) and after (right) material removal

Figure 14 shows one of the side walls of the UM2+ printer before and after the removal of material. Both sidewalls had material removed in an identical pattern. Two large triangles were removed from each side wall leaving a reinforcing member running diagonally. This reinforcing member was left in place to ensure the rigidity of the printer to prevent the removal of material from affecting the accuracy of the printer. While the rigidity of the printer before and after the removal of material from the sidewalls was not calculated, the pattern cut from the sidewall preserves a wider perimeter of material compared to the front wall of the printer and has a reinforcing member. This means that the side walls are still more rigid than the front wall of the printer preserving the rigidity of the printer. Approximately 700g of acrylic (Perspex) was removed from each of the side walls.

Removing material from the sidewalls of the printer also serves to allow heat generated by the printhead and buildplate during printing to be transferred to the surroundings more readily. The removal of some of the sidewall material provides the hot surfaces of the printhead and buildplate with a direct radiative path to the relatively cool walls of the vacuum chamber, reducing heat buildup in the printer volume.

3.6.1.2 *Wiring Sheaths*

The wiring sheaths of the UM2+ printer are made of Nylon, which has relatively high outgassing characteristics as seen above in Table 3. As the printer needed to be rewired to be placed in the vacuum chamber anyways it was decided that the wiring sheaths could be completely removed. Without the wiring sheaths abrasion of the wires could become an issue. When the printer was rewired, care was taken when routing the wires to prevent abrasion or interference with moving parts. The wires were routed to avoid contact with hot surfaces or moving parts. Where possible wires were secured to the printer structure or vacuum chamber walls with Kapton tape to ensure they did not shift during printing.

3.6.1.3 *Excess Filament, Filament Spool and Filament Spool Holder*

The filament spool holder and filament spool can be seen in Figure 15. These components are designed to keep the supply of filament organized and out of the way during the printing process and to allow the filament to easily unspool into the filament feed system during printing. The filament spool and spool holder are composed of ABS plastic with outgassing properties described in Table 3. Although the vacuum properties of ABS are reasonable the filament spool holder and

filament spool are relatively large masses of plastic that are not critical to the printing process and therefore do not need to be in the vacuum chamber during printing. As the filament spool and spool holder are unnecessary components they were removed from the experimental setup and were not exposed to the vacuum environment.



Figure 15: The filament spool holder (left) and the filament spool (right)

As the filament spool and spool holder were removed from the experimental setup the organization and feed system of the filament must be modified. There is 750 g of filament on the spool of Ultimaker PC filament used in testing. Using a normal printing process this entire mass of filament would be exposed to the vacuum environment causing unnecessary outgassing. As each print run only utilizes a small amount of filament having the entire spool of filament incorporated in the experimental setup is unnecessary. It was therefore decided that only the amount of filament needed for a print run would be loaded into the filament feed system for that print run. This serves a dual purpose of reducing the amount of plastic exposed to the vacuum environment, and therefore reducing outgassing, and eliminating the need for the filament spool and spool holder because there is not a large mass of filament that needs to be organized and kept out of the way.

3.6.1.4 Lubricants

Many components of the UM2+ printer are lubricated, including the filament feed system gears, the bearings in the servos and the bearings on the gantry rods. Ultimaker was contacted regarding the compositions of these lubricants however they did not know the exact compositions. Although the compositions of the lubricants are unknown it is safe to assume that they are not rated for vacuum environments as the UM2+ is a consumer printer that would have been optimized for cost, not vacuum performance, in the design process. These lubricants are therefore likely to outgas and should be removed if possible.



Figure 16: A servo motor (left) and a filament feed gear (right) showing green/grey lubricant

The lubricant on the filament feed system gears and in the bearings, see Figure 16, is used primarily to reduce friction and extend the lifetime of the relevant component. As the printer is only going to be used for a limited amount of time and number of print runs the longevity is not considered to be an issue. The lubricant in the filament feed system gears and bearings was therefore cleaned off to reduce outgassing. Any implementation of FFF on-orbit would use a custom-made printer that would be designed to function without lubricant or would use vacuum rated lubricants.

3.6.2 Removal of Printhead Fans

The printhead of the UM2+ incorporates three fans, one for helping to regulate the nozzle temperature and two for cooling the extruded material. These fans are seen below in Figure 17 along with their associated wiring and structure which secured the fans to the printhead. As these fans are not functional in a vacuum environment it was decided that they would be removed. This was done to reduce the outgassing, simplify the wiring and to prevent any unintended cooling by the fans during testing. In a real implementation of FFF on-orbit it would be exposed to a UHV environment. In this environment fans would not provide any cooling due to the extreme low pressure. The vacuum during testing is 1000 Pa, a much higher pressure than the UHV environment on-orbit. Because of this much higher pressure it is possible that the fans could provide some forced convective cooling to the printhead or component under fabrication during testing. To eliminate this variable the fans and associated wiring and structure were completely removed and were not used for printing in atmosphere or in vacuum.

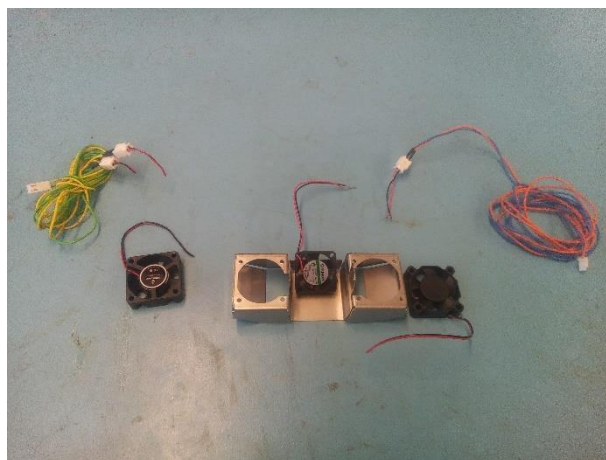


Figure 17: The regulating fan (centre) and cooling fans (left and right) of the UM2+, removed from the printhead

Removal of the fans from the printhead meant that they could not be used for printing in normal atmospheric conditions, where they would provide convective cooling. This may cause prints in

normal atmospheric conditions which would normally utilize the cooling of the fans to be fabricated sub-optimally. Johan Versteegh was contacted, and he indicated that it was possible to print without the fans. To confirm this several test components were printed without the cooling fans and were found to have acceptable dimensions and quality.

3.6.3 Wiring

The UM2+ printer needed to be rewired to function in the vacuum chamber as the printer power supply needed to be located outside the vacuum chamber to plug into the power mains. Power would then be passed from the power supply to the printer through the wall of the printer. The vacuum chamber has a series of four Dsub nine pin connectors that can be used for passing electrical signals into and out of the vacuum chamber. These connectors can be seen in Figure 18.



Figure 18: The four Dsub connectors inside the vacuum chamber

The UM2+ uses a GST220A24-R7B power supply from Mean Well Electronics seen in **Error! Reference source not found.** The power supply needed to be located outside the vacuum chamber for a variety of reasons. The first, as mentioned above, is because there is no outlet for the power supply to plug into in the vacuum chamber. The power supply is also a very large mass of plastic which would cause large amount of outgassing if exposed to the vacuum environment. Also, it was worried that the power supply would overheat without convective cooling, potentially damaging the power supply and causing safety hazards.

Because of this the power cable was cut between the power supply and the connector which plugs into the printer. The outer casing was removed to reduce outgassing and the appropriate Dsub connectors were soldered onto the wires. The new power supply configuration can be seen in Figure 19. On the left is the wiring to be placed in the interior of the vacuum chamber with female Dsub connectors and the connector for connecting to the printer. On the right is the wiring that is external to the vacuum chamber, connecting male Dsub connectors to the power supply.



Figure 19: the Dsub connectors on the rewired power supply

Although this wiring layout would allow the printer to function inside the vacuum chamber it left the circuit boards (PCBs) inside the chamber, exposed to the vacuum environment. This caused worries of the PCBs overheating and failing. It also, crucially, left the control interface of the printer inside the vacuum chamber. This meant that the print settings could not be controlled after the vacuum chamber door had been closed. This was particularly problematic because a vacuum could not begin to be drawn in the chamber until after the door closed. As the print run would have to be started before the vacuum was drawn this raised the risk of the printer beginning to print before a vacuum was fully drawn. This could render the results of testing invalid as the vacuum testing needed to be performed in a vacuum.

To prevent this issue, it was decided to move both PCBs, the main board and the display board, outside of the vacuum chamber. These PCBs are shown in Figure 20. The previous wiring which placed the power supply outside the vacuum chamber, seen in Figure 19, was discarded. New wiring therefore needed to be made.

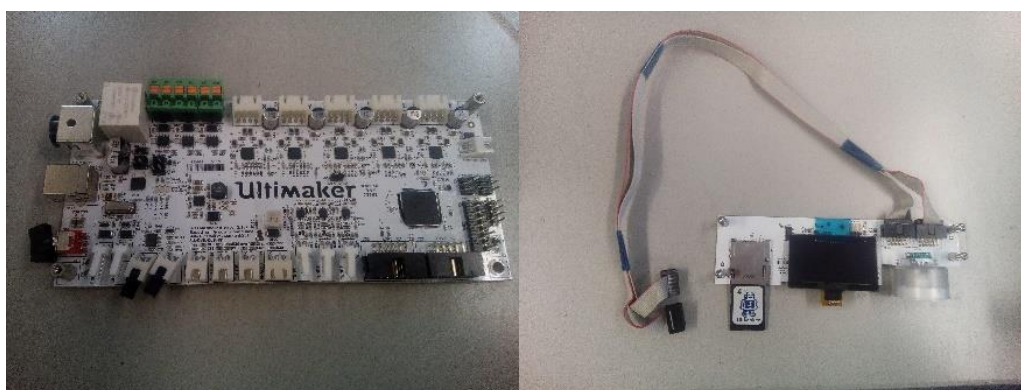


Figure 20: The main board (left) and display board (right) of the UM2+ printer

In this wiring layout the wires between the main PCB and the actuators and sensors of the printer would be cut and Dsub connectors would be soldered in where appropriate. It was found that 34 connections needed to be passed through the wall of the vacuum chamber to connect the printer inside to the PCBs outside. This was within the 36 possible connections afforded by the four, nine pin Dsub connectors available on the vacuum chamber. Once this was determined the pinout of the

wires on the four Dsub connectors was decided. This was done to minimize the lengths of wire inside the vacuum chamber to reduce outgassing. For example, the printhead heater wires emerged from the top of the printer and were therefore assigned to the topmost Dsub connector inside the vacuum chamber. The connectors were assigned a numerical value from one to four, with one being the lowest connector in the vacuum chamber and four being the topmost. Each connector was also assigned a colour to aid in identifying which connector held which wires. The complete pinout of the new wiring layout can be found in Appendix C – Connector Pinouts.

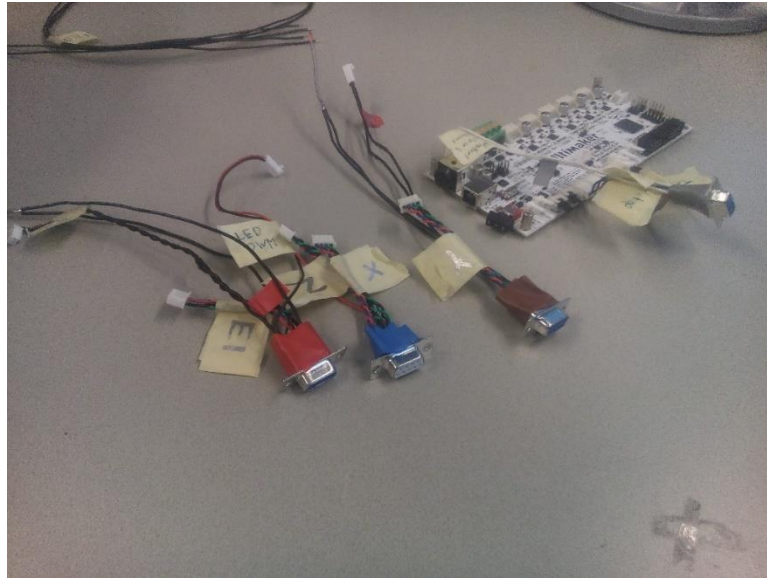


Figure 21: Four Dsub connectors for connecting the PCBs to the exterior of the vacuum chamber

Following the assignment of each wire to a pin on a connector the wires from the PCB to the printer were cut. Female Dsub connectors were soldering on the wires leading to the PCBs. These four exterior connectors can be seen above in Figure 21 along with their colour codes. The wires from the printer to the interior wall of the vacuum chamber were then soldered to the appropriate male Dsub connectors. These connectors can be seen below in Figure 22. After the soldering on each connector was completed it was checked using a multimeter to ensure all connections had been made properly and no unexpected short or open circuits existed.

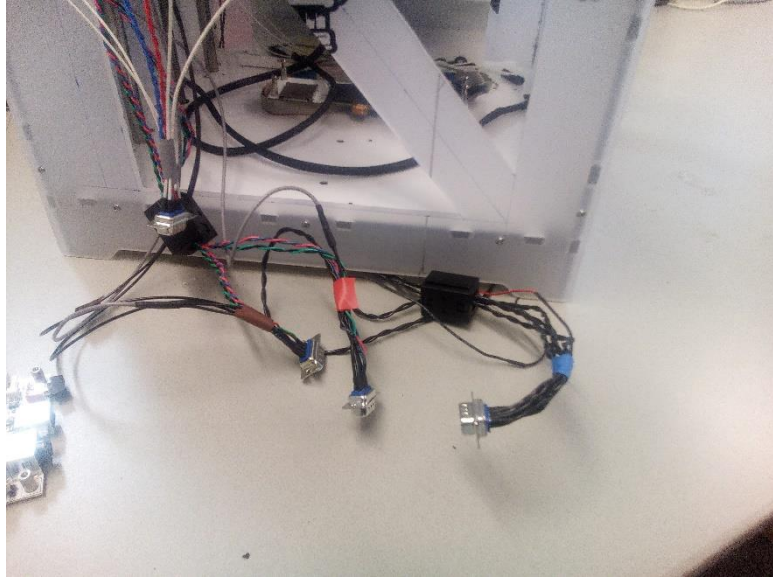


Figure 22: Four Dsub connectors for connecting the printer to the interior of the vacuum chamber

4 Experimental Setup Validation and Testing

This chapter shows the steps that were taken to validate the experimental setup. The problems that are expected to occur during printing in the vacuum environment are also discussed. The chapter begins with testing of the buildplate and printhead heaters to ensure they function correctly. The new wiring that was discussed in Chapter 3 is then tested to ensure all printer sub-systems function correctly and there are no safety hazards associated with the wiring. A short analysis of expected issues associated with performing the FFF process in a vacuum environment is then presented.

4.1 Printhead Heating and Cooling

The first thing that was checked was the ability of the printhead to heat up, maintain a constant temperature and cool down without the aid of the fan. To determine the effect of the fan on the printhead heating and cooling the temperature of the printhead was recorded while heating up and cooling down before and after the fan was removed. The behaviour of the printhead as it was holding the PC printing temperature of 260 °C was also recorded to determine how well it can hold temperature with and without the fan. 260 °C was chosen because it is the processing temperature for PC and it is the maximum temperature of the UM2+ printhead.

Figure 23 shows the temperature of the printhead as it heated up in atmosphere from roughly room temperature to 260 °C with and without the fan. The temperature was recorded by reading the temperature directly off the UM2+ display. It can be seen in Figure 23 that the printhead took approximately the same amount of time, roughly one minute and ten seconds, with and without the fan. The slight offset in Figure 23 between the fan and no-fan curve is likely due to a delay when starting the timer when recording the temperature. This shows that the printhead heats up at the same rate with and without the fan.

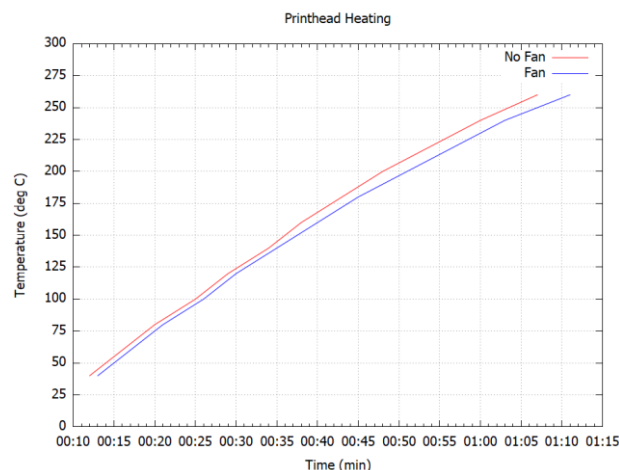


Figure 23: The heating curve of the printhead, with and without fan

Figure 24 shows the temperature of the printhead as it cooled down from 260 °C to room temperature, roughly 25 °C, with and without the fan. The temperature was recorded by reading the temperature directly off the UM2+ display as the printhead cooled. It can be seen in Figure 24 that the printhead took approximately six minutes to cool down with the fan and approximately twenty-two minutes without the fan. While this is significantly longer the printhead can cool effectively without the fan. The printer can therefore be operated without a fan however extra care must be taken to make sure nothing contacts the printhead for at least twenty minutes after printing finished.

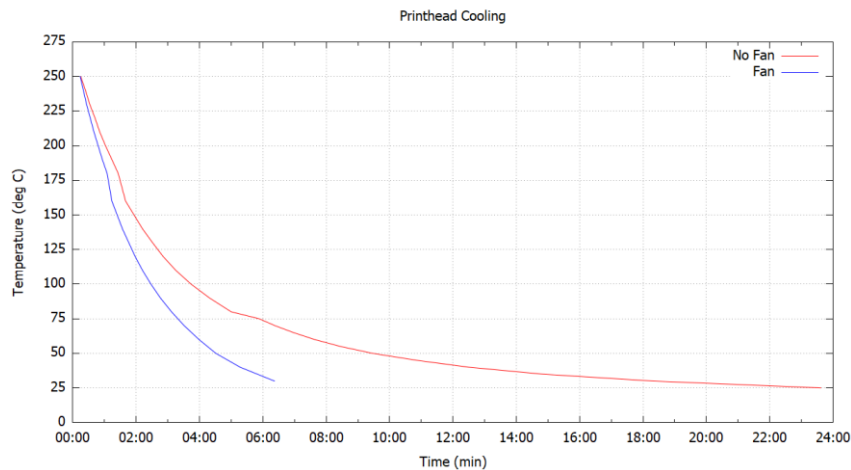


Figure 24: The cooling curve of the printhead, with and without fan

Table 8 below shows the performance of the printhead as it held a temperature of 260 °C with and without the fan. The maximum temperature reached by the printhead is very similar with and without the fan, only differing by a degree. This shows that the printhead will not overheat without the fan. The time between the start of heating and reaching the maximum recorded temperature is also very similar. The slightly faster heating of the printhead without the fan is similar to the slightly faster heating observed at higher temperatures in Figure 23. The time taken for the printhead to return to 260 °C from the maximum temperature is also very similar with and without the fan, only differing by one second. This clearly shows that the printhead can regulate its temperature without the fan. Finally, the minimum temperature is shown. Again, these values are very similar with and without the fan. After this minimum temperature was achieved the printhead temperature oscillated slightly, reaching lower maximum and higher minimum temperatures each time. The printhead eventually stabilized at 260 °C. Table 8 clearly shows that the UM2+ can regulate the printhead temperature without the fan. This means that printing can be carried out correctly without the fan and that the temperature of the printhead will not be a contributing factor to poor quality prints.

	Fan	No Fan
Maximum Temp (°C)	266	267
Time to max temp (s)	87.2	82.0
Time from maximum temperature back to 260 °C (s)	11.7	12.7
Minimum temperature (°C)	258	257

Table 8: The temperature holding of the UM2+ printhead at 260 °C

4.2 Buildplate Heating and Cooling

The next thing that was checked was the ability of the buildplate to heat up, maintain a constant temperature and cool down. This was done to establish a baseline for the temperature performance of the buildplate. The behaviour of the buildplate as it was holding the PC printing temperature of 110 °C was also observed to determine how well it can hold temperature. 110 °C was chosen because it is the processing temperature for PC and it is the maximum temperature of the UM2+ buildplate.

Figure 25 shows the temperature of the buildplate as it heated up from roughly room temperature to 110 °C. The temperature was recorded by reading the temperature directly off the UM2+ display.

It can be seen in Figure 25 that the printhead took approximately eighteen minutes to reach 110 °C. The buildplate took approximately twelve minutes to reach 100 °C.

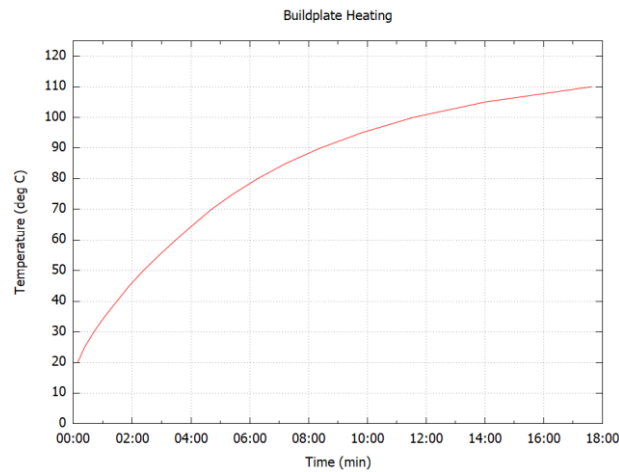


Figure 25: The heating curve of the buildplate

Figure 26 shows the temperature of the buildplate as it cooled down from 110 °C to room temperature, roughly 25 °C. The temperature was recorded by reading the temperature directly off the UM2+ display as the printhead cooled. The buildplate took approximately twenty-one minutes to cool down.

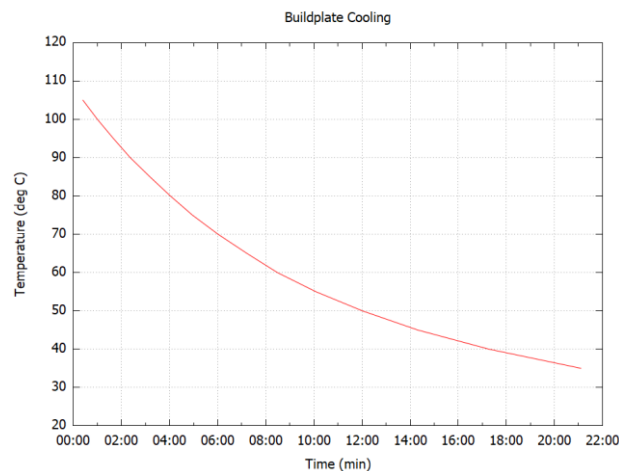


Figure 26: The cooling curve of the buildplate

Because the buildplate took so long to heat up and the heating was slow low as the temperature approached 110 °C, the temperature of the buildplate did not fluctuate once it reached 110 °C. This observation, along with the data presented in Figure 25 and Figure 26 gives a baseline for the buildplate performance.

4.3 Validation of New Wiring

To validate the new wiring of the UM2+, all the actuators and sensors of the printer needed to be tested. First the printer was powered on and checked for any issues in its standby state. Each sensor or actuator was then tested individually at first to isolate any issue. This testing was done by sending commands to the printer from pronterface, a piece of software that gives direct control over individual components of the printer. The commands from pronterface were sent to the printer via a USB connection. Following individual testing the sensors and actuators were then used in

combination to print test components. Each sensor and actuator tested is listed below along with a brief explanation of the test and any problems identified.

- Power on
 - When the printer was first powered on the functionality of the display, selector wheel and SD card reader were checked. The display functioned normally displaying all menus and responding appropriately to inputs from the selector wheel. The selector wheel functioned normally as well, scrolling between menu options and selecting options correctly. The SD card reader did not function normally. When the print option was selected on the display, which begins reading of the SD card, the display showed the message “Reading card...” and stayed on that screen indefinitely, necessitating a power cycle. When connected to pronterface it gave a message saying “echo:SD init fail” indicating that the SD card reader was not initializing. This was found to be an issue with the main PCB. The PCB was replaced with a new one supplied by Ultimaker after which there were no problems with the SD card reader.
- LEDs
 - After powering on the printer, the LED strips were visually checked to ensure they turned on. The LEDs turned on as normal.
- X, Y and Z Steppers:
 - The X, Y and Z steppers were tested by sending movement commands in both directions of varying distances. The movement of the printhead, for the X and Y axes, and the buildplate, for the Z axis, were measured with a measuring tape. All three axes responded to the commands from pronterface and moved the appropriate distance.
- Filament Feed Stepper
 - The filament feed stepper was tested by commanding it to forward a certain length of filament via pronterface. A mark was made in the filament before the command and another mark was made after. The distance between the marks was then measured and compared against the length of material that was forwarded. The filament feed stepper was commanded to forward 20 mm of filament and a length of 18.9 mm was measured as having been forwarded. Johan from Ultimaker was consulted and the difference between these values was found to be normal.
- X, Y and Z Stops
 - The X, Y and Z stops were tested individually by sending successive home commands to each axis from pronterface. The home command commands the printhead, for the X and Y axes, and the buildplate, for the Z axis, to move to its home position. The home position for the printhead in the X axis is at the leftmost position and for the Y axis to at the furthest back position in the print volume. The home position for the buildplate is the lowest position. The axis finds its home position by moving towards it and activates the stop switch when it reaches the home position. Accurate homing therefore indicates proper functionality of the X, Y and Z stops. All three axes responded to the commands from pronterface and homed correctly.
- Combined Homing
 - To further test the X, Y and Z switches they were commanded to move to their home positions simultaneously via pronterface. All axes responded correctly.
- Printhead heater
 - To test the printhead heater it was given commands via pronterface to heat up to, and hold, a specified temperature. The printhead was given commands to heat from

40 °C up to 260 °C in 20 °C increments. At each temperature increment it was checked via pronterface that the temperature had been reached and was stable. The wiring was also checked at each temperature to ensure there was no overheating or degradation of the wire. The printhead heater heated up to, and held, each temperature correctly and no damage of the wiring was observed.

- Buildplate heater
 - To test the buildplate heater it was given commands via pronterface to heat up to, and hold, a specified temperature. The printhead was given commands to heat from 30 °C up to 110 °C in 10 °C increments. At each temperature increment it was checked via pronterface that the temperature had been reached and was stable. The wiring was also checked at each temperature to ensure there was no overheating or degradation of the wire. The buildplate heater heated up to, and held, each temperature correctly and no damage of the wiring was observed.
- Combined heating
 - To further test the heaters and provide a worst-case scenario to the wiring the heaters were tested to ensure they can heat up simultaneously. To test this the heaters were commanded to heat up to and hold a temperature simultaneously via pronterface, 260 °C for the printhead and 110 °C for the buildplate. As the two heaters were commanded to heat directly to their maximum temperature simultaneously this put the maximum amount of current through the new wiring. The maximum current condition is the condition most likely to cause overheating or damage to the wiring. The wires showed no signs of damage and the printhead and buildplate heated normally.
- Printing
 - As a final validation of the experimental setup several test components were fabricated in atmosphere. These components were only used to validate the functionality of the experimental printer after modification and no conclusions were drawn from them. They were given the designation “T” (for test) and are listed in “Component Database” Excel sheet which is available upon request. Over the course of fabricating these test components the main PCB of the printer needed to be replaced several times for a variety of reasons. These reasons included accidental short circuiting, incorrect wiring of the vacuum chamber and incorrect PCB software. These issues were troubleshooted during fabrication of the T components. The troubleshooting process is not discussed in detail as none of the problems were caused by the experimental environment. The same PCB was used to print all components for evaluation of printer performance and mechanical testing.

4.4 Estimation of Decreased Cooling in Vacuum

To determine the effects of the vacuum environment on the cooling of fabricated components an estimate of the cooling rates with and without convection was created in MATLAB. This estimate assumed there was no convection at all when printing in the vacuum environment. This is not perfectly accurate as there will be a small amount of air present in the chamber due to the rough vacuum. The estimate also assumed that the temperature of the air in the vacuum chamber remained at room temperature and that all radiation from the fabricated component was radiated directly to the wall of the vacuum chamber which were also assumed to be at room temperature. Figure 27 shows the heat transfer rate, with and without convective cooling, in W/m^2 from a component at temperatures ranging from room temperature to 290 °C. The convective heat transfer takes up an increasingly large percentage of the total heat transfer as temperature increases.

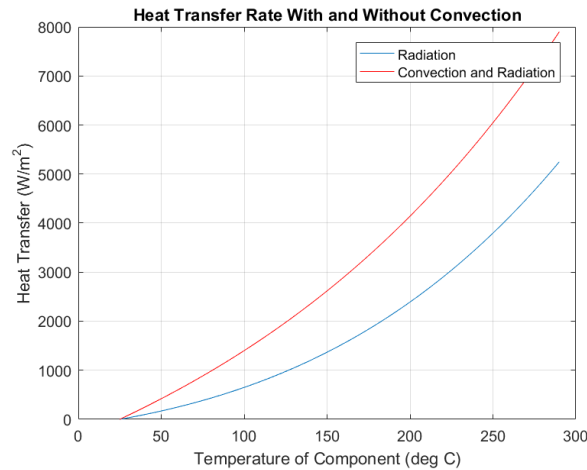


Figure 27: Cooling rate of a component with and without convective heat transfer

Figure 28 shows the convective heat transfer of a component across the same temperatures as above. Using the data in Figure 27 and Figure 28, along with the surface area and mass of the component and the cooling curve of the buildplate the cooling rate of the component can be estimated both in atmosphere and in vacuum. This information can be used to investigate differences in the dimensional accuracy, quality or material properties between components printed in atmosphere and vacuum. It can also be used to help estimate the cycle time of a print run allowing for better scheduling of test component fabrication.

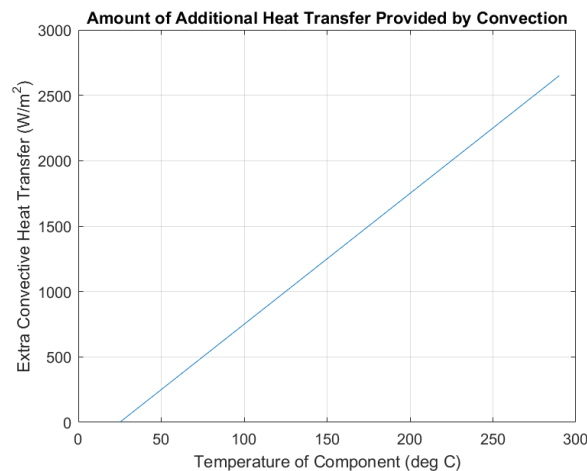


Figure 28: Convective heat transfer of a component

4.5 Analysis of Expected Problems Related to FFF in Vacuum

This section presents a short analysis of the expected problems associated with the FFF process in a vacuum environment. The expected issues are presented, and a preliminary analysis is performed. As this analysis was done prior to testing in a vacuum environment it is possible these issues will not manifest during testing and it is likely unforeseen issues will occur.

4.5.1 Reduced Cooling of Printed Component

When exposed to a vacuum environment the hot printed component will cool more slowly than in an atmosphere due to the lack of convective cooling. This slower cooling may present many challenges to the FFF process in vacuum. A layer which cools more slowly will remain above the glass transition temperature of the polymer for a longer period of time and will therefore be malleable for

a longer period of time. This lengthened period of malleability will cause decreased quality of overhangs and bridges as these features will be more likely to slump given a less rigid layer of polymer. This longer period of malleability can also cause printing to occur on still soft layers. If the preceding layer of polymer is not rigid when the following layer is printed on top of it the preceding layer may be dragged around by the movement of the nozzle. This could cause severe dimensional distortions. It is therefore very useful to determine how much more slowly a thread of extruded polymer cools in a vacuum in comparison to in an atmosphere.

To address this a model was created in MATLAB to simulate the cooling of a small segment of extruded polymer. This script can be found in Appendix E – MATLAB Script for FFF Thread Cooling. It was assumed that the thread of polymer is extruded as a rectangular prism with a constant rectangular cross-section with a width equal to the diameter of the nozzle and a height equal to the layer height. In the model used these were 0.4 mm and 0.2 mm respectively, the most common setting used during test prints. This constant cross-section thread was assumed to be extruded with an initial temperature equal to the processing temperature, 260 °C for polycarbonate, onto a previous layer of polymer at the same temperature.

To evaluate the cooling rate a small segment with a length equal to the width of the thread, 0.4 mm in this case, of the extruded thread was considered. This segment has a certain initial mass, heat capacity and temperature. This segment has six surfaces which can be sorted into three different groups. The top surface is exposed to the ambient environment and has the hot nozzle positioned directly above it. The side surfaces are exposed to the ambient environment but do not have a line of sight to the hot nozzle. Finally, the end and bottom surfaces are touching the surrounding polymer. It was assumed that the polymer surrounding the segment was at the same temperature, 260 °C. While this is not strictly speaking true, the segment is so small that if the printhead moves at a reasonable speed then the segment and its surrounding polymer will have been extruded at almost the same time and therefore have the same temperature.

The segment could cool itself by rejecting heat from each of its six sides. In an atmosphere the top surface could radiate heat to the room temperature surroundings and to the nozzle, the side surfaces could radiate heat away to the room temperature surroundings only and the bottom and end surfaces could not radiate any heat. In atmosphere the top and side surfaces could also cool using natural convection across their surface area. While there would be conduction between the bottom and end surfaces and the surrounding polymer it was assumed that they were the same temperature resulting in a ΔT of zero and no conductive heat transfer. In a vacuum the same conditions were assumed with the exception that there was no convection from the top or side surfaces of the segment.

The heat transfer regime above was combined with the specific heat capacity equation and the properties of polycarbonate to determine the temperature of the segment over time. The temperature started at 260 °C and decreased as the segment cooled and can be seen below in Figure 29. The segment exposed to atmosphere, with convective heat transfer, cools much more quickly than the segment in a vacuum environment. This can be used to estimate how rigid an extruded thread will be after a certain amount of time and help prevent the issues relating to the longer period of malleability of the polymer in the vacuum environment.

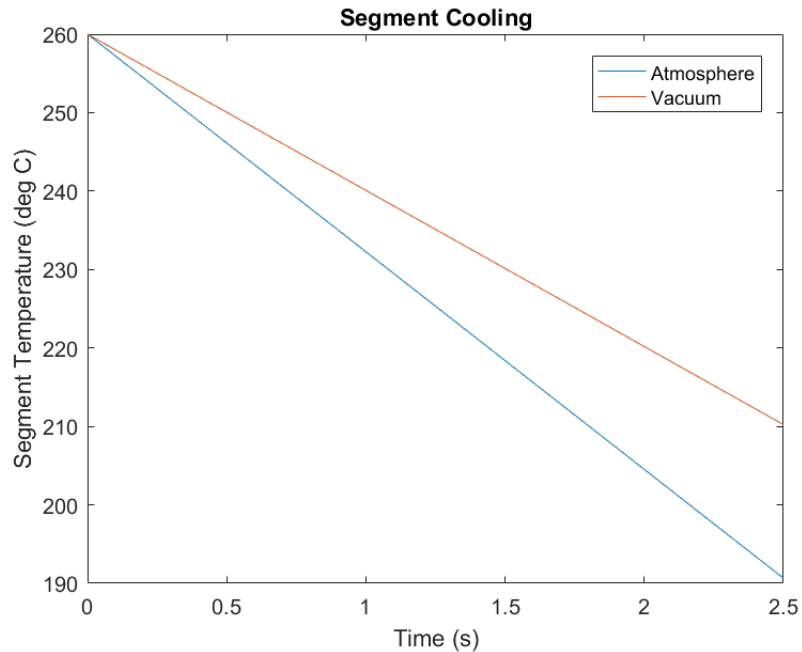


Figure 29: Cooling of a segment of an extruded polymer thread

4.5.2 Heater Temperature Control

The elimination of convective cooling in a vacuum environment leads to potential problems with the temperature control of the heated parts of the 3D printer, the printhead and the buildplate. The different thermal environment could cause temperature control issues in two main ways; overshooting the set temperature when heating up and less accurate temperature control at the set temperature.

Ultimaker was consulted and it was found that both the printhead and the buildplate temperatures are controlled by a PID controller. The behaviour of the temperature control can therefore be altered by changing the proportional (P), integral (I) and derivative (D) constants. These constants will likely need to be altered for both the printhead and the buildplate. These constants can easily be determined by using the M303 command [65]. This can be sent to the printer to the printer from a computer running pronterface via USB. The PID constants can also be changed manually via the M301 or M304 commands for the printhead and buildplate respectively [65].

The main issue with the temperature control is the potential for the temperature to overshoot and trip the maximum temperature cut-off. This is because the processing temperatures for polycarbonate are at the maximum value the UM2+ is rated to, 260 °C and 110 °C for the printhead and buildplate respectively [40]. The printhead had a maximum temperature cut-off of 275 °C. If the printhead temperature exceeds this temperature the printer will shut off and needs to be reset, disrupting the printing process. This makes the most important parameter the temperature overshoot as the printhead temperature must stay below 275 °C. This means that the P constant will likely have to be reduced and the D constant must be increased [66]. These values will likely be generated automatically but can be adjusted manually if needed. The only requirement for the new PID coefficients is that the maximum temperature stays below the cut-off point. The buildplate cut-off temperature is unknown but will be treated the same way as the printhead.

The other problem that must be addressed with new PID constants in the vacuum environment is the temperature stability at the set temperature. It is possible that the vacuum environment and new PID constants may cause oscillations around the set temperature. These fluctuations in temperature

could cause irregularities in the printed component. As the PID coefficients will be generated automatically it is assumed that the temperature holding at the set point will be sufficiently accurate. If large oscillations are noted with the new PID coefficients they can be adjusted by hand using the suggestions in Table 1 of [66].

4.5.3 Servo Motor Overheating

The temperature of the servo motors used to actuate the X, Y and Z axes as well as the filament feed system was also of concern. Due to the reduced cooling in the vacuum environment it is possible the servo motors may overheat while performing operations in the vacuum environment that are normal in an atmosphere. An estimate of the expected temperature of the servo motors during operation in the vacuum environment was therefore required to determine the risk of overheating.

To determine the estimated temperature of the servo motors during operation in the vacuum environment a steady state thermal model was created in MATLAB and combined with temperature data of the servos operating in atmosphere. The servo motors used on the UM2+ are NEMA 17 standard motors with external dimensions of 42.3 x 42.3 x 38 mm [67]. The specific servos used are manufactured by Pololu and have the serial number SY42STH38-1684A. The MATLAB model assumed that each servo could be modeled as a metal cube with these dimensions with an internal heat generation. This cube was assumed to expel heat by natural convection and radiation in the atmospheric case and only by radiation in the vacuum case. Convective heat transfer was assumed to act equally on all six sides of the cube. The emissivity of the cube was assumed to be 0.875. Radiative heat transfer was assumed to act equally on all six sides of the cube and the radiation was assumed to be toward a surface that is held at a constant temperature of 25 °C.

To estimate the temperature of the servo motor in vacuum the internal heat generation of the servo motor needed to be determined. To determine the internal heat generation the maximum temperature of one of the servos while printing in atmosphere was needed. This temperature was recorded while the printer was printing a component in atmosphere by means of a type K (Nickel-Chromium/Nickel Alumel) thermocouple taped to the exterior of the servo. This thermocouple was monitored using an NI 9211 DAQ and LabView software. The maximum temperature of any of the servos while printing in atmosphere was found to be approximately 46 °C. This value was then inserted into a heat balance with both radiative and convective heat transfer in the MATLAB script seen in Appendix D – MATLAB Script for Servo Cooling. As the only heat input of the servo is the internal heat generation the internal heat generation is equal to the sum of the heat leaving the servo. The internal heat generation was found to be $2.29 \cdot 10^{-6}$ W with a low convective heat transfer coefficient of 5 W/m²K and $8.61 \cdot 10^{-6}$ W with a high convective heat transfer coefficient of 35 W/m²K.

To calculate the temperature of the servo in vacuum it was assumed that the internal heat generation of the servo remains constant regardless of the environment. It was also assumed that there is no convective heat transfer away from the servo. The low and high values of the internal heat generation were then inserted into the heat balance for the servo in vacuum. These were then evaluated using MATLAB to solve for the temperature of the servo in vacuum. The expected temperature of the servo in the vacuum environment was found to range from approximately 61.3 °C to 125.6 °C with the low and high values of internal heat generation respectively.

The specification sheet for the SY42STH38-1684A servo motor gives a maximum temperature rise of 80 °C [67]. With an 80 °C temperature rise over room temperature, (25 °C) this gives a maximum temperature 105 °C. To confirm this value, Johan Versteegh from Ultimaker was consulted to see if testing had been carried out by Ultimaker to determine the maximum temperature of the servo

motors. Johan Versteegh said that the SY42STH38-1684A motor functioned normally with a core temperature of up to 100 °C but not for hours on end. There is potential for overheating of the servo in vacuum as the estimated values of servo temperature in vacuum, 61.3 °C to 125.6 °C, can be above the maximum operating temperature of 100 °C. This depends heavily on the value of the coefficient of convective heat transfer of the servo when it atmosphere. As it is possible that the temperature of the servos may rise above the maximum temperature when printing in vacuum the temperature should be closely monitored to establish the actual temperature in vacuum, evaluate the accuracy of the model used and prevent damage to the printer.

4.5.4 Outgassing of Component While Printing

Outgassing of the component as it is being printed in vacuum is also potentially of concern.

Outgassing of printed material could create bubbling of the surface of the component. When the polymer filament is exposed to a normal atmospheric environment, atmospheric gases, including oxygen, nitrogen and water vapour, dissolve and diffuse into the polymer. When exposed to a vacuum environment these absorbed gases are desorbed from the polymer and outgas into the vacuum. [22] It is possible that the absorbed gases in the polymer filament will damage the surface of the component as they outgas.

To investigate problems associated with outgassing the areas where it is most likely to happen need to be identified. This is important as the absorbed gas will take the path of least resistance when outgassing. As the rate of outgassing increases with both increasing temperature and decreasing pressure it is assumed that the plastic will outgas most heavily when it is hottest. This means that outgassing will likely occur immediately after it is extruded and bubbling, if present, will be observed on the thread of polymer between the nozzle and the component and on the top surface of the component. It is also expected that if tests are carried out in a variety of pressures the ones at the lowest pressure will show the most deformation due to outgassing.

It is expected that the absorbed gas in the polymer will expand and pressurize when it is heated during the extrusion process in accordance with the ideal gas law. These small bubbles of pressurized gas could then breach the surface of the component when a high enough pressure is reached. The pressurized gas could also breach the surface at lower pressures in areas where the component is weak, such as between layers or at the topmost surface where the polymer is still molten or semi-molten. The main risk of this outgassing is a decrease in surface quality in areas where outgassing occurs. As the volumes of gas are very small and they are likely distributed evenly in the component and across the surface it is expected that this decrease in surface quality will manifest as an increased surface roughness or pitting. If larger bubbles breach the surface they could cause small holes in the surface. If large bubbles form on the topmost surface while printing it could cause issues due to parts of the surface being raised above the expected height. This could cause the still molten layer to catch on the print head and be dragged around. This could distort the component being printed. It is expected that outgassing issues could be prevented by treating the filament appropriately before printing. This could include purging all absorbed gases from the filament by baking it out and by storing it in a very dry environment.

5 Performance of FFF in Vacuum

After the experimental apparatus was sourced and modified it needed to be evaluated for performance to determine if it could carry out the FFF process in a vacuum environment. In this chapter the performance of the printer in the vacuum environment was evaluated. The test apparatus was placed in the vacuum chamber, exposed to a vacuum environment and evaluated on several parameters. The components that were printed to evaluate the printer performance were labeled with the PP, for “Printer Performance” designation. The outgassing effects of the printer and the FFF process on the experimental environment were also investigated.

5.1 Printer Functionality

The first item that needed to be established was the proper functionality of the printer. The most important printer subsystems which were evaluated were the heaters, both buildplate and printhead, and the positioning and filament feed servos. These subsystems were evaluated in the vacuum environment of 1000 Pa.

5.1.1 Heater Performance

The first printer subsystems that was evaluated in a vacuum environment were the heaters for the printhead and the buildplate. Proper functionality of these heaters is key to the printing process to ensure the filament is heated to the proper temperature for extrusion, to promote adhesion of the component to the buildplate and to regulate cooling of the component. As noted above in Section 4.5.2 the PID control of the printer heaters was identified as a potential issue.

5.1.1.1 Printhead Heater Performance

To assess the performance of the printhead heater in a vacuum environment polycarbonate filament was loaded into the printer. The filament was forwarded until it was being extruded from the nozzle to ensure the filament was fully inserted into the printhead. Filament was inserted in the printhead for this test because the printhead would have filament inserted during normal printing operations. The experimental apparatus was then placed in the vacuum chamber and a vacuum of approximately 1000 Pa was drawn. After the vacuum was drawn the pump was turned off and isolated from the vacuum chamber using the valve built into the vacuum chamber. The printer was then turned on and was connected by USB to a computer running pronterface to allow for direct control of the printhead temperature.

Using pronterface the nozzle was set to 100 °C and the temperature was carefully observed as the nozzle heated up. The printhead heated up normally reaching 100 °C, overshooting and then settling as normal. It was noticed that the temperature overshoot the set temperature by 15-20 °C, noticeably more than the 7-8 °C observed when bringing the nozzle to a set temperature in atmosphere. Fluctuations around the set temperature were as expected with fluctuations of 1-2 °C. As the nozzle heated to a temperature of 100 °C properly the nozzle set temperature was subsequently set to 150 °C and then 200 °C with the temperature being closely observed at each set point. At both temperatures the nozzle heated properly, reaching the set temperature and settling with acceptable fluctuations. The overshoot was as observed with the 100 °C test in the vacuum environment, 15-20 °C.

Following these successful tests, the set temperature was increased to 260 °C. The nozzle heated normally however as it overshoot the set temperature the printer stopped heating and pronterface displayed the error “: Extruder switched off. MAXTEMP triggered !Error: Printer stopped due to errors. Fix the error and use M999 to restart!. (Temperature is reset. Set it before restarting)”. This

error was caused by the overtemperature cut-off in the UM2+ which turns off the printer if the nozzle temperature exceeds 275 °C. This was noted above in Section 4.5.2 as a potential issue.

To address the issue of the nozzle overshooting and triggering the over-temperature cut-off the PID constants which control the nozzle heater needed to be changed. First the nozzle temperature constants were identified. These constants are displayed automatically when connecting the printer to pronterface, so the printer was power cycled, reconnected to pronterface and the nozzle PID constants were recorded. It was found that the initial PID constants were 10.03, 1.50 and 70.00 for P, I and D respectively. To limit the overshoot of the nozzle temperature in the vacuum environment new PID constants needed to be determined.

To find new PID constants for the nozzle heater the “M303: Run PID Tuning” gcode command was used. This gcode command that was passed to the printer via the pronterface command line which commands the firmware to determine new PID constants. The exact command passed to the printer was “M303 E0 S250 C5”. This line of code specifies that the M303 PID tuning should be carried out on the nozzle heater (E0) at a temperature of 250 °C (S250) and the program should determine the new PID constants using five cycles around the set temperature (C5). 250 °C was chosen as the tuning temperature because it was the maximum temperature that could be used while still allowing the nozzle to remain under the 275 °C over-temperature cut-off with an overshoot of 25 °C. This was done to prevent the printer from shutting down while the running the PID tuning. This attempt at PID tuning was done with the printer still in the vacuum environment of approximately 1000 Pa. Once the M303 command was passed to the printer PID tuning began with pronterface displaying the message “PID Autotune start”. Although the PID tuning successfully started it quickly stopped with pronterface displaying the error "PID Autotune failed! Temperature too high". This was unexpected as measures had been taken to prevent the nozzle from exceeding the 275 °C over-temperature cut-off. Successive attempts to run the M303 command in a vacuum environment using temperatures of 220 °C and 200 °C were also unsuccessful with the PID tuning starting correctly before failing and displaying the same error as above.

Johan Versteegh at Ultimaker was consulted to determine the problem with running the M303 command. Under certain conditions the M303 command will automatically display the over-temperature even if the temperature is below the 275 °C cut-off. This is because the temperature needs to stay in a certain band around the specified temperature during the PID tuning. If the temperature falls outside this range the PID tuning fails and gives the "PID Autotune failed! Temperature too high" error.

As it was not possible to use the M303 command to automatically tune the nozzle heater PID constants it was necessary to adjust the PID constants by hand. Table 1 of [66] was used as a reference to determine if the P, I and D values should be increased and decreased. New PID values were sent to the UM2+ via pronterface by using the “M301: Set PID Parameters” command and saving them to EEPROM using the “M500: Store parameters in non-volatile storage” command. To test the manually set PID constants the nozzle was allowed to cool to approximately 150 °C, the new values were sent to the printer and then the nozzle temperature was set to 260 °C. This process was repeated until a set of PID constants was found which kept the overshoot of the nozzle temperature below the over-temperature cut-off and minimized fluctuations when at the set temperature. The maximum fluctuation around the set temperature once the nozzle temperature had settled was 2 °C. This value was chosen as it was the maximum fluctuation seen when the printer was operating in atmosphere with the initial PID constants. In general, the P value was decreased, and the D value was increased to minimize overshoot. The I value was also slightly increased to reduce fluctuations around the set temperature.

This process of manually adjusting the PID constants resulted in PID values of 9.00, 1.55 and 73.00 respectively. The first PP series component, PP-01-01-V, a small cube with 1 cm sides, was then printed in a vacuum atmosphere to determine if the printer functioned properly with the new PID constants. Although PP-01-01-V did not print with good quality the nozzle temperature remained stable at 260 °C throughout the print. Although the temperature remained stable throughout the print the nozzle temperature reached roughly 272 °C during the initial overshoot. This is close to the 275 °C cut-off, potentially causing a cut-off in certain situations. The PID constants were manually adjusted again using the same procedure as before to further reduce overshoot. New PID constants of 8.50, 1.55 and 95.00 were found. PP-01-02-V, another 1 cm sided cube, was then printed in vacuum to assess performance. The temperature remained constant when fabricating this component and the overshoot was kept below 10 °C, reducing the chances of an unexpected over-temperature cut-off. These PID constants were used for all further prints, both in a vacuum environment and in atmosphere.

5.1.1.2 Buildplate Heater Performance

The performance of the buildplate heater was assessed in much the same way as the printhead heater. First the printer was exposed to the vacuum environment. The buildplate was commanded to heat to and maintain a set temperature via pronterface and the temperature was monitored as the buildplate heated up and for a few minutes after it reached the set temperature. The buildplate temperature was successively set to 40, 60, 80, 100 and 110 °C and the temperature was monitored. The buildplate heated to each set temperature normally and settled around the set temperature with maximum temperature fluctuations of 1 °C or less and no appreciable overshoot. This behaviour mirrored the behaviour seen when heating the buildplate in an atmosphere. As the buildplate successfully reached the maximum temperature of 110 °C and did not exhibit excessive overshoot or fluctuation around the set temperature, no modification of the buildplate PID constants was needed.

5.1.2 Servo Performance

The other major printer subsystem that was evaluated for performance in a vacuum environment was the servos. This included the printhead positioning servos and the filament feed servo which are required to accurately position the printhead and to feed filament to the printhead at the appropriate rate. As noted in Section 4.5.3 the possibility of the servos overheating was identified as a potential issue.

5.1.2.1 X, Y and Z Servo Performance

The X, Y and Z servo motors were tested following a similar procedure to how they were tested in atmosphere with the revised wiring which was discussed in Section 4.3. As with all the other tests of the printer in a vacuum environment the printer was placed in the vacuum chamber, a vacuum of 1000 Pa was drawn, the pump was turned off and isolated and the printer was connected to pronterface.

The first step in assessing the positional servos was a homing test. The X, Y and Z servos were sequentially commanded to move to their home position via pronterface. All three servos responded normally to these commands. This showed that the servos responded normally and could rotate properly in vacuum. Next a combined homing command was sent where the X, Y and Z axes were commanded to home at the same time. The servos again completed this command normally. These tests also served as a test for the X, Y and Z end-stop switches. As the homing process was carried out normally these switches must be functioning properly in the vacuum environment.

The next assessment that was carried out was to see if the X, Y and Z servos moved the correct distance. To test this a ruler was placed in the vacuum chamber along with the printer and aligned with one of the three axes so that the distance moved by the axis could be see from outside the chamber. The relevant axis was then commanded to move specific distances via pronterface and the distance the axis moved was checked on the ruler and compared against the commanded distance. This was then repeated for the other two axes. It was found that all three axes moved nominally with no problems.

The temperature of the servo motors as they functioned in a vacuum environment was also assessed. The potential of overheating of the servos was discussed above in Section 4.5.3. The maximum acceptable temperature of any servo was chosen to be 100 °C [67]. To determine if there is a risk of the servos overheating type K thermocouples were taped to the exterior of the X, Y and Z servos. The temperature of these thermocouples was monitored while printing two PP series test components in atmosphere, PP-01-04-A and PP-02-01-A. PP-01-04-A is a small cube with 1 cm sides while PP-02-01-A is much larger component with a rectangular prism geometry and a very sparse infill Figure 30. These geometries were selected so the temperature could be recorded while printing a geometry that had already been printed and to see how the temperature responds when printing a larger component with a longer print time. Printing of these PP series components also served as a test of the positional accuracy of the X, Y and Z servo motors while printing in vacuum.



Figure 30: (L) PP-01-04-A and (R) PP-02-01-A

To determine the temperature performance of the X, Y and Z servos in a vacuum environment a baseline temperature while printing in atmosphere was recorded first. With the thermocouples recording the temperatures of the servos of the Y and Z servos, component PP-01-04-A, the small cube with 1 cm sides was printed in atmosphere. The temperature of the X servo was not recorded in this test due to a data acquisition malfunction. The temperature peaked at 39.6 °C for the Y servo and 31.0 °C for the Z servo.

Next, component PP-02-01-A, the long, thin, sparse volume was printed in atmosphere, and the servo temperatures were recorded. For this longer print the temperature peaked at 42.5 °C for the X servo and 46.1 °C for the Y servo. The temperature of the Z servo was not recorded for this test as the previous test showed that the Z servo remains at a much lower than the X and Y servos in atmosphere.

Two components with the same geometry, designated PP-01-05-V and PP-02-02-V, were then printed in a vacuum environment. For the 1 cm cube, PP-01-05-V the temperature peaked at 40.3 °C for the X servo, 42.5 °C for the Y servo and 31.1 °C for the Z servo. While printing the larger sparse

volume, PP-02-02-V, the temperature peaked at 49.6 °C for the X servo, 52.0 °C for the Y servo and 32.9 °C for the Z servo.

The temperatures recorded in the vacuum environment fall below the maximum allowed temperature of 100 °C showing that the servo motors can function correctly in a vacuum environment. The components printed in vacuum PP-01-05-V and PP-02-02-V were also analyzed to assess the positional accuracy of the X, Y and Z servos in vacuum. This clearly shows that the X, Y and Z servos can position the printhead accurately in a vacuum environment and overheating is not an issue. To ensure there is no danger of overheating the temperatures of the X and Y servos were recorded during several later prints in vacuum to ensure they remained below the 100 °C threshold. The servos remained below 100 °C during all printing operations where temperature was recorded.

5.1.2.2 Filament Feed System Servo Performance

The filament feed servo was also evaluated for performance in the vacuum environment. This was tested at the same time as the X, Y and Z servos. As with all the other tests of the printer in a vacuum environment the printer was placed in the vacuum chamber, a vacuum of 1000 Pa was drawn, the pump was turned off and isolated and the printer was connected to pronterface.

The first test of the filament feed servo was to command it to forward a certain length of material via pronterface. The filament feed servo was commanded to forward 20 mm of material and the results were observed. As there was no simple way of measuring the amount of material that was forwarded due to the location of the printer in the vacuum chamber the results were only assessed in a qualitative manner. When commanded via pronterface material was observed being extruded from the nozzle in the same manner as in atmosphere. The amount of material and time taken to forward 20 mm of material were roughly the same as when forwarding the same length of material in atmosphere.

Having passed the initial test, the filament feed servo performance was evaluated by printing two PP series components, PP-01-05-V and PP-02-02-V, in vacuum. These components are the same components that were used in evaluating the performance of the X, Y and Z servos in vacuum. The temperature of the filament feed servo was recorded during these two prints. The filament feed servo temperature peaked at 29.6 °C and 36.5 °C for the PP-01-05-V and PP-02-02-V components respectively. This is a much lower temperature than the X or Y servos and well below the 100 °C threshold. This lower temperature is likely due to the fact the filament feed servo does not need to accelerate and decelerate as much as the X and Y servos. This testing shows that the filament feed servo can accurately forward filament material for extrusion and will not over heat in a vacuum environment of 1000 Pa.

5.2 Issues with Printed Component

As mentioned several times the print quality of the PP-01 geometry, the small cube with 1 cm sides, was observed to very bad in vacuum. Images of several PP-01 components fabricated in vacuum can be seen in Figure 31. These components usually have good quality printing on the brim and first few layers with very poor quality in the following layers. This poor-quality printing is characterized by rounded corners and sides and a general “birds nest” appearance. As components with other geometries, such as the long, flat rectangular prisms of the PP-02 and PP-03 components, printed very well the problem must be with the geometry of the PP-01 component, not with the printer, the process or the printing environment.



Figure 31: (L-R) PP-01-01-V, PP-01-05-V and PP-01-11-V

5.2.1 Reduced Cooling

The PP-01 geometry has a very small cross-sectional area and therefore it does not take long for the nozzle to print a layer. As the time to print a layer is very short it is possible that the nozzle will begin printing the following layer before the preceding layer has had enough time to be rigid enough to support further printing. It is hypothesized that the reduced cooling in the vacuum environment is causing the layers of a print to cool more slowly, remaining malleable when further layers are printed. As the preceding layers are still malleable when printed on they are dragged around by the printhead leading to the rounded corners and “birds nest” appearance of the PP-01 components. This is supported by observing PP-01-05-V shown in Figure 32 which clearly shows a counter-clockwise twist in the upper layers. As the printhead moves in a counter clockwise motion while printing the PP-01 component it is assumed that this twist is caused by the still malleable filament being dragged and deformed by the printhead as it prints the following layers. Movement and deformation of already printed layers was also observed when printing PP-01 components in a vacuum environment and was video recorded for several components.

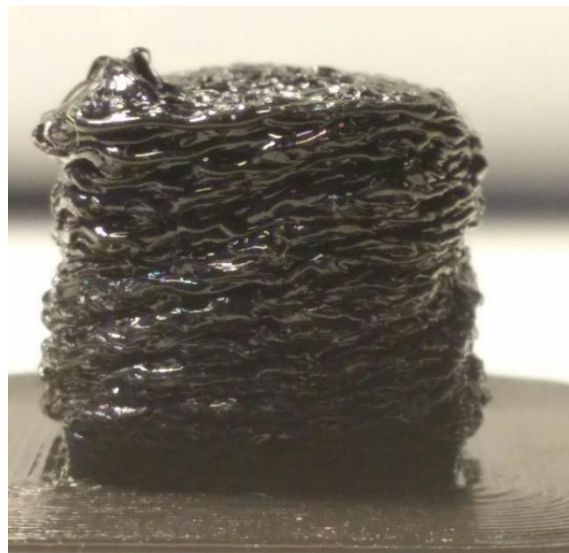


Figure 32: PP-01-05-V showing a counter clockwise twist

While this issue of poor quality printing was only observed while fabricating PP-01 components the hypothesis as to why it is occurring applies to all components with a small cross-sectional area that are printed in vacuum. This problem would likely be exacerbated in a vacuum environment with even lower pressure as convective cooling of the layer would be even further reduced. It is therefore

important to better understand the thermal environment experienced by the component as it is fabricated.

The first step to better understanding the thermal environment of the component was establishing the glass transition temperature. This is important as the glass transition temperature is the temperature at which an amorphous plastic, such as PC, shifts from being a rigid, glasslike material to being soft and malleable. The Ultimaker brand PC filament being used is stated to have a glass transition temperature of 111-112 °C. [68] To confirm this a differential scanning calorimetry (DSC) test was carried out to determine the exact glass transition temperature of the spool of polycarbonate that was being used for this research. This was done in the DASML chemistry lab on a PerkinElmer DSC machine. In this test a sample of 14.8 mg of polycarbonate filament was heated from 30 °C to 300 °C at a rate of 10 °C/min and was held at 300 °C for 5 minutes. The sample was then cooled back to 20 °C at a rate of 5 °C/min with the aid of a compressed air stream. The glass transition temperature was then calculated to be 117.3 °C, very close to the stated value. This validates the processing conditions that were used to fabricate components. It also gives a value at which the polycarbonate will be rigid enough to support the following layers. The DSC results are seen in Figure 33.

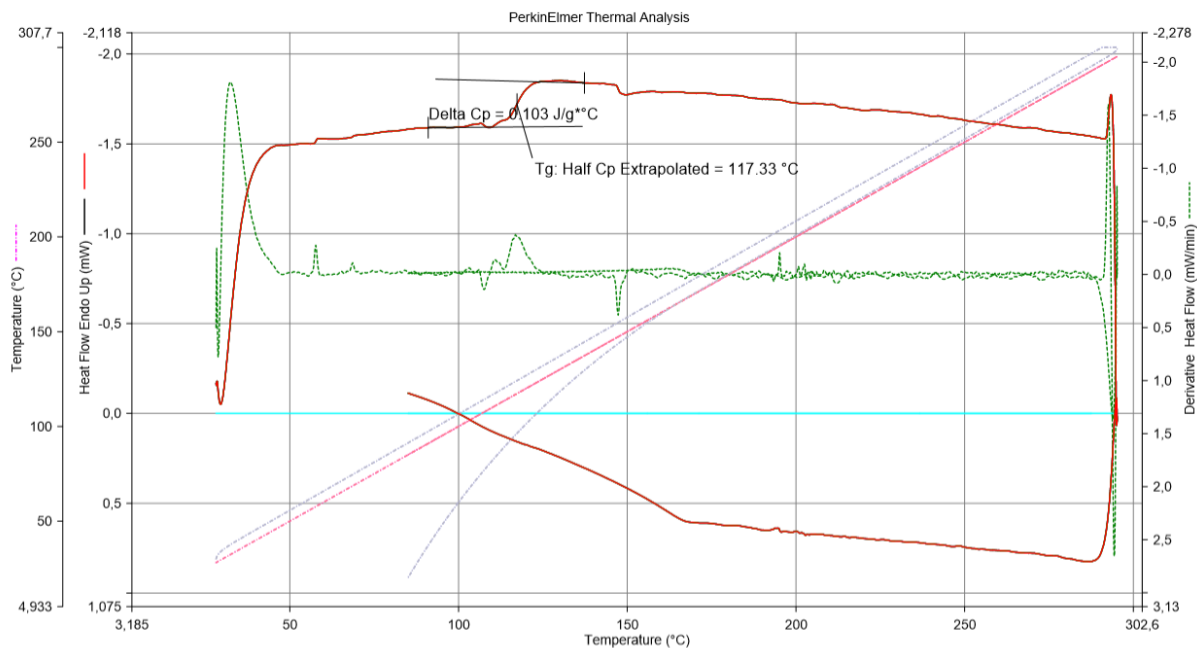


Figure 33: Results of the DSC test including T_g

The next step in better understanding the thermal environment was to simulate the cooling of a layer of polycarbonate as it is extruded. This simulation was done in COMSOL Multiphysics software. To begin with, a very simple model was created in SolidWorks and imported to COMSOL. This geometry is an 8 mm wide by 8 mm long by 0.2 mm prism and simulates a layer of polycarbonate fabricated using FFF. These dimensions were chosen to represent a single layer of a PC component which had side lengths of 0.8 cm (8 mm) and layer heights of 0.2 mm. This closely simulated a layer of the PP-01 component which had side lengths of 10 mm and a layer height of 0.2 mm.

The solid polycarbonate material was applied to this geometry and several boundary conditions were applied to represent the thermal environment of a layer of polycarbonate fabricated with FFF. A constant temperature constraint of 110 °C was placed on the lower surface as though the layer were sitting on the buildplate. The four sides and top surface were specified to be diffuse surfaces

which radiated to an environment with an ambient temperature of 25 °C to simulate the radiation from the component to the chamber walls. Reflectivity of the chamber walls and the radiation between the component and the buildplate and printhead was not considered. Finally, a constraint of external natural convection was applied to the sides and top surface. The sides were specified to be external natural convection on a vertical wall with a wall height of 0.2 mm. The top surface was specified to be external natural convection on the upside of a horizontal plate with a diameter of 8 mm. The initial temperature was specified as 260 °C. The ambient temperature for convective heat transfer was 25 °C. This simulation was run twice to simulate the cooling in atmosphere at a pressure of 1 atm and to simulate cooling in vacuum with a pressure of 1000 Pa. The appropriate pressure was specified in the natural convection constraint of each side for each simulation. The component was meshed with normal sized elements and a time dependent study was conducted from 0 to 0.5 seconds in increments of 0.01 s. The average temperature of the top surface of the component was recorded at every time step of the study and is presented in Figure 34.

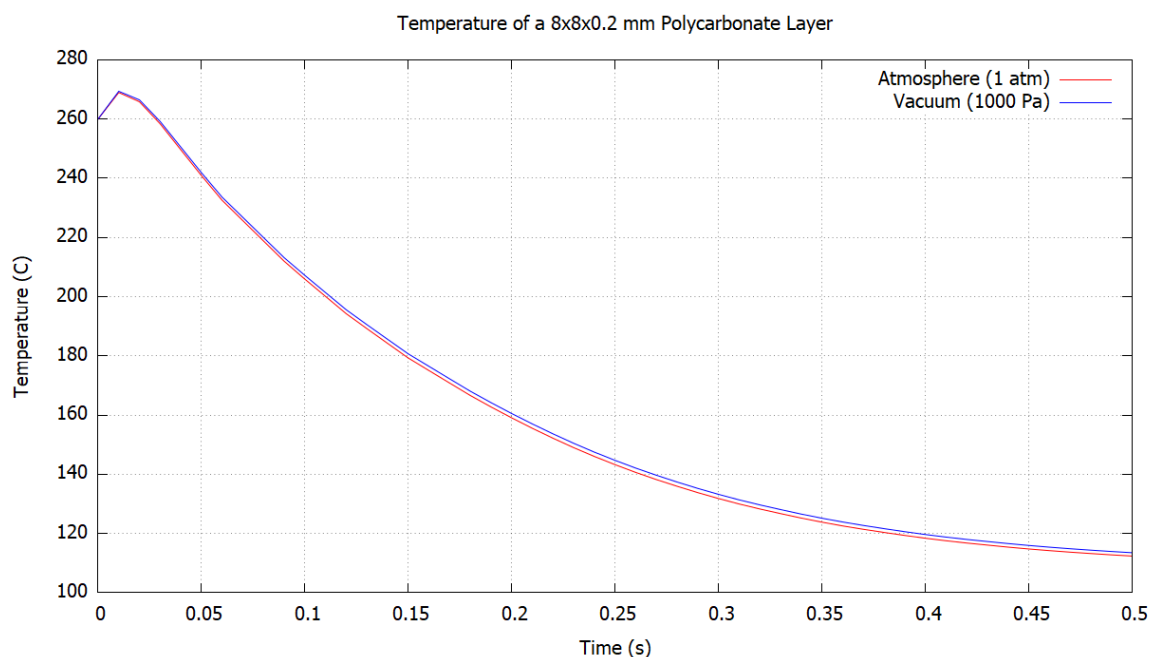


Figure 34: Temperature of the 8x8x0.2 layer over time

Figure 34 shows the average temperature of the top surface of the 8x8x0.2 mm component in atmosphere and vacuum as simulated in COMSOL. There is almost no difference in the rate of cooling between the components in atmosphere and vacuum. While this may suggest that there is little difference in cooling between the two thermal environments it was found that this was due to the extremely large thermal flux from the component though the bottom surface, held at 110 °C, which simulates the buildplate. This very large flux overwhelms the effects of the changes in convective flux from the component due to the different pressures. No real conclusions can be drawn from this simulation except that the first layer, and likely the first few layers, are cooled very quickly by conductive heat transfer to the buildplate.

To better model the cooling of a layer of FFF fabricate polycarbonate a new component with the same length and width as before (8 mm) and a height of 5 mm was created. Due to this larger height the top surface is better insulated from the relatively cool temperature of the buildplate by several mm of polycarbonate. As polycarbonate is a good thermal insulator the conductive heat transfer to

the bottom surface will be reduced allowing the effect of changing pressure on the temperature of the top surface to be better isolated and analyzed.

This new component was set up in much the same way as the preceding component with the bottom surface being held at 110 °C, diffuse radiation from the sides and top surface to an ambient temperature of 25 °C and natural convective heat transfer with an ambient temperature of 25 °C from the sides and top surface. The wall height for the convective transfer from the sides was set to 5 mm and the perimeter for the convective transfer from the top surface was again 8 mm. The initial temperature was set to be a gradient increasing linearly from a temperature of 110 °C at the bottom surface to 260 °C at the top surface. This initial temperature more closely models the actual temperature distribution in a component which has just finished printing with the lower layers being near the buildplate temperature and the upper, more recently printed layers, being nearer to the processing temperature.

This simulation was run as a time dependent study up to a time of 60 seconds with time steps of 0.2 s. This simulation was run at three different pressures, 1 atm (101.325 kPa), 1000 Pa and 0 Pa. This simulates the cooling of the component in an atmosphere, in the testing pressure in the vacuum chamber and in a real on-orbit environment respectively. This allows the testing conditions, at 1000 Pa, to be compared against printing in atmosphere and to the conditions that would be expected of a real implementation on-orbit. Figure 35 shows several images of the component as it cools from its initial temperature to the final temperature simulated after 60 seconds. In these images white indicates a temperature of 260 °C and dark red a temperature of 110 °C with other hues representing the range in between.

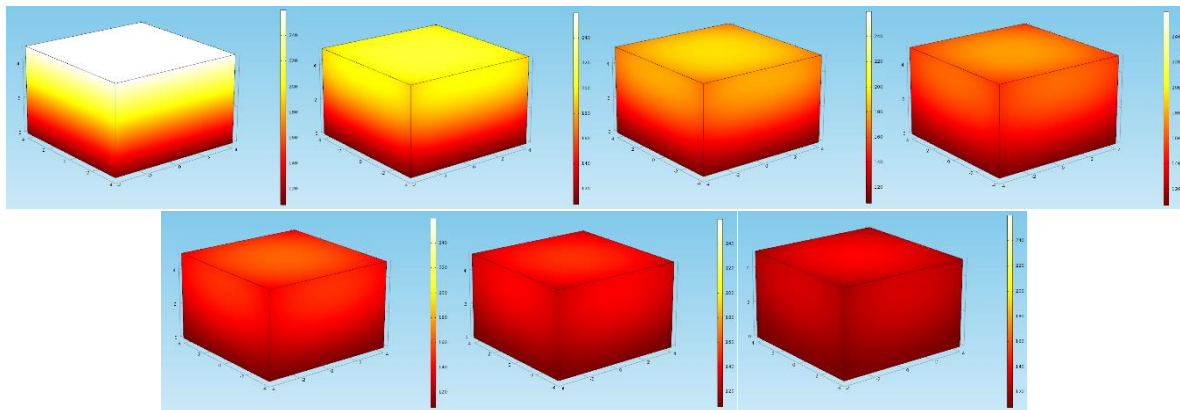


Figure 35: 8x8x5 mm COMSOL component temperature in a 0 Pa environment at (L-R) 0s, 10s, 20s, 30s, 40s, 50s, 60s

The average temperature of the top surface of the 8x8x5 mm component is shown in Figure 36. Figure 36 shows a clear difference between the temperatures in atmosphere and those in a vacuum of 1000 Pa. The temperature in atmosphere is consistently lower than the temperature in 1000 Pa with the difference growing over time. The temperature in a true vacuum (0 Pa) is consistently higher than the temperature in both atmosphere and 1000 Pa as expected due to the complete lack of convective cooling. Although the 0 Pa environment lacks convective cooling it follows the same trend as the temperatures in atmosphere and 1000 Pa. This validates the results gained from testing components fabricated in a 1000 Pa environment. If the cooling of the component in the 1000 Pa environment follows the same trend as in a 0 Pa environment, the effects caused by the 0 Pa thermal environment will also be present in the 1000 Pa environment just to a lesser extent. It can therefore be assumed that any differences in components fabricated 1000 Pa, when compared to components fabricated in atmosphere, will also be present in components printed in the, essentially,

0 Pa environment on-orbit. It can also be assumed that any observed differences will be more exaggerated if the component was fabricated in 0 Pa as opposed to 1000 Pa.

Another thing to note from Figure 36 is that the temperature curve at 1000 Pa is much closer to the curve at 0 Pa than it is to the atmosphere curve. This means that the 1000 Pa vacuum environment is closer, in a thermal sense, to the environment that would be experienced on-orbit than it is to a normal atmosphere. This validates the choice of 1000 Pa as the testing pressure.

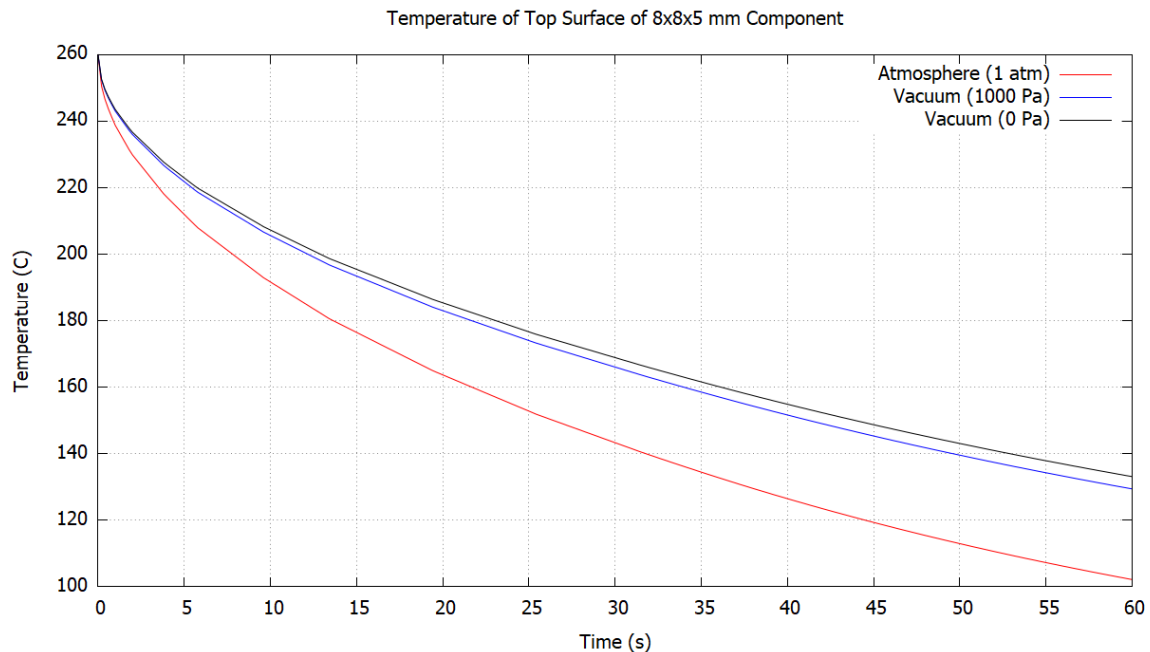


Figure 36: Average temperature of the top surface of the 8x8x5 component over time

Although the information gained in the second COMSOL simulation with the 8x8x5 mm component is very interesting and useful for validating the choice of pressure for testing it is still an incredibly simplified model. To start with, the temperature at any given height within an FFF fabricated component is not uniform as each layer is not printed as a single monolithic layer. Each layer is extruded in a pattern and the temperature of the layer follows this pattern with more recently printed material being hotter. Additionally, the vertical temperature distribution would not follow a linear distribution from the buildplate temperature to the processing temperature but would follow a pattern based on the geometry of the component and the path taken by the printhead. The previous COMSOL models also neglect radiation between the component and parts not at 25 °C such as the buildplate, nozzle and printer frame.

Creating a COMSOL model which incorporates all these aspects would be a very complex and time-consuming task. As the purpose of this research is to determine if FFF can be carried out in an environment representative of an on-orbit environment the creation of this sort of model is out of scope. The printer has already proven itself of being able to fabricate components in a vacuum environment. A better thermal model allows better prediction of printing and would assist in the design of processes to fabricate components with small-cross sectional areas however it does not assist in the goals of this research. Although a complete thermal model is out of scope, the thermal fluxes leaving a component in a variety of environments can be easily determined using COMSOL. These fluxes can be used to assist with calculations and to inform the creation of a better thermal model in the future.

To determine these flux values a very thin component with a width and length of 1 mm and a height of 0.05 mm was created in COMSOL. The bottom surface of the component was set to increase in temperature from 25 °C to 260 °C at a rate of 1 °C/s. Due to the extremely small component, and correspondingly small thermal mass, it can be assumed that the entire component is at the temperature of the bottom surface. The sides of the components were thermally insulated with no thermal flux passing through them. The top surface was specified to have a single thermal flux. The type and parameters of this thermal flux was changed to simulate a variety of environments with a time dependent study being carried out for each environment. There were five environments, and therefore fluxes, that were considered:

- Convective Flux
 - Atmosphere: $P = 1 \text{ atm}$, $T_{\text{ambient}} = 25 \text{ °C}$
 - Vacuum Chamber: $P = 1000 \text{ Pa}$, $T_{\text{ambient}} = 25 \text{ °C}$
 - On-orbit: $P = 10^{-3} \text{ Pa}$, $T_{\text{ambient}} = 25 \text{ °C}$
- Radiative Flux
 - Atmosphere/vacuum chamber: $T_{\text{ambient}} = 25 \text{ °C}$
 - On-orbit: $T_{\text{ambient}} = 3 \text{ K}$

The COMSOL study was run for each of the five environments mentioned above with the average flux leaving the top surface of the component being recorded each time across the entire temperature range. The resulting data can be see in Figure 37 for convective flux and Figure 38 for radiative fluxes.

Figure 37 shows the average convective flux leaving the top surface of the component in atmosphere and in a vacuum of 1000 Pa. The average convective flux in a vacuum environment of 10^{-3} Pa was also recorded however it could not be shown in this figure as it never rose above 1 $\text{W/m}^2\text{K}$ causing it to be hidden by the x-axis. The convective flux in the vacuum environment of 1000 Pa is generally about one-tenth of the flux in atmosphere, a large difference.

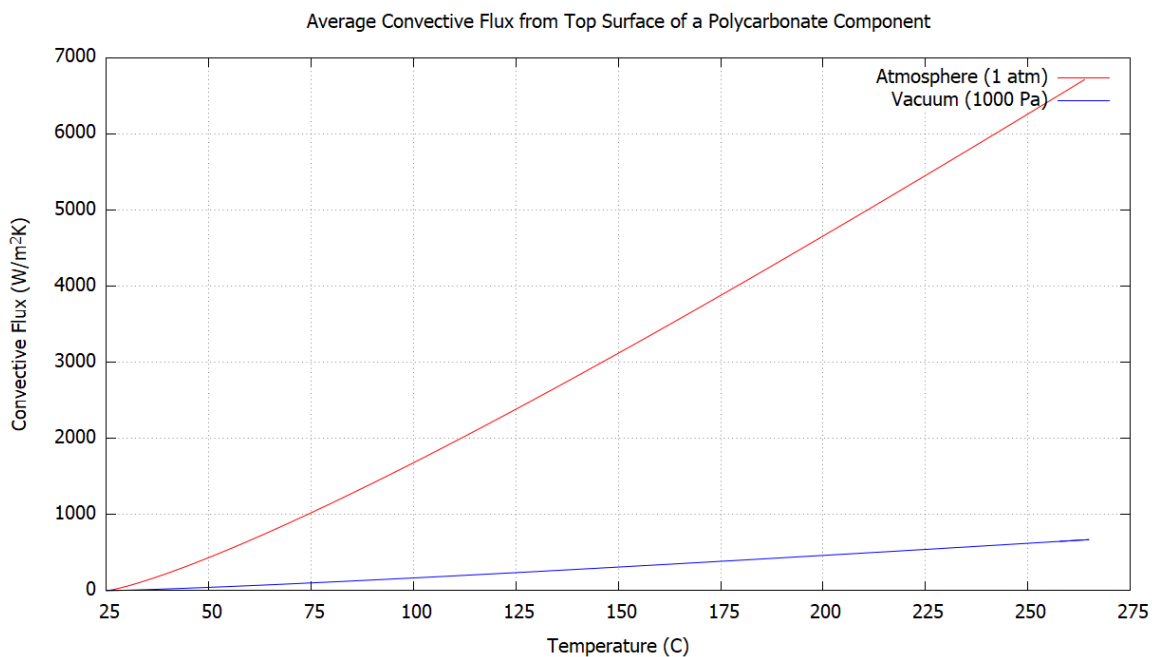


Figure 37: Convective flux from a polycarbonate component

Figure 38 shows the average radiative flux leaving the top surface of the component toward ambient temperatures of 25 °C (298.15 K) and 3 K. These first of these two environments represent the radiative environment experienced by components printed in atmosphere or in the vacuum chamber. The second environment represents the real environment that would be experienced on-orbit. It is seen that the radiative flux for the real on-orbit environment at 3 K is consistently about 400 W/m²K more than the radiative flux to an ambient temperature of 25 °C. While not useful by themselves these values can be used in future thermal models and to inform choices made when choosing further testing, processing or environmental parameters.

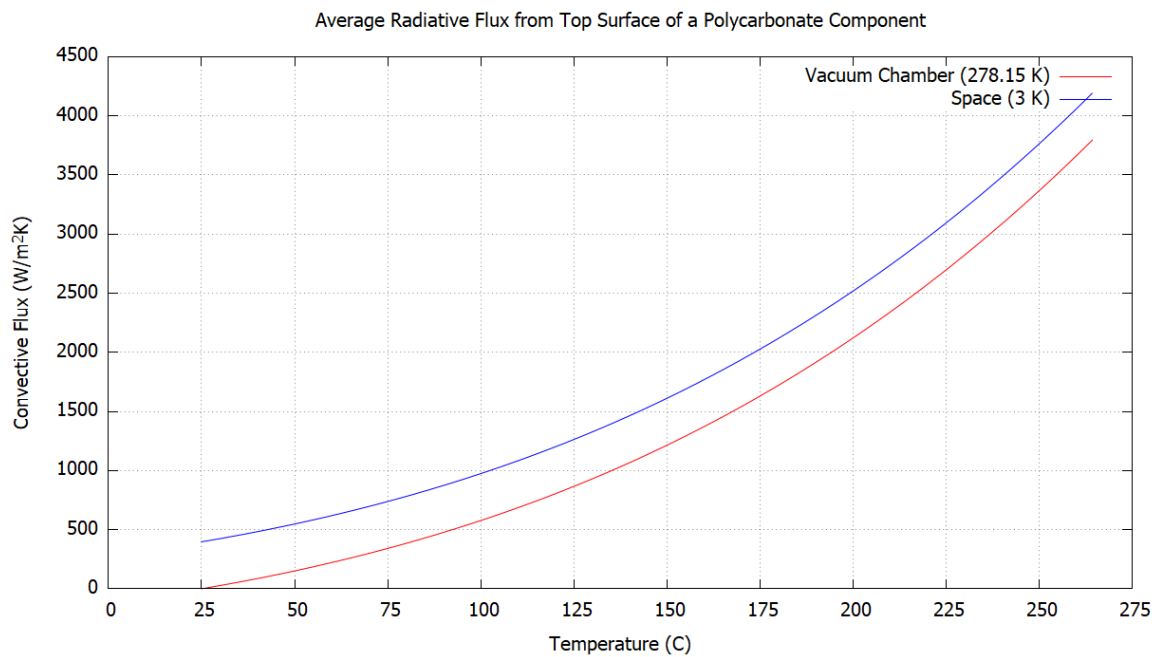


Figure 38: Radiative flux from a polycarbonate component

5.2.2 Bubbling of Upper Layers

Another issue that was noticed when printing the PP-01 components was bubbling of the top layer. While printing these components in a vacuum environment bubbles were observed forming and bursting on the top, most recently fabricated layer, of the component. One of these bubbles can be seen below in Figure 39. These bubbles may be contributing to the poor printing of the PP-01 components and even if they are not they will result in a poor surface finish on the top surface of components with small cross-sectional area.

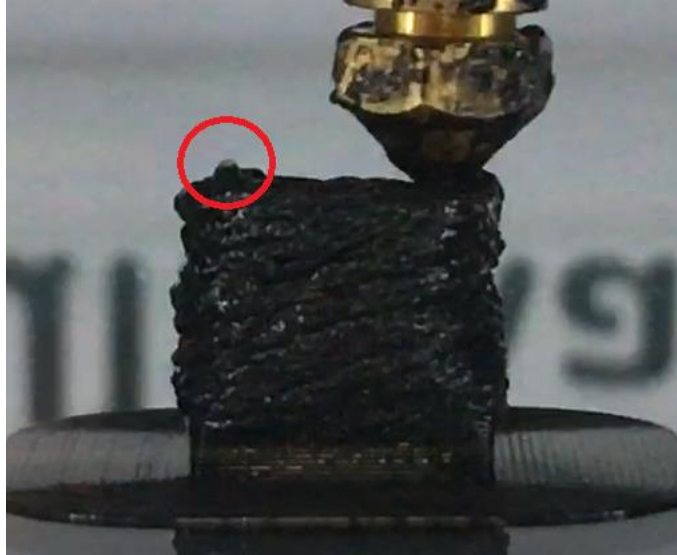


Figure 39: Bubble on top surface of component printed in vacuum

The first hypothesis to explain these bubbles was that the absorbed water in the polycarbonate filament was vaporizing as it is heated, producing pockets of high pressure steam in the filament. As the filament was further heated it would soften allowing the high-pressure pockets to burst from the surface, causing bubbles. To determine if this was the case a thermogravimetric analysis (TGA) was carried out. The TGA takes a small sample of material and heats it up, measuring the changes in mass as a function of time. If there was water present in the used polycarbonate filament it would boil at 100 °C and there would be a corresponding decrease in mass. If the steam could not escape the filament when it was rigid than it would escape after the glass transition temperature which for the polycarbonate filament in use was established to be 117.3 °C with the DSC test.

The TGA test, carried out in the DASML chemical laboratory, used a 3.118 g sample of polycarbonate filament taken from a section of spare filament that had been left out in atmosphere for several months. The sample was taken from filament that had been left out, as opposed to stored in a sealed bag or exposed to a vacuum environment, because it will have been more likely to absorb the most moisture from the surrounding air providing the most visible drop in mass. The sample was enclosed in an aluminum crucible and heated from 25 °C to 500 °C at a rate of 10 °C/min. the mass of the sample was recorded automatically as a function of temperature and is displayed in Figure 40.

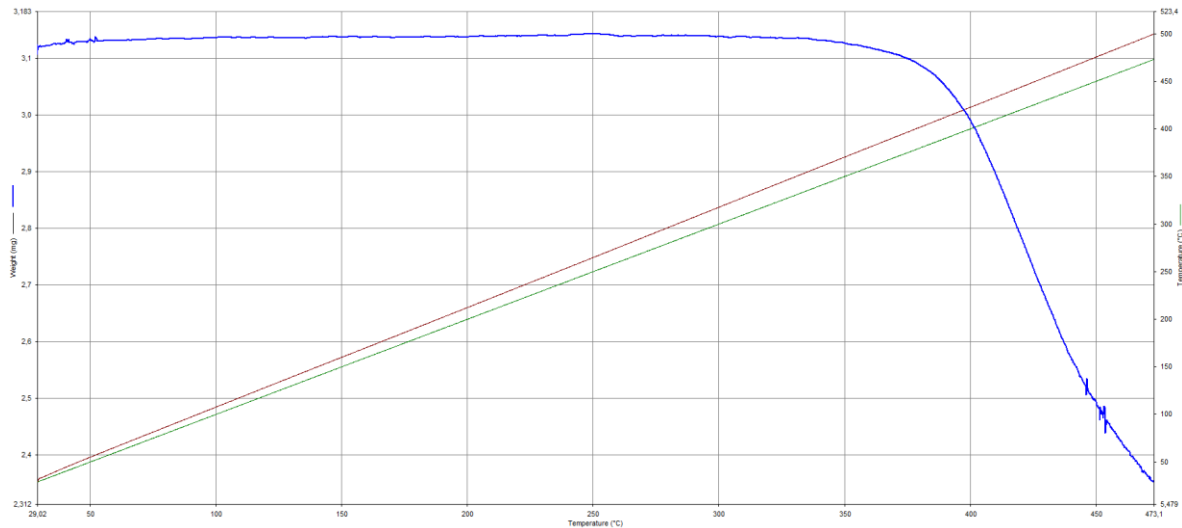


Figure 40: Results of the TGA testing

Figure 40 shows that the mass of the polycarbonate sample remains very steady up until approximately 350 °C at which point it begins to decompose. There is no noticeable decrease in mass around the 100 °C point where it would be expected that absorbed water would be released. The only conclusion that can be made from this is that there is little to no water absorbed in the polycarbonate filament and that the bubbles occurring on the top surface are not caused by absorbed water.

With the original hypothesis disproved another hypothesis needed to be generated. The only alternate hypothesis that was generated was that the polycarbonate material itself was boiling. This was thought to be possible due to the elevated temperature, 260 °C, and low pressure, 1000 Pa, that the material was exposed to. The problem with this theory is that bubbling should be observed on all components, not just those with a small cross-sectional area, and when the material is just leaving the nozzle. Bubbling was not observed in these situations. Further research needs to be conducted to determine the cause of these bubbles and their effect on the quality of components fabricated in vacuum.

5.3 Issues with the FFF Process

This section discusses the issues with the FFF process that were observed during the testing carried out in Chapter 5. The two main issues that are analyzed are the clogging of the nozzle and outgassing. Clogging of the nozzle was observed during the initial printing of the PP series of components and caused a complete stoppage of extrusion resulting in incomplete or extremely poor-quality components. The outgassing caused by the FFF process in the vacuum environment was also quantified and analyzed.

5.3.1 Nozzle Clogging

On several occasions, while printing PP series components in vacuum, the printer unexpectedly stopped extruding material. This first occurred when printing PP-01-01-V and PP-01-02-V, the first two components printed in vacuum. These components are small cubes with 1 cm sides and were printed one after the other without bringing the vacuum chamber to atmospheric pressure in between. They are shown below in Figure 41.

PP-01-01-V was printed first, in the centre of the buildplate, and completed printing with an appropriate amount of polycarbonate material extruded. PP-01-02-V was then printed immediately after, beginning printing approximately two minutes after PP-01-01-V had completed. The first

indication of a problem was the brim of PP-01-02-V, seen in Figure 41, which was so thin that it was almost see through. As the printer continued to fabricate the component extrusion became sporadic with the first few layers printing adequately and extrusion stopping for entire sections of later layers. At this point the print was stopped as it was assumed that the printer had run out of filament.

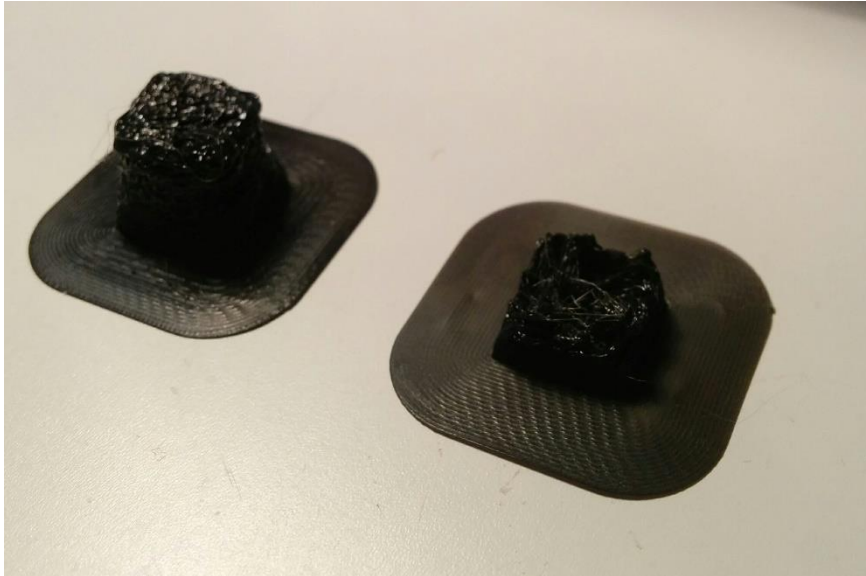


Figure 41: (L) PP-01-01-V and (R) PP-01-02-V

After removing the printer from the vacuum chamber, it was found that there was still considerable filament left that could be used for printing. When an attempt was made to remove the filament from the printer it was found that the filament was stuck in the printer. The filament was removed from the printer by pulling on the end. As the filament was pulled through the Bowden tube it was observed that the end of the filament was a very tight fit on the inside of the Bowden tube. After the filament was removed it was inspected to determine what caused it to become stuck in the printer. The end of the filament which was in the hot section of the printhead is shown in Figure 42 and was determined to be the problem. A length of end of the filament had a diameter of 3.1 to 3.4 mm, larger than the nominal 2.85 mm diameter of the filament. This expansion seemed to be caused by softening of the filament at elevated temperatures. This was suspected because the track marks of the filament feed system are not visible on the expanded section although they clearly visible immediately above the expanded section. The lack of track marks on the filament can be seen in Figure 42. Within this expanded section is a small ring with an even larger diameter of 3.68 mm and length of 1.8 mm.

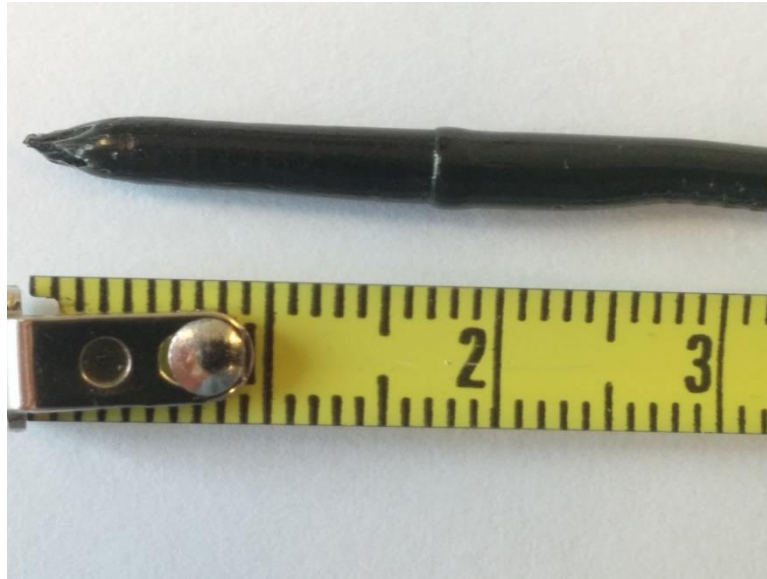


Figure 42: Expanded section and ring on filament when printing PP-01-01-V and PP-01-02-V

It was hypothesized that the expanded section of filament had softened during printing due to the reduced cooling in the vacuum environment. As the end of the filament was now soft it expanded when more filament was fed into the nozzle when the nozzle was not extruding, such as during travel moves. As the filament pushed down on the softened section the section expanded in volume to accommodate the additional material. The ring on the expanded section may have been caused by this expanded section catching on a flaw on the internal surface of the printhead. As extrusion continued the ring grew larger until it filled the inside of the printhead, preventing the filament feed system from pushing filament out the nozzle and halting extrusion.

After the clogging filament was analyzed fresh filament was inserted into the printer and another 1 cm cube, PP-01-03-A, was printed in atmosphere to check to see if the printer was damaged by the clogged filament. PP-01-03-A printed as expected so the next step was to try to replicate the clogging problem. This was done by printing components PP-01-05-V and PP-02-02-V in a vacuum environment. These are the components that were used when measuring the servo temperature in vacuum as discussed in Section 5.1.2.1. These components were a 1 cm cube and long rectangular prism with a sparse 15% infill. These components were printed one after another, on the same buildplate without bringing the vacuum chamber to atmospheric pressure in between. The first component, PP-01-05-V, printed as expected with no clogging or under extrusion noted. The second component, PP-02-02-V, printed as expected for the first few layers however when the layers with infill began to be printed extrusion became sporadic. This was quickly followed by a complete stop of extrusion approximately 15 seconds later.

The print was stopped, the vacuum chamber was brought to atmospheric pressure and the printer was removed. An attempt was made to remove the filament from the printer by pulling it through the Bowden tube. This time the filament did not come through the Bowden tube no matter how much force was applied. The filament was eventually removed by disassembling the printhead and pulling the filament out the end of the Bowden tube that was connected to the printhead. This was done so that the expanded section did not need to move through the Bowden tube. Examining the end of the filament an expanded section was observed, similar to the first incident of clogging. This is shown below in Figure 43.



Figure 43: Expanded section and ring of the second clog

The filament exhibited the same issues with an expanded section with a diameter of 3.2 to 3.55 mm and a ring with a larger diameter within the expanded section. The ring in this case had a much larger diameter of 6.3 mm however this is due to the ring being deformed when an attempt was made to remove the filament by pulling it through the Bowden tube. This is evidenced by the flat surface of the ring on the side of the Bowden tube, showing that it was pushed up against the flat face at the end of the tube.

Once it was established that this was a repeatable phenomenon a solution needed to be found. Johan Versteegh was consulted, and he suggested that the ring structure on the expanded section may be caused due to improper assembly of the printhead. If the printer parts which make up the printhead are not properly mated to each other malleable filament may be pressed into the gap, causing the ring. To test if this was the case the printhead was disassembled and cleaned to ensure mating surfaces could sit flush against each other. The end of the Bowden tube was squared off and great care was taken to ensure the Bowden tube was seated properly when reassembling the printhead.

To test the reassembled printhead two more components were printed in a vacuum environment, PP-01-05-V and PP-03-01-V. These components were again printed one after another, on the same buildplate without bringing the vacuum chamber to atmospheric pressure in between. Both PP-01-05-V, another 1 cm cube, and PP-02-02-V printed as expected. This suggested that the problem may have been fixed however when another component with the same geometry as PP-02-01-V was printed there was no extrusion at all. The print was aborted, the printer removed from the chamber and the filament extracted. The recovered filament can be seen in Figure 44 and shows the same characteristics of the previous two clogs.

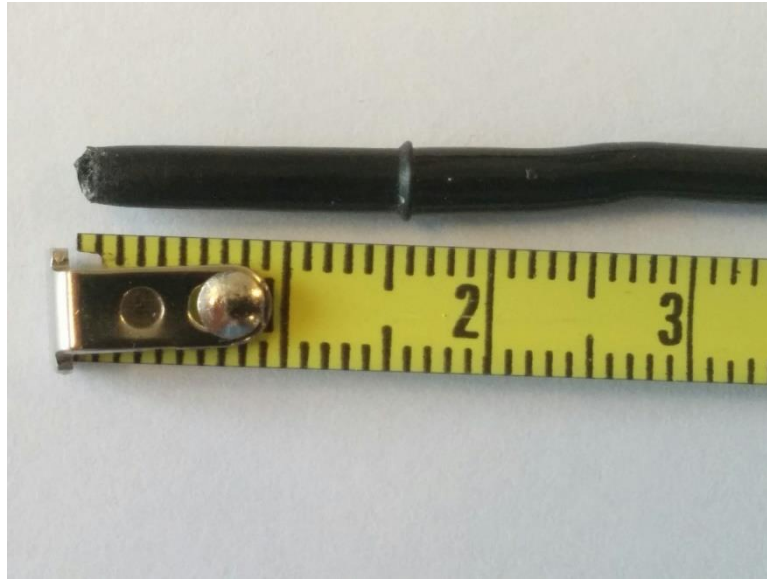


Figure 44: Expanded section and ring of the third clog

This suggests that the reassembly of the printhead did not solve the clogging issue. To confirm this the printer was loaded with new filament and four components PP-01-06-A, PP-03-02-A, PP-02-03-A and PP-01-06-A were printed. These components were printed immediately after extracting the third clogged filament in atmosphere. The printhead was not altered, the printer was left in the vacuum chamber, the wiring used the exact same wiring that was used in the vacuum print and the door of the vacuum chamber was closed. The printing setup was the same except vacuum was not drawn in the chamber leaving the pressure at atmospheric pressure. All four of these components printed perfectly showing that the clogging issue was due to the vacuum environment alone.

As the reassembly of the printhead had not solved the clogging issue a new hypothesis needed to be formed. The idea of the filament prematurely (at a greater distance than expected from the nozzle outlet) softening and being expanded in diameter by the pressure of the filament being fed was analyzed in depth and the idea of better isolating the hot section of the printhead was raised. By better isolating the hot section, including the heater block and nozzle, from the rest of the printhead the filament would remain rigid until just before it is extruded. As the filament is rigid it will not be able to expand in diameter when pressed upon by the filament feed system.

To better isolate the hot section from the rest of the printhead a new printhead was required with a better heat break. Johan Versteegh supplied a custom made printhead which he had previously used to print PEEK plastic at temperatures of up to 500 °C. Figure 45 shows stock printhead that had been used for previous prints on the left and the PEEK rated printhead on the right. This custom, PEEK rated printhead has a much better heat break which better separates the hot section from the cold section. This better insulation is mostly because the hot section is suspended from the rest of the printhead by a small tube with very thin walls. The small cross-sectional area of this tube limits the conductive heat transfer that can move through it.

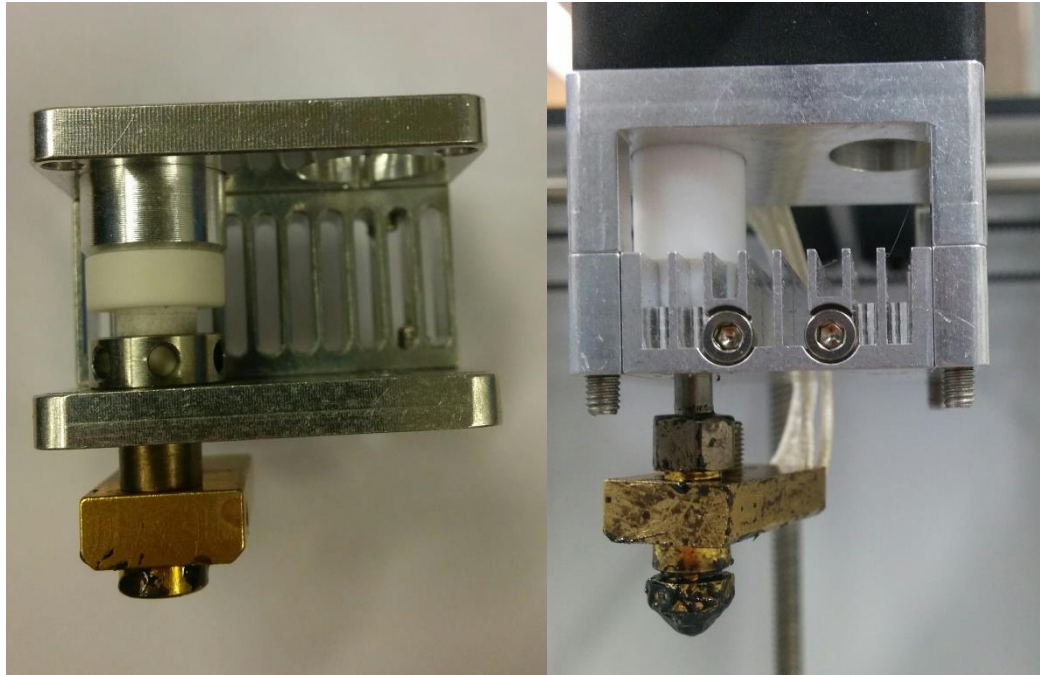


Figure 45: Stock printhead (L) and PEEK rated printhead (R)

The PEEK rated printhead was assembled and installed on the printer in place of the stock printhead. Four components, PP-01-07-A, PP-03-03-A, PP-02-04-A and PP-01-08-A were then printed in atmosphere to ensure the new printhead functioned correctly. As these components printed as expected the printer was placed in the vacuum chamber and a vacuum of 1000 Pa was drawn. Three components, PP-01-09-V, PP-03-04-V and PP-01-10-V were then printed one after another in the vacuum environment. These components all printed to the same quality as observed in the components that were printed in atmosphere. No under extrusion or clogging was observed. As the PEEK printhead had demonstrated that it would not clog in the vacuum environment it was used to fabricate all further components. Further research could be done to more accurately determine the thermal environment experienced by the filament inside the printheads in atmosphere and in vacuum.

5.3.2 Outgassing Test

Outgassing during the FFF process in a vacuum environment was a major concern that was raised in Section 3.5. The potential of contamination of the vacuum chamber by the outgassing caused by the heating of the thermoplastic filament during the FFF process was of particular concern. This was analyzed in detail in Section 3.5.1 and it was concluded that outgassing of the printer and the FFF process posed no contamination risk to the vacuum chamber. Although it was concluded that outgassing would not be an issue, an experiment was carried out to gather quantitative outgassing data and validate the conclusion that the outgassing from the printer and FFF process would not contaminate the vacuum chamber.

5.3.2.1 Outgassing Test Procedure

To gather this data two FTIR glass windows were acquired from Dr. Ugo Lafont to measure the amount of volatile material outgassed by the modified UM2+ printer and the FFF process. These windows measure outgassing by being placed in the vacuum environment with the object of interest allowing outgassed volatiles to condense on the surface of the window. After the test is completed the window can be removed from the vacuum environment and analyzed using FTIR to identify any condensed volatile contaminants. As the windows are numbered and the background spectra of

each window is known very accurately any deviation in the spectra from the background level indicates the presence of a contaminant. The contamination of the chamber during printing would be evaluating by running two tests: one with the printer printing and one with the printer in the vacuum chamber and powered on but not printing.

To begin the outgassing test, the vacuum chamber was cleared of as much unnecessary polymer material as possible. This is to minimize the amount of outgassing coming from sources other than the UM2+ printer and FFF process. Only the wiring needed for data acquisition and non-removable wiring was left in the vacuum chamber. The polymer material in the vacuum chamber was kept exactly same for both tests.

Before each outgassing test the vacuum chamber was connected to the vacuum pump and the vacuum pump was run for one hour. This purged the vacuum chamber of any contaminants and served to reduce the background contaminants that would be detected by the FTIR windows. While the vacuum chamber was being purged 2.4 m of polycarbonate filament was loaded into the printer. A set amount of filament, coming from the same spool, was used for both outgassing tests so that the amount of filament exposed to the vacuum environment was not a factor.

After the vacuum chamber was purged and brought back to atmospheric pressure the printer was placed in the chamber, wired up and checked for functionality. FTIR window #169 was then placed on the bottom surface of the vacuum chamber. It was placed approximately 17 cm from the left wall of the printer with the top of the window tangent to the front plane of the printer. The location of the FTIR window with respect to the printer can be seen in Figure 46. The FTIR window is the small circle on the bottom surface in from of the printer.

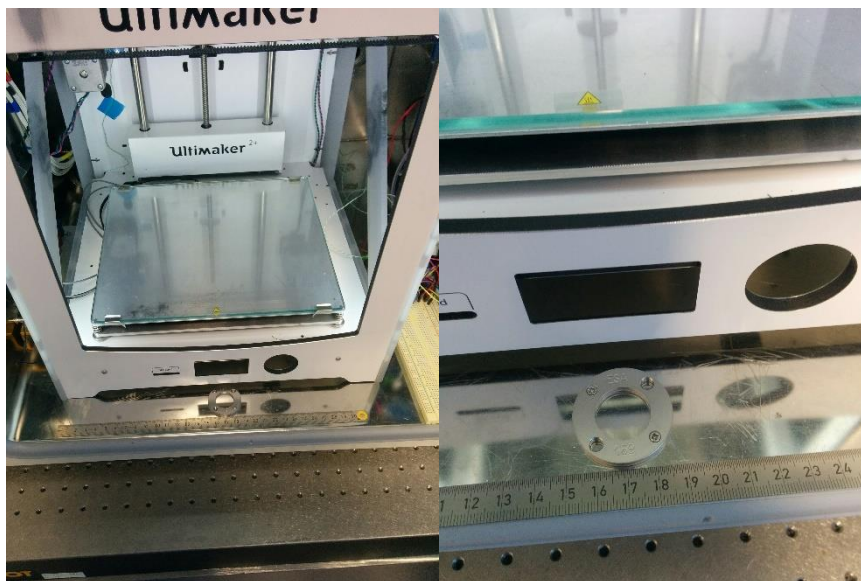


Figure 46: FTIR window #169 in position in the vacuum chamber

This location was chosen as the window is exposed to the general environment of the vacuum chamber and is not shielded by any equipment. The window was placed directly on the bottom surface of the chamber as the metal of the chamber walls stays around room temperature during printing. This cool temperature allows the maximum amount of volatile material to condense on the window. Placing the window directly on the bottom surface also allows the temperature of the window to be very similar during both tests. The FTIR window was handled with gloves and was stored in a tightly closed container when not in use to prevent accidental contamination.

After the printer and FTIR window were in place the vacuum chamber door was closed and the printer was turned on, but the print was not started, and no commands were sent. The vacuum pump was turned on and vacuum was drawn. A running timer was started at the same time as the vacuum pump was turned on and was used as a timing reference. The timing of the events can be seen in Table 9. The vacuum pressure reached 1000 Pa after 35 minutes and 53 seconds at which point the vacuum pump was turned off and isolated from the chamber. Isolation from the chamber was an important consideration as the vacuum pump could draw contaminants out of the chamber and away from the FTIR window if left running. At this point the printer was inspected to ensure everything was functioning correctly. The print was started after an elapsed time of 46 minutes and 22 seconds. The component printed was PP-04-01-V, a dog bone shaped component which had the same geometry as the MP-02 components that were used for tensile testing. The outgassing test therefore served as a test bed to see if a component with this geometry could be fabricated. The print completed successfully after 1 hour, 59 minutes and 50 seconds with extrusion stopping, the axes returning to home positions and the nozzle and buildplate beginning to cool down. The buildplate temperature reached 45 °C after 2 hours, 40 minutes and 39 seconds at which point the chamber was vented to atmosphere, the FTIR window was removed and the PP-04-01-V component was removed.

Event	Time (h:mm:ss)
-Vacuum pump turned on	0:00:00
-Pressure reaches 1000 Pa	0:35:53
-Vacuum pump turned off	
-Vacuum pump isolated from chamber by way of built in valve	
-Start of printing	0:46:22
-Buildplate and printhead home after completing print	1:59:50
-Buildplate temperature reaches 45 °C	2:40:39
-Vacuum chamber vented	
-FTIR window removed	

Table 9: Event times during outgassing test (FTIR window #169)

For the second outgassing test the vacuum chamber was again purged by pumping constantly for one hour. While the vacuum chamber was being purged, 2.4 m of polycarbonate filament was measured out and loaded into the printer. Following completion of the purge cycle the printer was placed in the chamber, wired up and checked for functionality. The second FTIR window, #170, was placed in the vacuum chamber in the same location as window #169 that was used for the first test. The printer was then turned on, the door was closed and vacuum was drawn. A timer was again started at the same time as the vacuum pump was turned on. The vacuum pump was turned off and isolated from the chamber when the pressure had reached 1000 Pa. After the vacuum pump was turned off and isolated the printer soaked in the vacuum environment, powered on but not printing, until 2 hours, 40 minutes and 39 seconds had elapsed since the vacuum pump was turned on. This is the exact same amount of time that the printer spent in the vacuum environment as it printed PP-04-01-V with FTIR window #169 present in the chamber. The chamber was then vented to atmospheric pressure and FTIR window #170 was removed and stored in its sealed container. Following these two tests the two FTIR windows were sent to Dr. Ugo Lafont at ESTEC for analysis.

5.3.2.2 Outgassing Test Results

The two FTIR windows were analyzed for contaminants at the Materials' Physics & Chemistry Section, Components and Materials' Physics and Chemistry Evaluation & Standardisation Division at ESTEC according to procedure "ESA-TECQTE-LAB-PR-0894 iss. 1, rev. 3, 12/06/2017". The results were returned in the form of Table 10 below and two FTIR spectra which can be found in Appendix F

– FTIR Analysis of Outgassing Windows. Table 10 shows the contaminants that were found on each of the two FTIR windows.

Window #169 was exposed to the vacuum environment with the printer printing component PP-04-01-V and window #170 was exposed to the same vacuum environment, with the printer present and turned on but not printing, for the same amount of time. Table 10 gives the contamination level for four types of contaminants along with the uncertainty (Δ) for both windows. The four types of contaminants measured were: A – Hydrocarbons, B – Esters, C – Methyl silicones, D – Methyl-phenyl silicones. All values are given with the units 10^{-7} g/cm^2 .

Sample	Location/ Description	A*	B*	C*	D*	Total MOC
		ΔA^{**}	ΔB^{**}	ΔC^{**}	ΔD^{**}	$\Delta \text{Total MOC}$
#169	Contamination during 3D printing	0.6	<0.5	<0.1	<0.2	0.6
		0.3	0.5	0.2	0.3	0.0.7
#170	Contamination during 3D printing	0.5	<0.5	<0.1	<0.2	0.5
		0.3	0.5	0.2	0.3	0.0.7

Table 10: Contaminants recorded in the vacuum chamber while printing (#169) and not printing (#170)

Table 10 shows that there is little difference in the levels of detected contaminants between the tests. The values for all contaminants, except for A, are identical for both windows. While the value of the A (hydrocarbon) is larger for the window that was exposed to the vacuum environment while the UM2+ was printing it only differs by $0.1 \cdot 10^{-7} \text{ g/cm}^2$, a value well below the $0.3 \cdot 10^{-7} \text{ g/cm}^2$ uncertainty of the measurement. There is therefore no noticeable increase in volatile outgassing products while the FFF process is being carried out in this vacuum environment.

Although there is no noticeable difference this is only applicable to the FFF fabrication of a component from polycarbonate filament, a printhead temperature of 260 °C, a buildplate temperature of 110 °C and a pressure of roughly 1000 Pa. The use of a different thermoplastic filament, processing temperatures or environmental pressure may result in noticeable outgassing during the FFF process. The use of a different printer or printhead could also change the level of outgassing. Tests with different FTIR window placement could also yield different results. Outgassing risks should still be carefully considered in future testing, especially if polymers with higher TML, higher processing temperatures or lower environmental pressures are used however this test shows that the FFF process can be carried out in a vacuum environment with undue risk of contaminating the test equipment providing outgassing is carefully considered.

6 Mechanical Property (MP) Series Components

To assess the feasibility of using the FFF process in an on-orbit environment the quality of components must be investigated. The quality of polycarbonate components fabricated in the vacuum environment includes both qualitative and quantitative parameters. Aspects of the fabricated components that need to be quantitatively investigated include the dimensions, mass, and mechanical properties. Qualitative analysis of polycarbonate components fabricated in a vacuum environment is mainly focused on the number and severity of defects in the components. To investigate these parameters a series of components needed to be designed to allow for accurate observations to be made. These components were named the “Mechanical Property” (MP) components and include the MP-01 flexural component, the MP-02 tensile component and the MP-03 compressive component

6.1 Overview

When designing the components used for evaluating the FFF process in a vacuum environment the most important factor that was considered was the testing standards. The tests which are used to determine the mechanical properties of materials typically require the test components to have specific geometries. This is to ensure the data generated by the test is accurate. These tests usually follow standards from organizations such as ASTM or ISO. As the mechanical tests require components of specific geometry they were chosen to be the components used for evaluation of the performance of the FFF process in a vacuum environment. Using the mechanical testing components to evaluate the FFF process maximizes the number of aspects of the process that can be investigated by using the limited vacuum chamber time in the most efficient manner.

Following the decision to use the mechanical property testing components for evaluation of the FFF process the specific mechanical tests, and the appropriate test components, needed to be chosen. As there is no data available at the time of writing on the mechanical properties of polymers fabricated using FFF in an on-orbit environment it was decided that the focus of the mechanical testing would be on very basic properties such as tensile and compressive strength and Young’s modulus. To determine the specific tests that should be carried out, NASA’s plan for material characterization of components fabricated by the 3DP on the ISS was consulted. The NASA test plan included three mechanical tests for components fabricated using FFF in a microgravity environment aboard the ISS. These tests were a tensile test, compressive test and flexural (3-point bending) test. These tests were carried out according to ASTM standards, following D638, D697 and D790 for the tensile, compressive and flexural tests respectively. [7]

With the mechanical tests chosen the actual test components themselves could be designed in CAD. Although the geometry of these components was based on the geometry given in the relevant ASTM standard some modifications needed to be made to ensure the component was compatible with the available testing equipment. Technicians at DASML were consulted to ensure the component geometry was appropriate for the testing machines. In addition to being used for the mechanical property testing, these components were used to investigate the performance of the FFF process in a vacuum environment including parameters such as mass, density and dimensional accuracy.

To accurately determine the quality of components fabricated using FFF in a vacuum environment they needed to be compared against the exact same components which were fabricated in a normal atmosphere. Each set of MP series components was further broken down into two distinct sub-sets: components fabricated in a normal atmospheric environment and components fabricated in a vacuum environment. Components fabricated in an atmospheric environment were given a suffix of

“-A” in their component ID and those fabricated in vacuum received a suffix of “-V”. Each sub-set of components consists of at least five components printed in the appropriate pressure environment. The vacuum and atmosphere component sub-sets were fabricated with the exact same printing variables except for the pressure.

6.2 Flexural Component

The flexural test that was to be carried out was a 3-point bending test which followed the ASTM D790 standard. The component associated with this test was given the designator MP-01 and will be referred to as the MP-01 component or the flexural test component later in this report. To determine the geometry of the flexural test component the lab manual for the ASTM D790 test from DASML and the ASTM D790 standard itself were consulted. The DASML manual for the D790 test suggests using a thickness, in the vertical direction, of 2 mm for all tests. This thickness was chosen for the MP-01 component as it would ensure the component was compatible with the available testing equipment. After the thickness had been chosen the ASTM standard was consulted for the other dimensions.

There is no category in ASTM D790 specifically for components fabricated using FFF, so the most appropriate category needed to be chosen. It was decided that the FFF printed polycarbonate best fit in Section 7.3 of ASTM D790, “Sheet Materials (Except Laminated Thermosetting Materials and Certain Materials Used for Electrical Insulation, Including Vulcanized Fiber and Glass Bonded Mica)” and Subsection 7.3.1 “Materials 1.6 mm (1/16 in.) or Greater in Thickness”. This sub-section of the ASTM D790 standard specifies that “Specimens 3.2 mm or less in depth shall be 12.7 mm (1/2 in.) in width. The specimen shall be long enough to allow for overhanging on each end of at least 10 % of the support span, but in no case less than 6.4 mm (1/4 in.) on each end. Overhang shall be sufficient to prevent the specimen from slipping through the supports. A support span of 16 ± 1 times the depth of the specimen is used for these specimens.” [69]. This specifies the width of the MP-01 flexural test component as 12.7 mm. The only remaining dimension that needed to be determined was the length which, when using a span to thickness ratio of 16:1 and an overhang of 6.4 mm on each side, must be at least 44.8 mm long. The final length of the flexural test component was chosen to be 50 mm to allow for extra overhang of 2.6 mm on each side. This additional overhang would prevent defects in the corners of the flexural component from influencing the test and help prevent the component from slipping between the supports. The final flexural test component was therefore chosen to be a rectangular prism 2 mm x 12.7 mm x 50 mm and is shown in Figure 47.

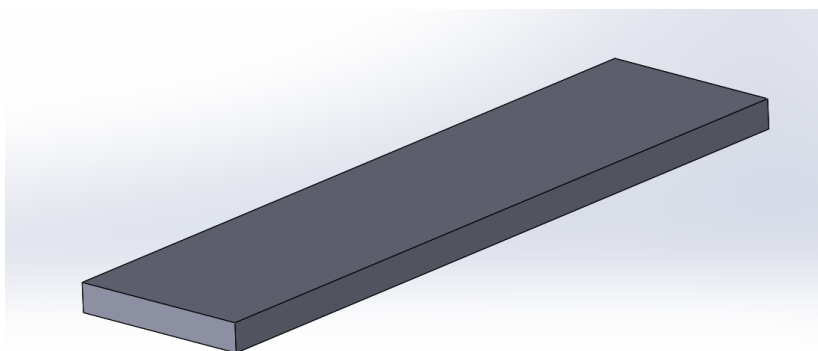
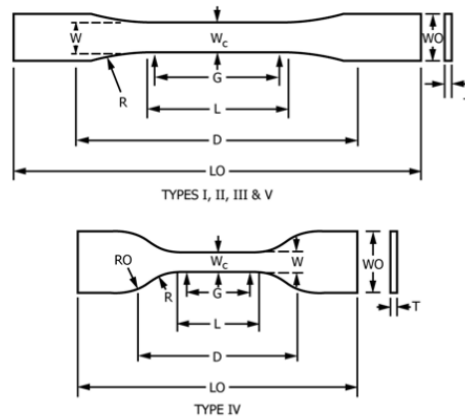


Figure 47: MP-01, a modified ASTM D790 flexural testing component

6.3 Tensile Component

The tensile test that was carried out followed ASTM D638. The component associated with this test was given the designator MP-02 and will be referred to as the MP-02 component or the tensile test

component later in this report. The general geometry of this component follows the Type I component laid out in the ASTM D638 standard as shown below in Figure 48 with the Type I dimensions highlighted in yellow. The Type I component was chosen as the basis for the MP-02 component because ASTM D638 states that the Type I component is the preferred component geometry. [70]



Dimensions (see drawings)	Specimen Dimensions for Thickness, T , mm (in.) ^A				Tolerances	
	7 (0.28) or under	Over 7 to 14 (0.28 to 0.55), incl	4 (0.16) or under			
	Type I	Type II	Type III	Type IV ^B	Type V ^{C,D}	
W —Width of narrow section ^{E,F}	13 (0.50)	6 (0.25)	19 (0.75)	6 (0.25)	3.18 (0.125)	±0.5 (±0.02) ^{B,C}
L —Length of narrow section	57 (2.25)	57 (2.25)	57 (2.25)	33 (1.30)	9.53 (0.375)	±0.5 (±0.02) ^C
W_O —Width overall, min ^G	19 (0.75)	19 (0.75)	29 (1.13)	19 (0.75)	...	+ 6.4 (+ 0.25)
W_O —Width overall, min ^G	9.53 (0.375)	+ 3.18 (+ 0.125)
L_O —Length overall, min ^H	165 (6.5)	183 (7.2)	246 (9.7)	115 (4.5)	63.5 (2.5)	no max (no max)
G —Gage length ^I	50 (2.00)	50 (2.00)	50 (2.00)	...	7.62 (0.300)	±0.25 (±0.010) ^C
G —Gage length ^I	25 (1.00)	...	±0.13 (±0.005)
D —Distance between grips	115 (4.5)	135 (5.3)	115 (4.5)	65 (2.5) ^J	25.4 (1.0)	±5 (±0.2)
R —Radius of fillet	76 (3.00)	76 (3.00)	76 (3.00)	14 (0.56)	12.7 (0.5)	±1 (±0.04) ^C
R_O —Outer radius (Type IV)	25 (1.00)	...	±1 (±0.04)

Figure 48: Geometry of an ASTM D638 component with Type I highlighted in yellow [70]

The MP-02 tensile component differs from the Type I component detailed in ASTM D638 [70] as it has slightly extended sections at either end where the machine grips the component. This is to ensure that the testing machine grips have enough area to grip the component and to allow the component to reach the alignment tabs on the testing machine. The final MP-02 test component is shown in Figure 49.

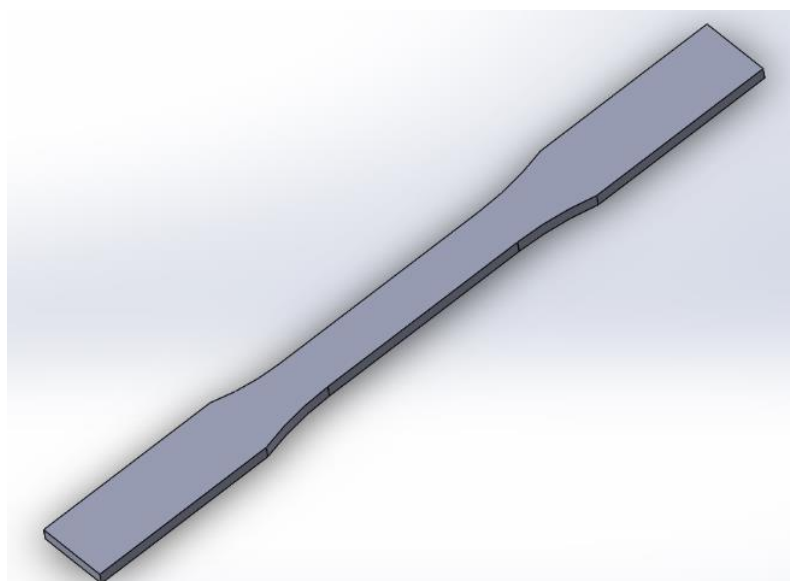


Figure 49: MP-02, a modified Type I ASTM D638 tensile testing component

6.4 Compressive Component

The compressive test that was to be carried out followed the ASTM D695 standard. The component associated with this test was given the designator MP-03 and will be referred to as the MP-03 component or the compressive test component later in this report. ASTM D695 specifies that the test component *“shall be in the form of a right cylinder or prism whose length is twice its principal width or diameter. Preferred specimen sizes are 12.7 by 12.7 by 25.4 mm (0.50 by 0.50 by 1 in.) (prism), or 12.7 mm in diameter by 25.4 mm (cylinder).”* [71] After discussion with DASML technicians it was determined that a cylindrical component 12.7 mm in diameter, 25.4 mm in height would be compatible with the available testing machines. Therefore, the compressive test component, MP-03, was chosen to exactly follow the ASTM D695 recommended geometry. The MP-03 component is shown in Figure 50 and has a nominal diameter of 12.7 mm and a nominal height of 25.4 mm.

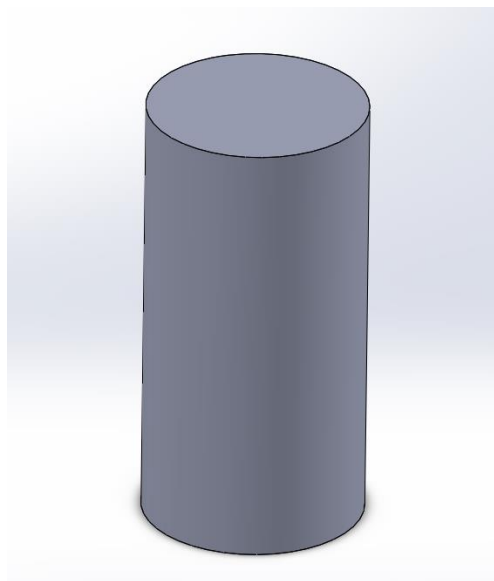


Figure 50: MP-03, a ASTM D695 compressive testing component

6.5 Control of Variables While Fabricating MP Series Components

A large amount of care was taken to control all variables during the fabrication process of the MP series components. Care was also taken to control the variables within the set of components to ensure that the only difference between the vacuum and atmosphere subsets is the pressure.

6.5.1 Controlled Variables

To best control the variables all components were printed on a single FFF printer, the modified Ultimaker 2+ printer discussed in the Section 3.3. This printer used a non-standard hot end supplied by Johan Versteegh which was used for all printing of MP series components. All other parts of the printer were the standard parts from the Ultimaker factory and were not repaired or replaced over the course of the thesis work. The exception to this is the X, Y and Z bearings which were non-standard oil-less bearings. These were pre-installed on the printer by Ultimaker and were used for all printing. The firmware parameters of the printer itself were not changed over the course of fabrication of the MP series of components.

The pump, a vacuubrand MD-1, used to draw the vacuum was the same for the fabrication of all MP series components. This pump was turned off and isolated from the vacuum chamber by means of the valve built into the Heraeus VT 6130 M vacuum chamber. The pressure was brought to 1000 Pa for every vacuum component in the MP series. Printing was not started unless the pressure within

50 Pa of 1000 Pa. If the pressure was too high the vacuum pump was turned back on and if the pressure was too low a small amount of air was let into the chamber. As the vacuum pump was turned off and isolated from the chamber during printing the pressure could not drop during printing. Although the pressure could not drop over the course of printing it did rise slightly due to outgassing and imperfect sealing. As the same chamber was used for each vacuum print this rise in pressure was the same across each MP set of components. The pressure in the vacuum chamber during printing never exceeded 2000 Pa.

The cooling of every MP series component, both atmosphere and vacuum, was also controlled. After the fabrication process had finished the buildplate began cooling down toward room temperature. To ensure that the cooling regime of the components was consistent the components were only removed from the buildplate when the buildplate had reached 45 °C. For components printed in atmosphere the temperature was monitored and the component simply removed from the buildplate by hand when the temperature reached 45 °C. For the vacuum components the printer was left in the vacuum environment until the buildplate reached 45 °C. The vacuum chamber was then brought up to atmospheric pressure, the door opened and the component removed. Although the buildplate takes longer to cool down in the vacuum environment this ensures that each component has reached the same, relatively low, temperature before being handled.

Care was also taken to ensure the material used to fabricate all MP series components was kept consistent. The material used to fabricate all MP series components came from a single 750 g spool of Ultimaker brand, 2.85 mm diameter, black, polycarbonate filament. This spool of material was stored in a sealed bag in the cleanroom which was only opened when needed.

6.5.2 Uncontrolled Variables

There were also several variables which changed between the atmosphere and vacuum components. The most important of these is the ambient temperature. The atmosphere components were printed in the open atmosphere of the cleanroom and the ambient temperature was therefore very constant at ~25 °C. The vacuum components were printed in an enclosed volume causing the temperature to rise over the course of printing. This is due to the high temperatures of the buildplate and printhead during printing. The wall temperature of the vacuum chamber was recorded for several components and found to peak at ~28 °C. It is possible that this raised temperature, when compared to the temperature of the atmosphere environment, could change the material properties. It is important to note that this temperature rise is the same for all vacuum components and that the vacuum chamber heaters were not used at any point.

Another difference was how the material was fed to the printhead. When fabricating MP series components in atmosphere material was fed directly from the spool into the printer. When fabricating MP series components in the vacuum environment the needed length of filament was measured and separated from the spool which was then returned to the sealed bag. The separate length of material was then inserted into the printer which then fabricated the MP series component in the vacuum environment. This was done to avoid exposing the entire spool of polycarbonate material to the vacuum environment each time an MP component was fabricated in the vacuum environment. This served to reduce outgassing and to prevent degradation of the material. It is possible, although unlikely, that this difference could have effects on the properties of the fabricated components.

The amount of material in the vacuum chamber also varied from print to print. This was because the vacuum chamber was in use by other researchers during the thesis research. Objects, particularly

wiring, were added and removed from the chamber between prints. This additional material could outgas differently, altering the properties of the fabricated components.

6.6 MP Series Cura Profile

Cura, a piece of slicing software developed by Ultimaker, was used to convert the geometry in the CAD file to g-code which could be sent to the printer. Cura provides an enormous number of parameters which can be changed to change how the g-code is generated and ultimately how the components are printed. For the entire MP series of components, a single Cura profile was used. This profile was titled “Solid No Brim” and is shown in Appendix G– “Solid No Brim” Cura Profile.

There are several key points of this profile. The infill percentage for this profile is 100% which means that the component is solid. This was done to allow for a mass analysis and to provide an upper boundary of the strength of polycarbonate fabricated using FFF in a simulated on-orbit environment. The solid infill also allows the grips of the mechanical testing machines to firmly grip the component without the risk of crushing it and altering the mechanical properties.

The infill is printed in layers alternating at 45° and 135°. This was chosen as it creates a quasi-isotropic component and because it is the most common orientation for infill. There are three concentric threads (a wall thickness of 1.2 mm) of PC which run along the perimeter of each layer. This was chosen as it was the minimum number of threads which gave dimensionally accurate printing in previous tests. The layer height chosen was 0.2 mm to keep print times low.

7 Quality of Components Printed in a Vacuum Environment

After it was established that the experimental apparatus could function in the vacuum environment the quality of the components fabricated in the vacuum environment was evaluated. The quality of the fabricated components includes the dimensional accuracy, the mass and the volume of the components. It also includes a qualitative analysis of the components including identifying defects or systemic errors in the components. Statistical t-tests were applied to compare various parameters of the vacuum and atmosphere sub-sets, with a confidence level of 0.05. Where data for both atmosphere and vacuum components is presented in tables, the atmosphere components are colour coded yellow and the vacuum components are colour coded blue.

7.1 Dimensional Analysis

The first aspect of the MP series components that was investigated was the dimensional accuracy. This was done by selecting several dimensions of interest for each of the three sets of MP series components. These dimensions were measured with digital calipers and the dimensions of the vacuum and atmosphere sub-sets were compared with statistical t-tests. The results were analyzed and conclusions were drawn.

7.1.1 Procedure

The dimensional accuracy of the components fabricated in a vacuum environment was the first aspect that was investigated. Dimensional accuracy of components fabricated is very important in situations where components interface with each other or where accurate positioning is required. To investigate the dimensional accuracy of components fabricated with FFF in a vacuum environment several dimensions on each component were measured using a set of digital calipers. Each dimension was measured several times at various points along the dimension with the measurements being averaged to arrive at a more accurate final dimension. After all the dimensions had been measured the dimensions of the atmosphere and vacuum subsets were compared with each other, and with the nominal dimension from the CAD file, to determine any patterns. Statistical t-tests were also carried out for each measured dimension to determine any statistical differences between the atmosphere and vacuum subsets. These t-tests were carried out in Excel using the built in “T.TEST” function. The test assumed two-tailed and Type 2 (Two-sample equal variance (homoscedastic)). Analysis and statistical tests were also applied to the volumes of the components to identify any differences.

7.1.2 Flexural Components

The MP-01 flexural component is a rectangular prism with three dimensions that were measured and analyzed: the height, the width and the length. Nominally the MP-01 component has a height of 2 mm, a width of 12.7 mm and a length of 50 mm. The measured dimensions are shown below in Table 11 along with the error of the measured dimension compared to the nominal dimension in both mm and percentage. As noted above each dimension is the average of several measurements which are listed in the complete data set for the flexural components in the “Component Database” Excel sheet.

Component ID	Height (mm)	Height Error (mm)	Height Error (%)	Width (mm)	Width Error (mm)	Width Error (%)	Length (mm)	Length Error (mm)	Length Error (%)
MP-01-01-A	2.15	0.15	7.40	12.64	-0.06	-0.47	49.93	-0.07	-0.14
MP-01-02-A	2.18	0.18	9.20	12.72	0.02	0.16	49.98	-0.02	-0.05
MP-01-03-A	2.15	0.15	7.70	12.70	0.00	-0.02	49.97	-0.03	-0.07

MP-01-04-A	2.16	0.16	8.10	12.71	0.01	0.11	49.94	-0.06	-0.12
MP-01-05-A	2.15	0.15	7.40	12.70	0.00	-0.02	49.94	-0.06	-0.12
Atmosphere Average	2.16	0.16	7.96	12.69	-0.01	-0.05	49.95	-0.05	-0.10
MP-01-06-V	2.16	0.16	8.10	12.78	0.08	0.60	49.98	-0.02	-0.04
MP-01-07-V	2.15	0.15	7.50	12.80	0.10	0.76	49.98	-0.02	-0.04
MP-01-08-V	2.16	0.16	8.10	12.79	0.09	0.69	50.00	0.00	0.01
MP-01-09-V	2.09	0.09	4.60	12.80	0.10	0.77	50.06	0.06	0.13
MP-01-10-V	2.16	0.16	8.10	12.77	0.07	0.54	50.01	0.01	0.01
Vacuum Average	2.15	0.15	7.28	12.79	0.09	0.67	50.01	0.01	0.02

Table 11: Dimensions of flexural components

It can be seen in Table 11 that the height of every flexural component, both vacuum and atmosphere, is larger than the nominal height of 2 mm. This may be due to roughness that was observed on the top of all flexural components. This roughness appears as a small ridge present on top of every polycarbonate thread that makes up the top surface of the flexural component. This roughness is discussed more in depth in Section 7.3. A statistical t-test was performed to compare the heights of the vacuum and atmosphere sub-sets and it returned a value 0.396. This is well above the chosen confidence level of 0.05 showing that there is no significant difference in the height of the two sub-sets of the flexural components.

The width of the MP-01 flexural components is nominally 12.7 mm. The width of the flexural components, shown in Table 11, appears to have more of an obvious pattern than the height. The components printed in atmosphere, with the exception of MP-01-01-A, are very dimensionally accurate differing from the nominal value by only 0.16%. MP-01-01-A differs from the nominal width by a much larger amount, -0.47% however this seems to be an outlier. The width of the components printed in vacuum are consistently farther from the nominal width with the closest width, MP-01-10-V, being 0.54% wider than nominal and MP-01-09-V being the most dimensionally inaccurate width with a width 0.77% wider than nominal. In addition to the greater dimensional error exhibited by the components printed in vacuum all the components printed in vacuum have a larger width than nominal. This is contrasted with the atmosphere components which have widths both larger and smaller than nominal. The t-test comparing the widths of the vacuum and atmosphere components returned a value of 0.0003. This shows that the widths of the two sub-sets are statistically different. It is hypothesized that this difference may be due to the slower cooling of components printed in a vacuum environment. This slower cooling may cause the component to remain soft for a greater period allowing it to squish and spread out on the buildplate as further layers are printed. It is expected that this phenomenon will manifest when measuring the dimensions parallel to the buildplate for all MP series components.

The length of the MP-01 flexural components is nominally 50 mm. The measured length of the flexural components seems to follow the same pattern as the width with the components fabricated in atmosphere having a smaller length than those printed in a vacuum environment. It is thought that this difference is caused by the phenomenon noted above where the components printed in vacuum remain malleable for longer causing the lower layers to compress and spread due to the weight of the layers printed above. Interestingly, the lengths of the components printed in the vacuum were more dimensionally accurate when compared to the nominal value. The vacuum fabricated components range from 0.04% smaller than nominal to 0.13% larger. This is contrasted with the atmosphere components which range from 0.14% to 0.05% smaller than nominal. The t-test

comparing the lengths of the vacuum and atmosphere components returned a value of 0.011, well below the confidence level of 0.05. This means there is a statistical difference between the lengths of the MP-01 flexural components fabricated in vacuum and atmosphere. It should be noted that both the lengths and widths of the flexural components are statistically different.

The volumes of the MP-01 flexural components were also calculated for comparison. The volume of each MP-01 component was calculated by multiplying the height by the width by the volume and is shown in Table 12 along with the error of the calculated volume compared to the nominal volume in both mm³ and percentage. The nominal volume of the MP-01 flexural component is 1270 mm³.

Component ID	Volume (mm ³)	Volume Error (mm ³)	Volume Error (%)
MP-01-01-A	1355.58	85.58	6.74
MP-01-02-A	1388.36	118.36	9.32
MP-01-03-A	1366.64	96.64	7.61
MP-01-04-A	1372.73	102.73	8.09
MP-01-05-A	1362.18	92.18	7.26
Atmosphere Average	1369.10	99.10	7.80
MP-01-06-V	1380.59	110.59	8.71
MP-01-07-V	1375.07	105.07	8.27
MP-01-08-V	1382.49	112.49	8.86
MP-01-09-V	1340.38	70.38	5.54
MP-01-10-V	1380.39	110.39	8.69
Vacuum Average	1371.79	101.79	8.01

Table 12: Volumes of flexural components

It can be seen in Table 12 that every flexural component, from both the atmosphere and vacuum sub-sets, is noticeably larger than the nominal volume. This ranges from 5.54% larger for component MP-01-09-V to 9.32% larger for MP-01-02-A. This larger volume is likely related to the heights of all flexural components being larger than nominal. It is possible that the measurement of the height measured to the top of the ridges on the component, causing an overestimation of volume as the ridges contain less volume than a filled volume with the same height. Comparing the vacuum and atmosphere sub-sets does not seem to show any pattern with a seemingly random distribution of volumes. This is confirmed by the t-test comparing the volumes, which returned a value of 0.789, showing that there is no statistical difference between the two volume subsets.

7.1.3 Tensile Components

For the dimensional analysis of the MP-02 tensile component only two dimensions were recorded and analyzed: the height and width of the narrow, central section. These dimensions were chosen as they needed to be recorded for the determination of the tensile stress during the tensile testing. While there were other dimensions that could have been analyzed on the MP-02 components, such as the height and width of the grip sections, these were not measured as they were only needed to hold the component during tensile testing and were not used for calculation of tensile strength.

Nominally, the thickness of the narrow section of the MP-02 component is 3.2 mm and the width of the narrow section is 13 mm. The measurements of these two dimensions are shown below in Table 13 with the error of the measured dimension compared to the nominal dimension in both mm and percentage. As noted above, each dimension is the average of several measurements which are listed in the complete data set for the tensile components in the "Component Database" Excel sheet.

Component ID	Average Thickness (mm)	Thickness Error (mm)	Thickness Error (%)	Average Width (mm)	Width Error (mm)	Width Error (%)
MP-02-01-V	3.29	0.09	2.94	13.25	0.25	1.94
MP-02-02-V	3.28	0.08	2.63	13.19	0.19	1.43
MP-02-03-V	3.33	0.13	4.12	13.19	0.19	1.49
MP-02-04-V	3.25	0.05	1.62	13.24	0.24	1.82
MP-02-05-V	3.27	0.07	2.06	13.23	0.23	1.80
Vacuum Average	3.29	0.09	2.67	13.22	0.22	1.70
MP-02-06-A	3.39	0.19	6.06	13.21	0.21	1.58
MP-02-07-A	3.32	0.12	3.75	13.20	0.20	1.57
MP-02-08-A	3.33	0.13	3.94	13.12	0.12	0.91
MP-02-09-A	3.35	0.15	4.75	13.09	0.09	0.72
MP-02-10-A	3.33	0.13	4.06	13.07	0.07	0.55
Atmosphere Average	3.34	0.14	4.51	13.14	0.14	1.07

Table 13: Dimensions of tensile components

Looking at the thickness of the narrow section of the tensile component in Table 13 the thickness of all the tensile components is larger than the nominal thickness, regardless of if the component was fabricated in atmosphere or vacuum. This is similar to the observed heights of the MP-01 flexural components which were all larger than nominal. This excess thickness could be caused by the same ridges on the top surface that were observed on the flexural components. This is further discussed in Section 7.3. The statistical t-test comparing the thickness of the narrow section of the tensile component returned a value of 0.016 which means there is a statistical difference. This can be seen when looking at the averages with the atmosphere components having an average height of 3.34 mm (0.14 mm above nominal) and the vacuum components have an average height of 3.29 mm (0.09 above nominal). This is interesting as there was no significant difference in the heights of the flexural components which is a very similar dimension. Further study with a greater sample size and a range of components with varying heights would be useful to determine if the environment a component is fabricated in results in a significant difference in height.

The width of the narrow section of the tensile component was also investigated. It can be seen in Table 13 that the widths of all the tensile components are greater than the nominal value of 13 mm showing that the UM2+ overprinted the width, even in an atmosphere environment. Comparing the atmosphere and vacuum subsets the atmosphere components have an average width of 13.14 mm while the vacuum components have an average width of 13.22 mm. A t-test comparing the widths of the narrow sections returns a value of 0.029, below the chosen confidence level of 0.05, showing that there is a statistical difference. This pattern of the vacuum components having a significantly lower thickness/height and a significantly larger width (and length in the case of the flexural components) correlates with the hypothesis that the reduced cooling in the vacuum environment is allowing the vacuum components to remain malleable for longer during fabrication. This could cause the component to be compressed and spread due to the weight of further layers.

A volumetric analysis was not conducted for the tensile components due to the difficulty in measuring the geometry. As the dimensions of the components were measured with calipers it was not possible to obtain accurate measurements of curved surfaces. The MP-02 tensile component contains a curved surface between each grip section and the central narrow section. As it was not

possible to establish accurate measurements of this section an accurate volume could not be calculated. Further studies on components with curved, of otherwise difficult to measure, geometries will need to use an alternative measuring technique, such as 3D scanning to obtain accurate measurements of volume for analysis.

7.1.4 Compressive Components

The MP-03 flexural component is a cylinder, allowing for two dimensions to be recorded for analysis: the height and the diameter. Nominally the MP-03 component has a height of 25.4 mm and a diameter of 12.7 mm. The measured dimensions are shown below in Table 14 along with the error of the measured dimension compared to the nominal dimension in both mm and percentage. Each dimension is the average of several measurements which are listed in the complete data set for the compressive components in the “Component Database” Excel sheet.

Component ID	Average Height (mm)	Height Error (mm)	Height Error (%)	Average Diameter (mm)	Diameter Error (mm)	Diameter Error (%)
MP-03-01-V	25.22	-0.18	-0.72	12.81	0.11	0.89
MP-03-02-V	25.27	-0.13	-0.52	12.70	0.00	0.02
MP-03-03-V	25.25	-0.15	-0.60	12.66	-0.04	-0.29
MP-03-04-V	25.27	-0.13	-0.52	12.75	0.05	0.42
MP-03-05-V	25.26	-0.14	-0.57	12.74	0.04	0.35
Vacuum Average	25.25	-0.15	-0.59	12.74	0.04	0.28
MP-03-06-A	25.36	-0.04	-0.17	12.79	0.09	0.73
MP-03-07-A	25.35	-0.05	-0.21	12.78	0.08	0.65
MP-03-08-A	25.31	-0.10	-0.37	12.72	0.02	0.12
MP-03-09-A	25.40	0.00	-0.02	12.78	0.08	0.61
MP-03-10-A	25.37	-0.03	-0.13	12.82	0.12	0.93
Atmosphere Average	25.35	-0.05	-0.18	12.78	0.08	0.61

Table 14: Dimensions of compressive components

It can be seen in Table 14 that every compressive component, except for MP-03-09-A, has a height smaller than the nominal value. It can also be seen that the average height of the vacuum components is 0.1 mm shorter than the components printed in atmosphere. The t-test on the height of the compressive components returned a value of 0.0004, indicating that there is a significant difference in the heights of the atmosphere and vacuum components to a very high level of confidence.

Looking at the diameter of the compressive components in Table 14 the diameter of the atmosphere components is on average only 0.04 mm larger than the vacuum components. This shows that the diameters are in general quite similar. The t-test comparing the diameters of the atmosphere and vacuum components returned a value of 0.203, well above the chosen confidence level of 0.05 showing that there is no statistical difference. This does not correlate the above-mentioned theory of vacuum components being shorter with larger dimensions in planes parallel to the buildplate. This may be due to the different shape of the diameter dimension, as the diameter is measuring a curved surface.

The volumes of the MP-03 compressive components were also calculated for comparison. The volume for each MP-03 component was calculated following the equation of the volume of cylinder

using the height and radius of each component. The volume of each MP-03 component is shown in Table 15 below, along with the error of the calculated volume compared to the nominal volume in both mm³ and percentage. The nominal volume of the MP-03 compressive component is 3217.6 mm³.

Component ID	Volume (mm ³)	Volume Error (mm ³)	Volume Error (%)
MP-03-01-V	3251.55	33.96	1.06
MP-03-02-V	3202.31	-15.28	-0.47
MP-03-03-V	3179.65	-37.94	-1.18
MP-03-04-V	3227.57	9.98	0.31
MP-03-05-V	3221.70	4.11	0.13
Vacuum Average	3216.56	-1.03	-0.03
MP-03-06-A	3259.41	41.82	1.30
MP-03-07-A	3252.78	35.19	1.09
MP-03-08-A	3213.49	-4.10	-0.13
MP-03-09-A	3256.28	38.69	1.20
MP-03-10-A	3273.56	55.97	1.74
Atmosphere Average	3251.11	33.52	1.04

Table 15: Volumes of compressive components

In Table 15 it is seen that the average volume of the vacuum components is very close to the nominal volume while the atmosphere components are approximately 1% larger on average. There also appears to be a large spread of the volume data with some components from each sub-set being above and below the nominal volume and a wide range in the magnitude of the volume errors. The t-test returned a value of 0.059, only slightly above the chosen confidence level of 0.05. Although this shows that there is no statistical difference it is possible this may change if studies are conducted with a larger sample size or difference geometries.

7.2 Mass Analysis

The masses of all MP series components were investigated to determine the differences between components printed in vacuum, components printed in atmosphere and an ideal reference component made of solid polycarbonate. Following determination of the masses of the components, statistical t-tests was carried out to determine if there were significant differences between the components printed in atmosphere and vacuum.

7.2.1 Procedure

The mass of each component in the MP series was determined by weighing the component on the Mettler Toledo Classic balance shown in Figure 51. Each component was weighed three times with the final mass being determined by taking the average of the three measurements.



Figure 51: The Mettler Toledo Classic analytical balance used for mass analysis

The mass of the reference component was determined by applying “High Viscosity PC” material to the Solidworks CAD model of the component and using the mass evaluation function. The “High Viscosity PC” material in SolidWorks assumes that the component is composed of polycarbonate with a constant density of 1.19 g/cm^3 .

After tabulation of the mass of each component a t-test was carried out to compare the mass of components produced in atmosphere and vacuum. The t-test used two sets of data with five data points each. The first set of data was the average mass of each component produced in atmosphere and the second set was the average mass of each component produced in vacuum.

7.2.2 Flexural Components

The MP-01 series of flexural test components, have a nominal mass of 1.511 g each. Table 16 below shows the measured mass of each component as well as the difference between the average mass and the nominal mass in grams and percentage. The mass shown is the average of several measurements which are listed in the complete data set for the flexural components in the “Component Database” Excel sheet.

Component ID	Mass (g)	Mass Error (g)	Mass Error (%)
MP-01-01-A	1.518	0.007	0.474
MP-01-02-A	1.522	0.010	0.688
MP-01-03-A	1.532	0.021	1.387
MP-01-04-A	1.535	0.024	1.588
MP-01-05-A	1.528	0.017	1.136
Atmosphere Average	1.527	0.016	1.055
MP-01-06-V	1.504	-0.007	-0.476
MP-01-07-V	1.513	0.001	0.088
MP-01-08-V	1.520	0.009	0.598
MP-01-09-V	1.481	-0.030	-1.992
MP-01-10-V	1.515	0.003	0.227
Vacuum Average	1.507	-0.005	-0.311

Table 16: Mass of the flexural test components

Table 16 shows that components produced in vacuum are generally slightly less massive than the nominal component while components produced in atmosphere are slight more massive than the nominal component. This is an interesting observation however the difference by which they vary, - 0.31% and 1.06% respectively, is very small. While this appears to be quite a small difference the t-test returned a p-value of 0.0258 well below the 0.05 threshold for statistical significance. This could be due to outgassing of the polycarbonate material in the vacuum environment.

7.2.3 Tensile Components

The MP-02 series of tensile test components have a nominal mass of 12.458 g each. Table 17 below shows the measured mass of each component as well as the difference between the average mass and the nominal mass in grams and percentage. The mass shown is the average of several measurements which are listed in the complete data set for the tensile components in the “Component Database” Excel sheet.

Component ID	Mass (g)	Mass Error (g)	Mass Error (%)
MP-02-01-V	12.37	-0.08	-0.68
MP-02-02-V	12.30	-0.16	-1.27
MP-02-03-V	12.45	-0.01	-0.09
MP-02-04-V	12.25	-0.20	-1.63
MP-02-05-V	12.28	-0.18	-1.45
Vacuum Average	12.33	-0.128	-1.02
MP-02-06-A	12.35	-0.11	-0.89
MP-02-07-A	12.42	-0.04	-0.29
MP-02-08-A	12.38	-0.08	-0.62
MP-02-09-A	12.35	-0.11	-0.87
MP-02-10-A	12.37	-0.08	-0.68
Atmosphere Average	12.38	-0.08	-0.67

Table 17: Mass of tensile test components

The mass of all the tensile components is below the nominal mass, the same as with the flexural components above. This is expected as the nominal mass was calculated assuming the entire volume of the component has the same density. As components fabricated FFF are fabricated by laying down successive thin threads of plastic there could be small gaps between the threads which reduce the mass. Comparing the masses with a t-test returns a value of 0.274, well above the confidence level of 0.05 therefore there is no difference between the masses of the tensile components fabricated in atmosphere and vacuum.

7.2.4 Compressive Components

The MP-03 compressive test components have a nominal mass of 3.829 g each. Table 18 below shows the measured mass of each component as well as the difference between the average mass and the nominal mass in grams and percentage. The mass shown is the average of several measurements which are listed in the complete data set for the compressive components in the “Component Database” Excel sheet.

Component ID	Mass (g)	Mass Error (g)	Mass Error (%)
MP-03-01-V	3.803	-0.026	-0.68
MP-03-02-V	3.738	-0.091	-2.37
MP-03-03-V	3.716	-0.113	-2.96
MP-03-04-V	3.782	-0.047	-1.22

MP-03-05-V	3.752	-0.077	-2.00
Vacuum Average	3.758	-0.071	-1.85
MP-03-06-A	3.833	0.004	0.10
MP-03-07-A	3.794	-0.035	-0.91
MP-03-08-A	3.738	-0.091	-2.37
MP-03-09-A	3.815	-0.014	-0.37
MP-03-10-A	3.800	-0.029	-0.76
Atmosphere Average	3.796	-0.033	-0.86

Table 18: Mass of the compressive test components

Nearly every compressive component, except for MP-03-06-A, is less massive than the nominal component. As noted above in the Section 7.2.3 this was expected because the components were fabricated using FFF. The vacuum components are about 1% less massive than the atmosphere components on average however both sets have components that differ by less than 1% from the nominal mass and components which differ by more than 2%. Components MP-03-06-A and MP-03-08 differ from the other atmosphere components with MP-03-06-A being much more massive than the atmosphere average and MP-03-08-A being much less massive. The t-test for the mass of the compressive components gave a value 0.129 which is much higher than the 0.05 statistical significance threshold. Therefore, there is no statistical difference between the masses of the compressive components when printed in atmosphere or vacuum. This may change if MP-03-06-A or MP-03-08-A, or both were considered outliers and removed or if a larger sample size was used.

7.3 Qualitative Analysis

The qualitative analysis section focuses on identifying defect in the MP series components and determining if there are differences in the type, location or quantity of defects between the atmosphere and vacuum sub-sets. This was done by individually examining each MP series component and identifying all defects and classifying the general quality of the surfaces. Each component was photographed from a variety of angles and all defects were imaged.

7.3.1 Procedure

In addition to the quantitative dimensional accuracy analysis a qualitative analysis was also carried out on the MP series components. The aim of this qualitative analysis was to identify any systematic defects in the MP series components. This was done by examining each individual MP series component and photographing and recording any defects. These photographs and records were then analyzed for any patterns.

7.3.2 General Defects and Observations

When fabricating a component, the printhead does not begin directly printing the component. First it primes itself by extruding a blob of material in the corner of the buildplate and then moves to the perimeter of the component which it begins fabricating. This leaves a single thread of material, called a tail, which crosses the area where the bottom layer of the component will be fabricated. This causes a disruption in the alignment of the bottom layer of the component. This occurred on all components and can be seen in Figure 52. The disruption caused by the tail could be prevented by having the printhead not travel over the area to be printed on after priming.

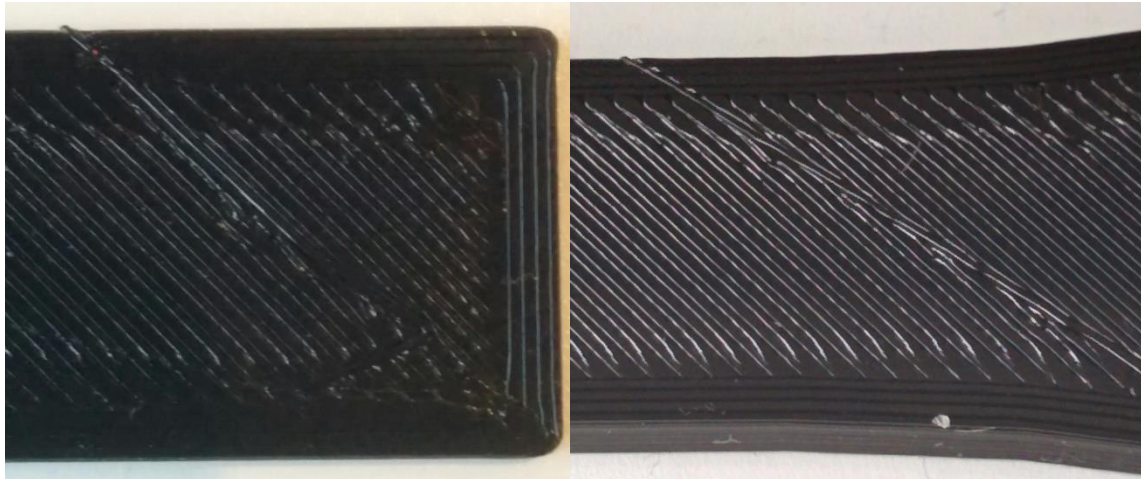


Figure 52: Tail on the bottom layer of MP-01 (L) and MP-02 (R) components

As the tail sticks out from the component it needed to be removed prior to performing any dimensional or mechanical analysis. The tail is a single thread of polymer and can therefore be removed very easily. The tail was removed with a sharp pull and snapped off from the component very close to the surface. Although the tail snapped off easily it still left a defect on the surface of the component as seen in Figure 53. This occurred on all components. It was thought that components would fracture at this defect during mechanical testing however this was not observed with fracture occurring elsewhere on the component in all mechanical tests. This defect could be avoided by changing how the printhead primes and travels.



Figure 53: Damage resulting from tail removal

There were also several instances of small bulges, dent or other defect on the components such as the bulge seen in Figure 54. These small defects occurred on various examples of all three sets of MP components. They did not seem to occur any more often on vacuum or atmosphere components and did not seem to have any effect on the mechanical testing.



Figure 54: Bulge on an MP-01 component

Another observation that was made was the difference in surface quality between the top and bottom surfaces. All components had very good surface quality on the bottom surface of the component. The bottom surface had a glassy, reflective surface as can be seen in Figure 55. The bottom surface had varying quality depending on the component however it was never as good as the bottom surface. This is because the bottom surface sits on the very smoother, glass buildplate during fabrication. While this is not an issue it is interesting to note. Components can be designed so that surfaces which require good surface finish are printed as the bottom surface.

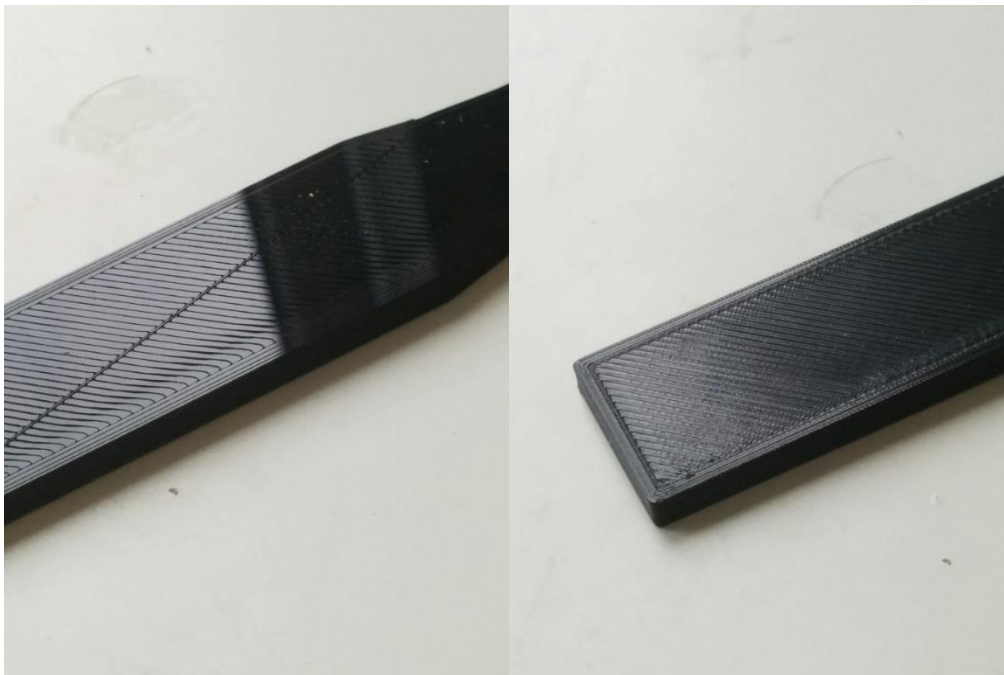


Figure 55: Top (L) and bottom (R) surfaces of an MP-02 component

7.3.3 Flexural Component Defects

The main issue that was observed on the flexural components was roughness on the upper surface. This roughness caused the height of the flexural components to consistently exceed the nominal height as discussed in Section 7.1.2. The roughness on the upper surface can be seen below in Figure 56 as the darker section on the left. It can clearly be seen that the roughness is only present in the centre of the top surface and does not occur along the perimeter. The roughness is therefore related

to the infill. The roughness occurred on all MP-01 components, both atmosphere and vacuum, and did not appear to cause any issues when testing. Although it did not cause any issues in testing it may present a problem if precise dimensions are required. This could be investigated further to determine the cause and to come up a solution.

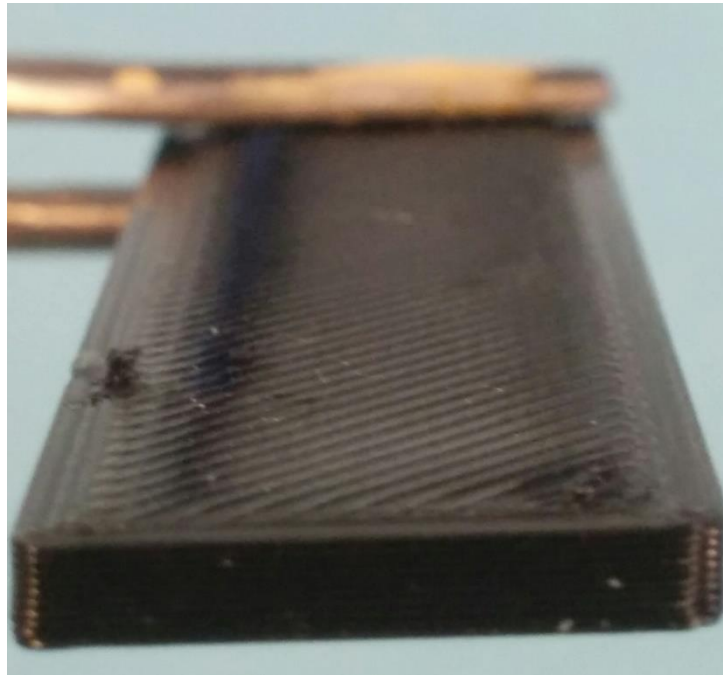


Figure 56: Roughness on the upper surface on an MP-01 component

7.3.4 Tensile Components Defects

It was observed that several tensile components had some distortion in the perimeter layers near the end. This occurred for only a few components and occurred in both atmosphere and vacuum components. This defect is characterized by non-uniformity of the perimeter threads, small gaps between perimeter threads and sometimes small bulges of material sticking out from the end. As this defect only occurred on either end of the tensile component it did not interfere with the mechanical testing however the cause should be identified. It is interesting that this defect occurred in the tensile components but not in the flexural components as the flexural components have the same geometry, with smaller dimensions, at either end.



Figure 57: Defect on bottom layer, end of MP-02 component

7.3.5 Compressive Components Defects

The only defect unique to the compressive components was a vertical seam on the outer surface. This appeared to be caused by the Z axis moving down at the same time after each layer was fabricated. This defect was present in all compressive components both atmosphere and vacuum. It was expected that this defect would be a point of failure in the compressive test however this was not the case as discussed in Section 8.3.3. This defect could be mitigated by varying the position of the printhead when the Z axis moves.



Figure 58: The seam on an MP-03 component

7.3.6 Qualitative Analysis Conclusions

In conclusion there was no noticeable qualitative difference between components fabricated in atmosphere and vacuum. There was no difference in frequency or severity of observed defects between the two sub-sets. Those defects that were observed either occurred on all components, regardless of fabrication environment or occurred seemingly randomly.

8 Mechanical Properties of Polycarbonate Fabricated Using FFF in a Vacuum Environment

The third and final goal of the thesis research was to determine the mechanical properties of PC components fabricated in vacuum using FFF. The mechanical properties of the components fabricated in vacuum were compared to those of the components fabricated in a normal atmosphere to gain insight into how the FFF process differs when carried out in vacuum and atmosphere.

It was determined that three tests would provide the most useful information for investigating the differences in the FFF process: a tensile test, a compression test and a three-point bending test. More testing, such as impact testing, fatigue testing or hardness would produce more data and yield more insight, but the above three tests would provide the most useful information in the time available. These three tests were chosen as they were the destructive tests chosen by NASA to characterize components fabricated on-orbit by the 3DP [7]. The principal goal of these mechanical tests was to compare the mechanical properties of polycarbonate fabricated using FFF in a vacuum environment and in a normal atmosphere. All mechanical testing was carried out in DASML on a Zwick 250 kN press.

8.1 Flexural Test

To investigate the flexural properties of polycarbonate printed in a vacuum environment a flexural test was carried out. This flexural test followed the ASTM D790 standard [69] as closely as possible with only a few modifications. The primary result of this test is the flexural stress at yield. The flexural test components were also qualitatively analyzed to determine how and where yielding occurred.

8.1.1 Flexural Testing Components

The components to be used for the flexural test were designated the MP-01 series of components. These components are based on the suggested test component from the ASTM D790 standard [69]. While the MP-01 components are based on the ASTM D790 standard different dimensions were chosen to make them more compatible with the available flexural testing apparatus. The MP-01 component is discussed in depth in Section 6.2

The MP-01 series of components consisted of ten test components numbered MP-01-01 to MP-01-10. This set of components consisted of two subsets, five in atmosphere and five in vacuum. These components have component IDs MP-01-01-A to MP-01-05-A and MP-01-06-V to MP-01-10-V for the atmosphere and vacuum subsets respectively.

8.1.2 Flexural Testing Procedure

The flexural test was carried out on the Zwick 250 kN press in the DASML. The basic structure of the tensile test followed the ASTM D790 standard. The three-point bending apparatus used for this test is shown in Figure 59 and came from the blue box in DASML. The three-point bending apparatus used had support and nose diameters of 10 mm, in accordance with ASTM D790 [69], and was adjusted to have a support span of 32 mm. The three-point bending apparatus was simply placed on the lower plate of the press and was not secured to the lower plate, being held in place only with the force of the moving, upper plate of the press.

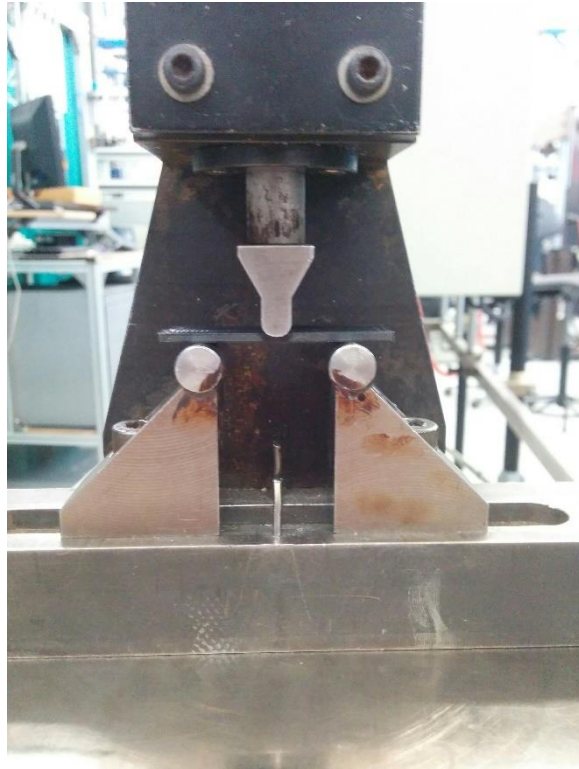


Figure 59: The three-point bending apparatus used for the flexural test

At the beginning of each flexural test the MP-01 component was removed from its labelled bag and placed in the three-point bending apparatus. The MP-01 component was placed in the three-point bending apparatus with the bottom side of the component (the smooth side which was printed on the buildplate) on the supports with the top side of the component being contacted by the moving nose. The component was aligned so that the nose of the three-point bending apparatus was parallel to the ends of the component and perpendicular to the long side of the component. The component was centred in the apparatus so that the component overhung each of the supports equally and so that it was centred along the length of the supports as seen in Figure 59. The component was aligned by eye without any aids.

The measured thickness and width the MP-01 component was then input into the connected computer to allow for automatic calculation of stresses. A preload force of 10 N was selected. The preload force was force at which the computer began recording load/displacement data. After selecting these parameters the proper displacement rate was determined using Procedure A from ASTM D790 [69]. The displacement rate was determined using Equation 1 where R is the rate of crosshead displacement, L is the support span (32 mm), d is the component thickness (the nominal value of 2 mm was used) and Z is the rate of straining in the outer fibre which according to Procedure A is equal to 0.01 mm/mm/min.

$$R = ZL^2/6d$$

Equation 1: Equation to calculate the rate of crosshead motion for the flexural test [69]

This yielded a rate of crosshead displacement of 0.85 mm/min This value was discussed with the DASML technician and was determined to be rather slow. A faster value of 2 mm/min was chosen for MP-01-01-A. This value was to be adjusted down to the Procedure A recommended value of 0.85 mm/min if the component fractured properly or adjusted to the value specified in ASTM D790 Procedure B if fracture or yield did not occur before maximum strain in the outer surface of the test

component had reached 0.05 mm/mm. This value was chosen as ASTM D790 states that the test must be terminated “when the maximum strain in the outer surface of the test specimen has reached 0.05 mm/mm (in./in.) or at break if break occurs prior to reaching the maximum strain” [69]

To determine the displacement at which the maximum strain in the outer surface of the test component had reached 0.05 mm/mm, Equation 2 was used. In Equation 2 D is the deflection at the centre of the flexural component, r is the strain (0.05 mm/mm in this limiting case), L is the support span (32 mm) and d is the component thickness (2 mm). This gave a value of 4.27 mm as the maximum crosshead displacement.

$$D = \frac{rL^2}{6d}$$

Equation 2: Equation to calculate the maximum displacement of the flexural component [69]

Although this was specified as the maximum displacement the behaviour of the polycarbonate component fabricated FFF was unknown. To gain a better understanding of the flexural behaviour the first component to be tested, MP-01-01-A, was tested to a much greater displacement. MP-01-01-A was tested until the displacement was slightly less than 14 mm at which point the test was terminated as it appeared the component might slip between the supports of the three-point bending apparatus.

As the MP-01-01-A component did not fracture before the maximum strain in the outer surface of the test component had reached 0.05 mm/mm it was decided that the flexural test would follow Procedure B from ASTM D790. Procedure B is the exact same as Procedure A except that “the rate of straining of the outer surface of the test specimen shall be 0.10 mm/mm” [69] a factor of ten increase from Procedure A. The new rate of cross head movement was then calculated using Equation 1 and was found to be 8.5 mm/min. This new value was then input as the rate of crosshead motion. A cut-off of 8 mm of displacement was also chosen. Although the displacement which ASTM D790 states the test should be terminated at is 4.27 mm it was decided that the test would be terminated at a displacement of 8 mm. This value, larger than the recommended value was chosen to allow the MP-01 component to be qualitatively analyzed at higher displacements. Terminating the test at a higher displacement does not affect the data gathered at displacements below 4.27 mm and therefore does not interfere with the quantitative analysis.

Flexural components MP-01-02-A to MP-01-10-V were then tested with the new displacement rate of 8.5 mm/min, maximum displacement of 8 mm and a preload of 10 N. During the test the top grip of the press moved downward at the specified displacement rate, pushing the loading nose of the three-point bending apparatus into the MP-01 component. The load and displacement data were recorded automatically until the component had reached a displacement of 8 mm. Displacement data was measured from the position of the loading nose with respect to the supports of the three-point bending apparatus (Type I from ASTM D790 [69]). The component was then removed from the press and stored in its labelled bag. The maximum force and the displacement at the maximum force were automatically recorded by the test computer.

Following the conclusion of flexural testing the components were photographed and analyzed. The zone of maximum stress at the centre of the bottom surface of the component was of particular interest. The data recorded by the test computer was also analyzed to determine any statistical differences between MP-01 components fabricated in atmosphere and vacuum.

8.1.3 Results and Analysis

The force/deformation curves resulting from the testing of the MP-01 flexural components are shown below in Figure 60. These figures clearly show the load on the component steadily increasing over the initial displacement of the loading nose, after which the component yields at the peak force and the load begins diminishing. As the flexural components did not fracture during testing the data acquisition ceased at chosen the termination displacement, 8 mm. Although MP-01-01-A was tested up to a displacement of almost 14 mm the data was truncated with only the first 8 mm of displacement being shown in Figure 60.

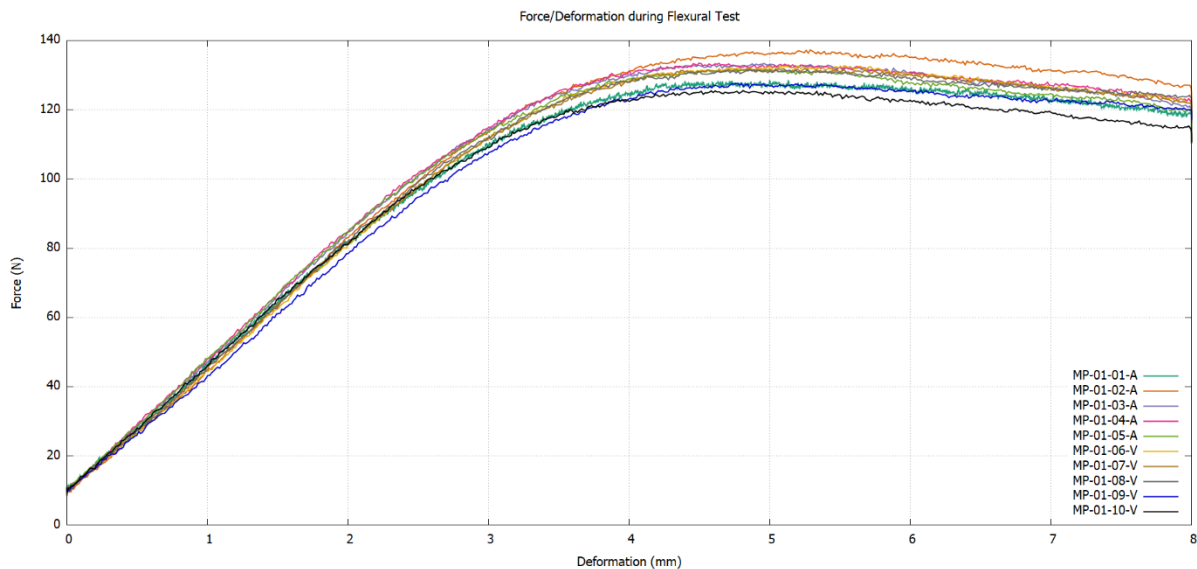


Figure 60: Force/deformation curves of the flexural test

The main parameter that was to be determined from the flexural testing was the flexural yield stress. The flexural yield stress can be calculated using Equation 3 where P is the maximum recorded force/force at yield, L is the support span (32 mm), b is the width of the component and d is the thickness of the component.

$$\sigma_f = \frac{3PL}{2bd^2}$$

Equation 3: Equation for calculation of flexural stress [69]

The maximum force, width and thickness for each flexural component, in addition to the calculated flexural yield stress are given below in Table 19. Table 19 also shows the displacement of the flexural component at the maximum force, which is also the displacement at yield.

Note 18 of ASTM D790 states that “Beyond 5% strain, this test method is not applicable” [69] meaning that flexural components which do not yield before a displacement of 4.27 mm (calculated above) should be discounted. None of the MP-01 flexural components yielded before this limit and if adhering exactly to ASTM D790 should be discarded. Although all MP-01 components yielded after the maximum 5% strain displacement of 4.27 mm all of them yielded very soon after the limit. The largest displacement at yield, MP-01-06-V was only 5.53 mm while MP-01-04-A yielded the closest to the limit at a displacement of 4.50. As the MP-01 components yielded at values only slightly above the recommended maximum displacement the data generated was still used to calculate flexural yield stress. Future testing which aims to follow ASTM D790 exactly would have to use a different

component geometry for flexural testing, perhaps a component with a greater thickness or smaller support span, to induce fracture or yield at a lower displacement.

Component ID	Max Force (N)	Flexural Yield Stress (MPa)	Displacement at Max Force (mm)	Thickness (mm)	Width (mm)	Area (mm ²)
MP-01-01-A	128.56	105.81	5.00	2.148	12.640	27.151
MP-01-02-A	137.25	108.58	5.29	2.184	12.720	27.780
MP-01-03-A	133.35	108.62	4.96	2.154	12.700	27.356
MP-01-04-A	133.48	107.85	4.50	2.162	12.710	27.479
MP-01-05-A	131.74	107.91	5.04	2.148	12.700	27.280
Atmosphere Average	132.88	107.76	4.96			
MP-01-06-V	132.74	106.66	5.53	2.162	12.780	27.630
MP-01-07-V	131.88	106.98	5.06	2.150	12.800	27.520
MP-01-08-V	131.68	105.72	5.04	2.162	12.790	27.652
MP-01-09-V	127.66	109.40	4.77	2.092	12.800	26.778
MP-01-10-V	125.51	100.93	4.81	2.162	12.770	27.609
Vacuum Average	129.90	105.94	5.04			

Table 19: Results of flexural testing

Looking at Table 19 the flexural yield strength for the atmosphere and vacuum sub-sets are very similar, differing by about 2 MPa. A t-test comparing the flexural yield stresses of the two sub-sets returns a value of 0.255, much larger than the 0.05 confidence level. This clearly shows that there is no statistical difference in flexural yield stress between components fabricated in atmosphere and those fabricated in vacuum. The result is similar when comparing the displacement at maximum force of the flexural components with the t-test returning a value of 0.655. This was expected as the average displacement at maximum force only differs by 0.08 mm between the atmosphere and vacuum components.

Qualitatively there was little to no difference between the atmosphere and vacuum flexural components. The outer surface of all atmosphere and vacuum components show the same damage with no discernable difference. This can be seen in Figure 61 which shows the outer surfaces of MP-01-03-A and MP-01-08-C, an atmosphere and vacuum component respectively. The yield zone can be seen on both components as an area which is slightly lighter than the black PC.

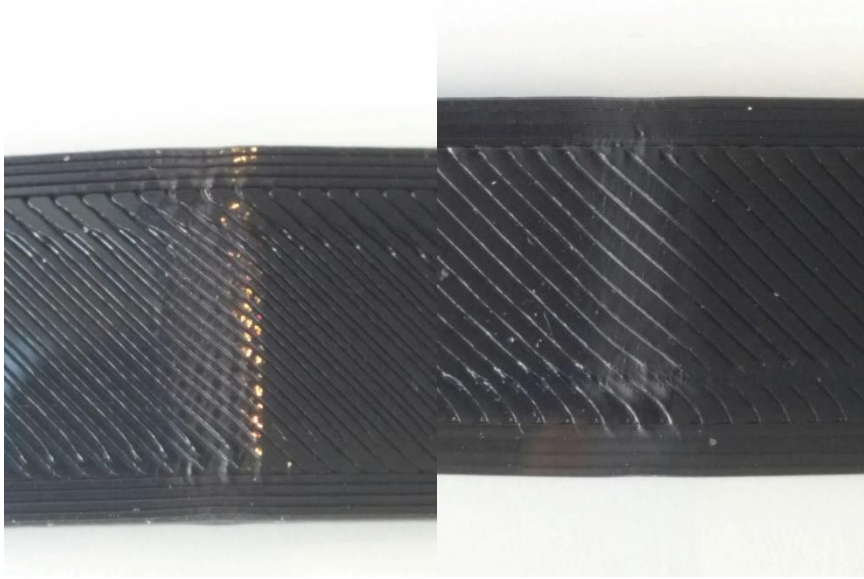


Figure 61: The yield zones of MP-01-03-A and MP-01-08-V

There was no discernable difference in the angle of the bend in the flexural components after they were removed from the 3-point bending apparatus. This can be seen in Figure 62. The exception to this is MP-01-01-A which was tested to a much higher maximum displacement and therefore shows a more acute bend angle after testing. None of the qualitative defects discussed in Section 7.3.3 appeared to be involved in the flexural yield of the MP-01 components.



Figure 62: MP-01-02-A and MP-01-07-V after flexural testing

In conclusion there was no noticeable difference in the flexural behaviour or properties of components fabricated in atmosphere and vacuum. There were no statistical differences in the flexural yield stress or the displacement at maximum force. Qualitative analysis of the MP-01 flexural components after flexural testing also failed to find any differences between the two sub-sets.

8.2 Tensile Test

To investigate the tensile properties of polycarbonate printed in a vacuum environment a tensile test was carried out. This tensile test followed the ASTM D638 standard [70] as closely as possible

with only a few modifications. The results of this test include the ultimate tensile strength, modulus of elasticity (Young's modulus), elongation at ultimate tensile strength and elongation at fracture. The tensile test components were also qualitatively analyzed to determine where the component fractured and to determine the type of fracture experienced.

8.2.1 Tensile Testing Components

The components to be used for the tensile test were designated the MP-02 series of components. These components are based on the Type I tensile test component from the ASTM D638 standard [70] as discussed above in Section 6.3. While the MP-02 components are based on the ASTM D638 Type I component they required slight modifications to make them more compatible with the available tensile testing machine. The main modification of the MP-02 components was the extension of the grip areas at either end of the dog bone shaped component to allow it to be more easily aligned in the testing machine and to be gripped more easily by the grips of the machine.

The MP-02 series of components consisted of thirteen test components numbered MP-02-01 to MP-02-13. Originally only ten MP-02 components were fabricated for the tensile test, five in atmosphere and five in vacuum however there was an issue during testing which affected two components, specifically MP-02-06-A and MP-02-08-A, which resulted in incorrect data. The problems with the extensometer experienced during testing are discussed below in the Section 8.2.2. As the data provided by the MP-02-06-A and MP-02-08-A components was incorrect it was discarded. As ASTM D638 specifies that there be a minimum of five samples in each set two additional components, MP-02-11-A and MP-02-12-A were fabricated. The MP-02 components fabricated in vacuum can be seen in Figure 63. The MP-02 components fabricated in atmosphere are seen in Figure 64.



Figure 63: MP-02-01-V to MP-02-05-V (left to right)



Figure 64: MP-02-06-A to MP-02-10-A (left to right)

8.2.2 Tensile Testing Procedure

As with all the mechanical testing the tensile test was carried out on the Zwick 250 kN press in the DASML. The basic structure of the tensile test followed the ASTM D638 standard. Unique to the tensile test an extensometer was used to measure the strain in the test component. The extensometer used has a resolution of 1 μm and continuously recorded the strain in the tensile component. The extensometer was used to measure the strain in the MP-02 test component as the ASTM D638 standard requires the use of an extensometer when determining the modulus of elasticity.

To begin the tensile test the MP-02 component to be tested was removed from its labelled bag and placed in the press as seen in Figure 65. The MP-02 component was placed in the press with the bottom side (the smooth side which was printed on the buildplate) facing to the right. It was aligned so that the long axis of the component was vertical, parallel to the gravity vector and clamped into place using the pneumatic grips on the press. The component was aligned by eye with the aid of the alignment tabs on both the top and bottom grips of the Zwick press. A pressure of 50 bar was used for the pneumatic grips to hold the component securely in place with no slippage.



Figure 65: Flexural testing set-up

The measured dimensions of the narrow part of each MP-02 component were entered into the connected computer to allow for automatic calculation of stresses. A preload force of 50 N and a displacement rate of 5 mm/min were selected. The displacement rate of 5 mm/min was chosen in accordance with ASTM D638 which states 5 mm/min as the preferred displacement rate for a Type I component. The extensometer was set to grip the testing component when the recorded force was 25 N. Recording and displacement of the press was set to stop when the force being recorded dropped to half of the peak recorded force. This effectively means that displacement and data recording would cease when the component fractured.

After all the parameters were specified the program was allowed to run with the top grip of the press moving upwards at a rate of 5 mm/min. The load and displacement data were recorded automatically until fracture of the test component. The component was then removed from the press and stored in its labelled bag. Parameters including the maximum force, the maximum stress, the elongation at maximum force, the force at break and the elongation at break were automatically recorded by the test computer. This procedure was repeated for each of the MP-02 tensile test components.

As mentioned above the extensometer did not properly grip two components, MP-02-06-A and MP-02-08-A. For these components one side of the top grip of the extensometer fouled on a protruding screwhead as it closed resulting in the extensometer having only three of the four points of contact needed to measure the strain of the component accurately. This fouling can be seen below in Figure 66 and resulted in incorrect load/displacement data being recorded. Any calculations or observations relating to the displacement data of these components was therefore discarded. As the load data was still recorded properly calculations utilizing the load data are still valid. These components could also still be used for qualitative analysis. Two new components, MP-02-11-A and MP-02-12-A, were fabricated to replace MP-02-06-A and MP-02-08-A and were tested following the same procedure as all the other MP-02 components. MP-02-11-A also had an issue during testing with the extensometer failing to record any data. No calculations using displacement data could be

carried out for this component however it could still be used for calculations based on load data and qualitative analysis.



Figure 66: Fouling of top extensometer grip

MP-02-05-V also presenting an issue during tensile testing, with strange data being recorded after yield as seen in Figure 67. The cause of this unexpected data is unknown. As the cause of the unexpected data is unknown all data, both load and displacement, was discarded for this component. MP-02-05-V was still used for qualitative analysis. Another component, MP-02-13-V was fabricated in a vacuum environment and tested according to the same procedure to replace the discarded data.

Following the conclusion of tensile testing the components were photographed and analyzed. The primary item that was investigated was the fracture zone and fracture surface. The data recorded by the test computer was also analyzed to determine any differences between MP-02 components fabricated in atmosphere and vacuum. The Young's modulus, or modulus of elasticity, was calculated from the automatically recorded load/displacement data.

8.2.3 Results and Analysis

The load/displacement curves resulting from the testing of all the MP-02 tensile components are shown below in Figure 67. Component MP-02-11-A is not shown in this figure as the strain data did not record properly. This figure shows the load on the component steadily increasing over the initial displacement, after which the component yields at the maximum force, followed by the load slowly diminishing until fracture of the component. The final displacements for each component vary as the test was terminated at component fracture, not at a set displacement.

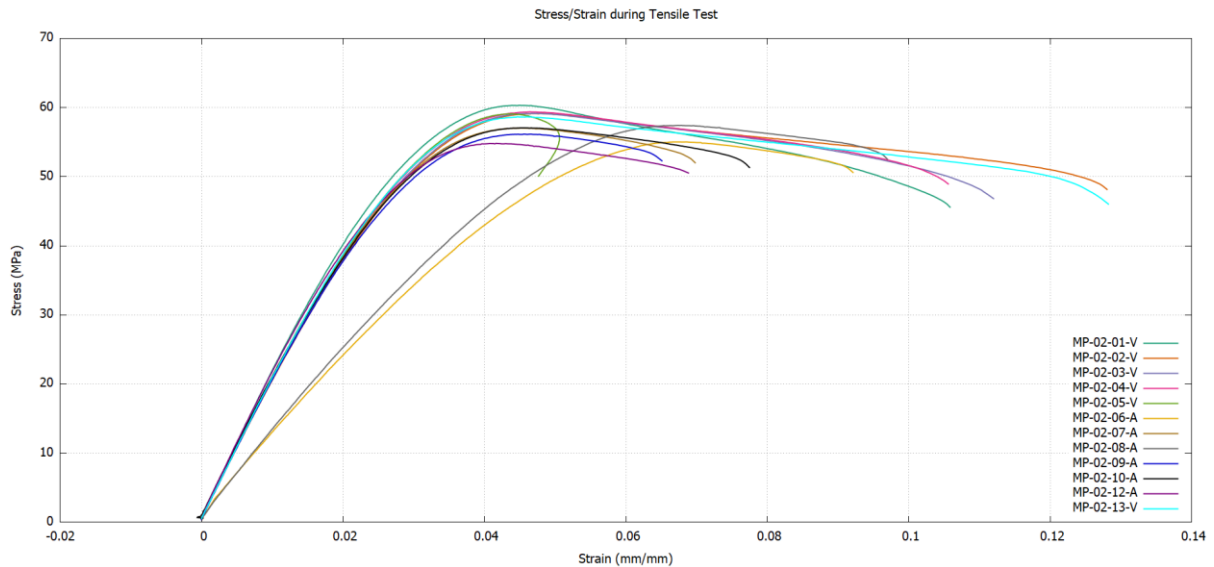


Figure 67: Stress/strain curves of the tensile components

In Figure 67 the strange data recorded for MP-02-05-V can be seen with the strain decreasing after yield. This is impossible as the test was terminated at component fracture. As MP-02-05-V fractured during the tensile test it could not have decreased in length. This behaviour is not consistent with what was observed for all other vacuum components and is what led to the data for MP-02-05-V being discarded. The data for the replacement component, MP-02-13-V is included in Figure 67.

Figure 67 also shows two components which stand out as outliers, MP-02-06-A and MP-02-08-A. These components follow a much different stress/strain curve than the other ten components with a much less steep initial linear section and yield at a much larger strain. As noted above these are the components which the extensometer did not grip properly as seen in Figure 66. Due to this, any measurements relating to the displacement or strain of these components was discarded however measurements related to load and stress were retained.

The numerical results of the tensile testing are presented below in Table 20. This table excludes results that would be derived from discarded data as discussed above. These excluded results are marked with an “N/A” and include all the results for MP-02-05-V and the Extension at Yield and Extension at Break for MP-02-06-A, MP-02-08-A and MP-02-11-A. Table 20 also shows the average values of each parameter for the atmosphere and vacuum sub-sets. These averages are only calculated from components which have good data for that parameter and therefore do not consider any data points which were discarded.

Component ID	Maximum Force (N)	Tensile Strength at Yield (MPa)	Extension at Yield (mm)	Force at Break (N)	Tensile Strength at Fracture (MPa)	Extension at Fracture (mm)
MP-02-01-V	2629.74	60.33	1.84	1986.89	45.58	4.33
MP-02-02-V	2559.06	59.15	1.79	2082.94	48.15	4.75
MP-02-03-V	2600.81	59.16	1.73	2058.47	46.82	4.15
MP-02-04-V	2554.71	59.35	1.75	2106.40	48.94	3.95
MP-02-05-V	N/A	N/A	N/A	N/A	N/A	N/A
MP-02-13-V	2515.16	58.63	1.81	1974.65	46.03	5.13
Vacuum Average	2571.90	59.32	1.78	2041.87	47.10	4.46
MP-02-06-A	2466.14	55.02	N/A	2268.13	50.60	N/A

MP-02-07-A	2499.87	57.03	1.74	2279.98	52.01	2.67
MP-02-08-A	2505.31	57.42	N/A	2291.71	52.53	N/A
MP-02-09-A	2464.68	56.15	1.87	2294.93	52.29	2.67
MP-02-10-A	2484.09	57.07	1.83	2233.82	51.32	3.15
MP-02-11-A	2446.84	56.28	N/A	2363.83	54.37	N/A
MP-02-12-A	2405.50	54.81	1.66	2217.57	50.53	2.75
Atmosphere Average	2467.49	56.26	1.78	2278.57	51.95	2.81

Table 20: Tensile testing results

The first parameter that was calculated was the ultimate tensile strength. This was calculated for each tensile component by dividing the maximum force by the cross-sectional area of the narrow section. Data of the dimensions of the tensile components can be found above in Table 13. Table 20 shows that the average tensile strength at yield is around three MPa higher for the vacuum components than the atmosphere components. The individual values of the tensile strength at yield are also very clustered with the lowest tensile strength at yield for a vacuum component, 58.63 MPa for MP-02-13-V, being larger than the highest tensile strength at yield for an atmosphere component, 57.42 MPa for MP-02-08-A. It is therefore very likely that the vacuum components have a significantly higher tensile strength at yield. This hypothesis is confirmed by the t-test which returned a value of 0.0001. This is an extremely low value and shows that the tensile yield strength is statistically different with a very high level of confidence.

This is a very interesting result as it shows that FFF printed polycarbonate components have a higher tensile performance when fabricated in a vacuum environment. It is theorized that the higher tensile strength at yield of the vacuum components is due to the slower cooling of each thread as it is extruded during the FFF process. As the thread cools more slowly, due to the reduction in convective cooling in vacuum, it will remain above its glass transition temperature for longer and will have more time to weld to adjacent threads. If the thread being extruded remains at a higher temperature for longer it will also heat up adjacent threads allowing them to weld to the thread being extruded more easily. As the MP-02 tensile components were printed in a vacuum environment with a pressure of approximately 1000 Pa there is still a small amount of convective cooling. It is therefore expected that the tensile yield strength of polycarbonate components fabricated using FFF will increase as the environmental pressure decreases. As the pressure decreases, the convective cooling will decrease, giving the thread more time at a higher temperature and a greater ability to weld to adjacent threads. The increased performance may also be due to contaminants being outgassed, resulting in a purer printing material and fewer voids in the final component.

The second parameter of the tensile testing that was investigated was the extension at yield. In Table 20 the average extension at yield for both the atmosphere and vacuum components is 1.78 mm. This shows that there is no noticeable difference between the extension at yield of the two sub-sets. This hypothesis that was confirmed by the t-test comparing the extension at yield which returned a value of 0.854, well above the confidence level of 0.05. It is interesting to note that the tensile strength at yield was extremely different between the atmosphere and vacuum sub-sets while the extension at yield showed almost no difference at all.

Moving away from the point of yield to the point of fracture the next parameter that was investigated was the tensile strength at fracture. Table 20 show the average tensile strength at fracture as 47.10 MPa for the vacuum components and 51.95 MPa for the atmosphere components. The t-test comparing these two subsets returned a value of 0.0001 showing a statistical difference to a very high confidence level. This shows that while the atmosphere components have a significantly lower tensile strength at yield they also have a significantly higher tensile strength at fracture.

To gain more insight into this phenomenon the extension at fracture was investigated. Table 20 shows that the average extension at fracture for the vacuum components is much larger than the extension at fracture for the atmosphere components, being 4.46 mm and 2.81 mm respectively. The difference in extension at fracture is statistically significant with the t-test returning a value of 0.0004. It is hypothesized that the difference in behaviour at fracture between the atmosphere and vacuum sub-sets may be due to necking occurring in the tensile component prior to fracture. Necking is a decrease in the cross-sectional area of a component when under tensile strain. As a smaller cross-sectional area reduces the ability of the component to carry stress it will result in a lower load at fracture however necking also results in high level of plastic strain in the necking zone, increasing displacement at fracture. This would explain both the lower stress at fracture and the higher displacement at fracture of the vacuum components. If greater necking occurred in the vacuum components during tensile testing it may be noticeable around the fracture. This is investigated in more depth below.

The final quantitative parameter that was investigated during the tensile testing was the modulus of elasticity, otherwise known as Young's modulus. The modulus of elasticity was calculated according to Section 11.4 of ASTM D638 [70] and involved fitting a curve to the initial, linear section of the stress/strain graph for each component. The slope of the curve of best fit of the initial, linear section is equal to the modulus of elasticity. The curve was fit to the stress/strain data up to a maximum strain of 0.2 mm as this was the section which was clearly linear. The calculated values of the modulus of elasticity are shown below in Table 21.

Component ID	Youngs Modulus (GPa)
MP-02-01-V	2.02
MP-02-02-V	1.87
MP-02-03-V	1.90
MP-02-04-V	1.93
MP-02-05-V	N/A
MP-02-13-V	1.95
Vacuum Average	1.93
MP-02-06-A	N/A
MP-02-07-A	1.92
MP-02-08-A	N/A
MP-02-09-A	1.89
MP-02-10-A	1.89
MP-02-11-A	N/A
MP-02-12-A	1.98
Atmosphere Average	1.92

Table 21: Modulus of elasticity of the tensile components

Table 21 shows the modulus of elasticity for each MP-02 tensile component, with the exception of components which did not have correct displacement data recorded by the extensometer. Table 21 also shows the average modulus of elasticity for each sub-set with the average being nearly identical. This lack of difference was confirmed statistically with a t-test value of 0.687. This shows the environmental pressure during fabrication does not affect the modulus of elasticity, an interesting conclusion given its influence over other parameters of the MP-02 tensile components.

A qualitative analysis was also done on the MP-02 components. Figure 68 shows the vacuum components, MP-02-01-V to MP-02-05-V after tensile testing. The vacuum components all fractured

properly within the narrow section of the component and at roughly the same position along the narrow section. The vacuum components did not fracture perpendicular to the sides of the narrow section but fractured at a roughly 45° angle. This suggests that the components failed along the length of the individual threads which followed a 45°/135° pattern during fabrication.

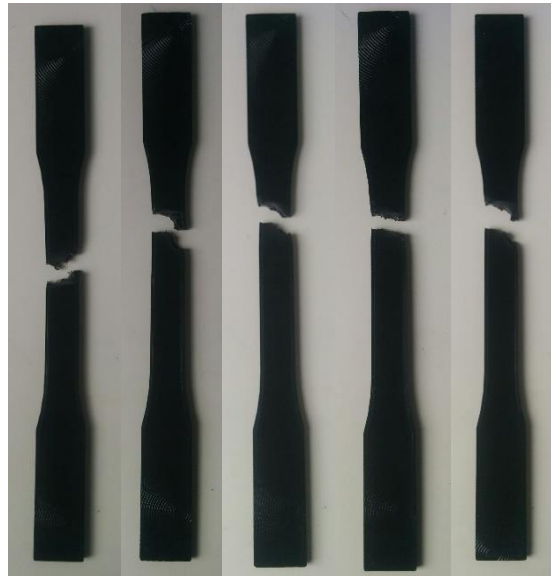


Figure 68: MP-02-01-V to MP-02-05-V (left to right) after testing

Figure 69 shows the fracture zone of two vacuum components more closely. Necking of the component can be clearly seen in Figure 69 with the sides of the component bending inward directly above and below the fracture itself. This immediately evident necking supports the above-mentioned hypothesis of necking causing increased displacement at fracture in the vacuum components. The threads seen on the fracture of the MP-02-01-V component in Figure 69 also suggest that the fracture included significant plastic deformation possibly due to a less brittle component. The angle of the fracture can also be clearly seen with the fracture occurring perpendicular to the sides of the component in the outer threads and proceeding at a 45° angle in the central portion of the component. The portion of the fracture which proceeds at an angle follows the angle of the threads of the top of component MP-02-01-V while it follows the stands on the bottom of component MP-02-03-V. This suggests that the difference in surface finish does not decide the angle at which fracture occurs and that other factors are more relevant. More testing with a larger sample size would be needed to determine that aspects of the component impact the fracture behaviour.



Figure 69: L-R, The fracture zones of MP-02-01-V (top), MP-02-03-V (top and bottom)

Figure 70 shows the atmosphere components, MP-02-06-A to MP-02-10-A after tensile testing. The atmosphere components all fractured properly within the narrow section of the component although MP-02-06-A and MP-02-07-A both fractured quite close to the upper rounded section. The atmosphere components fractured at roughly the same position as each other and the vacuum components along the narrow section. The atmosphere components appear to have fractured straight across the narrow section, perpendicular to the side. This contrasts with the vacuum components which fractured at approximately 45°.



Figure 70: MP-02-06-A to MP-02-10-A (left to right) after testing

Figure 71 below shows the fracture zones of three atmosphere components, MP-02-06-A, MP-02-07-A and MP-02-08-A, in greater detail. The differences between these components and the vacuum components shown in Figure 69 are immediately evident with the fracture in the atmosphere components of Figure 71 occurring perpendicular to the sides. The fracture does not seem to follow the 45° angle of the threads and appears to have fractured each thread across the entire width of the component. There are no threads hanging from the fracture surface and there is minimal

necking visible next to the fracture. Both observations are indicative of a brittle failure in which the component broke suddenly with minimal plastic deformation. The differences in the fracture, when compared to the vacuum components, supports the hypothesis that the atmosphere components are more brittle and helps to explain why the atmosphere components have a higher stress at fracture and lower displacement at fracture compared to the vacuum components.

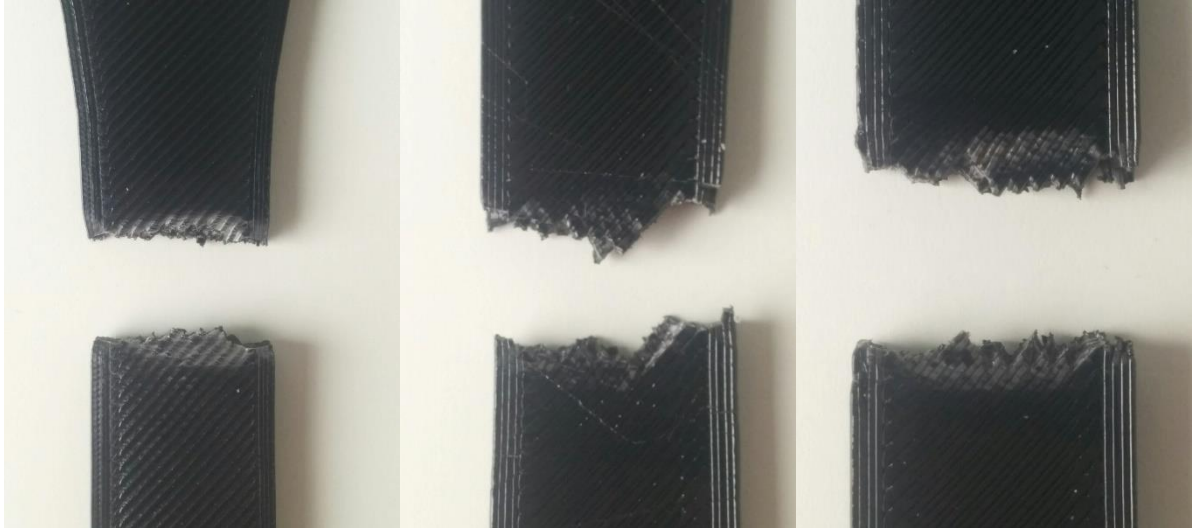


Figure 71: L-R, fracture zones of MP-02-06-A (top), MP-02-07-A (top) and MP-02-08-A (bottom)

The final important qualitative observation was the observation of the pattern of the press grips on the grip sections of the tensile components. This pattern can be seen on MP-02-01-V in Figure 72 below. The concentric circles seen on the component are the result of the grips holding the component. The fact that this pattern can be clearly seen, and the edges of the circles are crisp show that there was no slip between the grips and the component during testing. While this is not an indication of component performance it does validate the pressure used to hold the components and the lack of slip suggests that the displacement recordings can be taken as accurate.



Figure 72: The pattern of the pneumatic grips on MP-02-01-V

8.3 Compressive Test

To investigate the compressive properties of polycarbonate printed in a vacuum environment a compressive test was carried out. This compressive test followed the ASTM D695 standard [71] as closely as possible with only a few modifications. The primary result of this test is the compressive stress at yield. The deformation of the MP-03 component at yield was also investigated. The compressive test components were qualitatively analyzed to determine where along the component yielding took place and to determine the properties of the component when compressed to rupture.

8.3.1 Compressive Testing Components

The components used for the compressive test were designated the MP-03 series of components. The MP-03 compressive testing components exactly follow the preferred test component from the ASTM D695 standard [71]. The MP-03 component is a small cylinder with a nominal diameter of 12.7 mm and a nominal height of 25.4 mm.

The MP-03 series of components consisted of ten test components numbered MP-03-01 to MP-03-10. This set of components consisted of two subsets, five in vacuum and five in atmosphere. These components have component IDs MP-03-01-V to MP-03-05-V and MP-03-06-A to MP-03-10-A for the vacuum and atmosphere subsets respectively. The fabrication of the MP-03 series of components differs from the fabrication of the other MP components as each subset of was fabricated in a single print run. This means that all five components of each of the two MP-03 subsets were printed on the same buildplate as seen in Figure 73

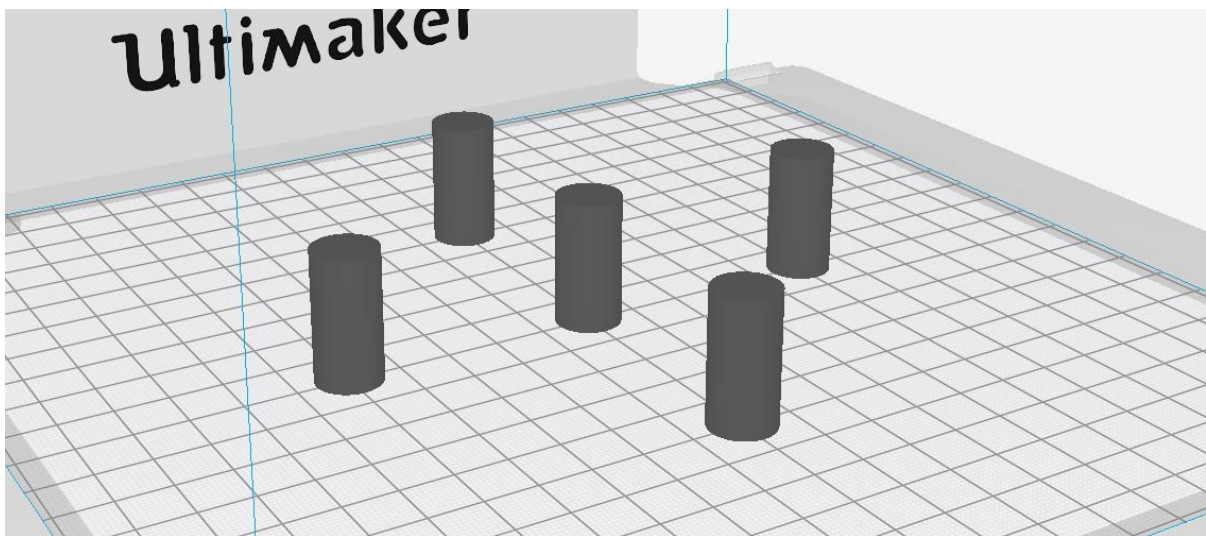


Figure 73: The buildplate layout for the MP-03 components

This contrasts with the other two sets of MP components where each component was fabricated in a separate print run without other components on the buildplate. The reason for fabricating the MP-03 components in sets of five is because each MP-03 component has a very small cross-sectional area. As noted above in Section 5.2 components with small cross-sectional areas printed very poorly in the vacuum environment, likely due to the reduced cooling. By printing each subset of MP-03 components using the “all at once” option in Cura the components could be printed with acceptable quality. The “all at once” option in Cura sequentially prints the first layer of each component before printing the second layer and so on. In this manner each layer has sufficient time to cool before being printed on, allowing components with small cross-sectional areas to be fabricated with good quality.

8.3.2 Compressive Testing Procedure

The compressive test was also carried out on the Zwick 250 kN press in the DASML. The basic structure of the tensile test followed the ASTM D695 standard. The compressive test did not require any additional apparatus as the MP-03 component was simply placed on the lower flat plate and compressed by the downward movement of the upper flat plate of the press. An MP-03 compressive component in the Zwick 250 kN press prior to compressive testing can be seen in Figure 74. The two flat, horizontal plates of the press and the black MP-03 component can be clearly seen.

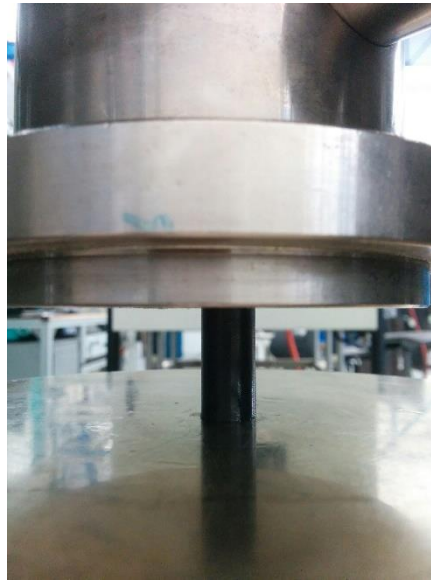


Figure 74: Compressive test set-up

At the beginning of each compressive test the MP-03 component to be tested was removed from its labelled bag and placed on the lower flat plate of the press. The MP-03 component was placed on the plate with the bottom side of the component (the smooth side which was printed on the buildplate) contacting the lower plate. The compressive component was centred on the flat plate of the press by eye.

The measured height and diameter each MP-03 component was input into the connected computer for each test to allow for automatic calculation of stresses. A preload force of 10 N and a displacement rate of 1.3 mm/min were selected. The preload was selected in consultation with the DASML technicians and the displacement rate is the standard speed of testing specified in ASTM D695. [71] A maximum displacement was specified in the computer as the termination of the test. For the first test component, MP-03-01-V, a maximum displacement of 20 mm was chosen. This displacement was chosen as it showed the complete compressive behaviour of the specimen and allowed for the approximate displacement range at which yield occurs to be identified. As yield was found to occur before 2.5 mm of displacement a maximum displacement of 5 mm was chosen to record yield data and see the behaviour of the component for a small displacement after yield. Components MP-03-05-V, MP-03-08-A and MP-03-10-A, in addition to MP-03-01-V, were also tested to maximum displacement of 20mm to allow qualitative analysis of the component after yield. The maximum displacement was always specified to be smaller than the height of the component to avoid the two plates of the press from contacted each other.

During the test the top grip of the press moved downward at the specified displacement rate, compressing the MP-03 component between the two flat plates of the press. The load and displacement data were recorded automatically until the component had reached the maximum

displacement. Displacement data was measured by recording the position of the top plate after it had reached the preload. After the maximum displacement was reached the top plate returned to the start position and the component was removed from the press and stored in its labelled bag. The maximum force and the displacement at the maximum force were automatically recorded by the test computer. The maximum stress was determined by dividing the maximum stress by the measured cross-sectional area.

Following the conclusion of compressive testing the components were photographed and analyzed. The location of yield was the most important qualitative parameter analyzed. The location of rupture in components that were compressed to a maximum displacement of 20 mm was also investigated. The data recorded by the test computer was analyzed to determine any statistical differences between MP-03 components fabricated in atmosphere and vacuum.

8.3.3 Results and Analysis

The force/deformation curves resulting from the testing of the MP-03 compressive components are shown below in Figure 75 and Figure 77. Figure 75 shows the force/deformation curves for the components which were tested to a final deformation of 20 mm while Figure 77 shows the force/deformation curves of the components which were tested to a deformation of 5 mm. These figures show the force on the component increasing as it is compressed, after which the component yields at the maximum force. The force then decreases slightly before beginning to increase again.

Figure 75 shows the force/deformation curves of the MP-03 components which were tested to a deformation of 20 mm. For these components the force increases greatly after yielding due to the increased cross-sectional area of the component caused by the high levels of deformation. The deformation of an MP-03 component during the compression test can be seen in Figure 76. The force eventually peaks and then decreases suddenly several times near the end of the curve. This is due to the component rupturing or cracking. At each sudden decrease the component ruptures, quickly decreasing the force before it begins to climb again. The peak force and the behaviour after the peak force is quite similar for the atmosphere and vacuum components. Although the behaviour of the components at or near the point of peak force is similar it can be observed that the vacuum components, shown in orange and green, have a higher force at yield. This suggests that the components fabricated in a vacuum environment have a higher compressive yield strength which will be investigated more thoroughly below.

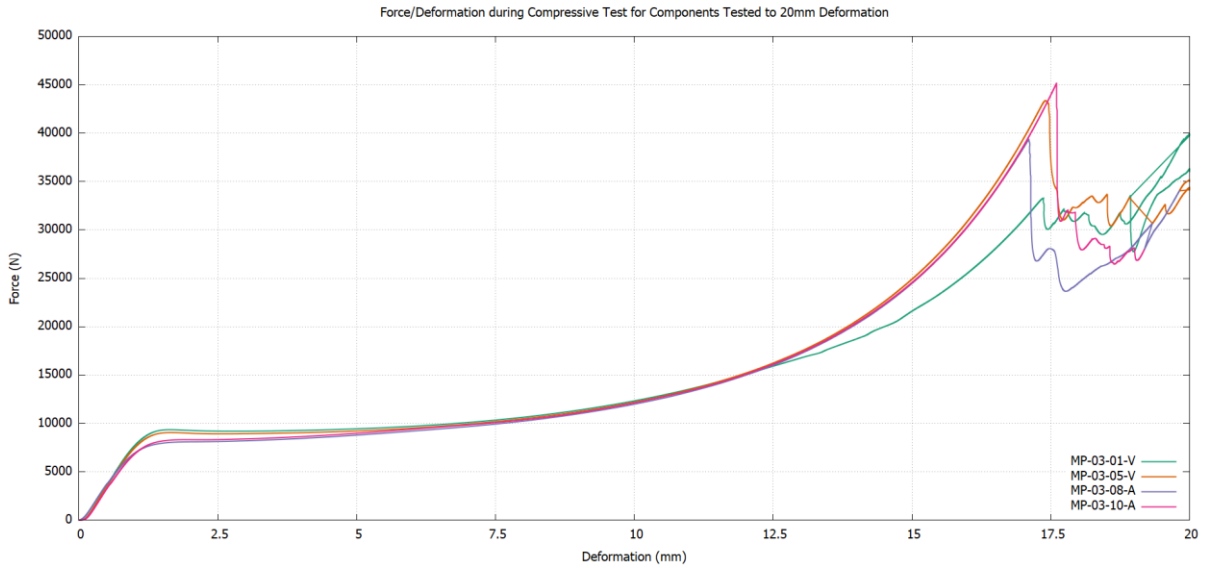


Figure 75: Force/deformation of components tested to 20mm compressive deformation



Figure 76: A MP-03 component deforming under high compressive load

In Figure 77 the force/deformation curves of the MP-03 compressive components which were tested to a deformation of 5 mm are shown. In these curves the force only has time to increase slightly before the test is terminated. This slight increase in force after yield is due to the increase in cross-sectional area after plastic deformation has occurred. The vacuum components, MP-03-02-V, MP-03-03-V and MP-03-04-V, again appear to have a higher force at yield than the components fabricated in atmosphere.

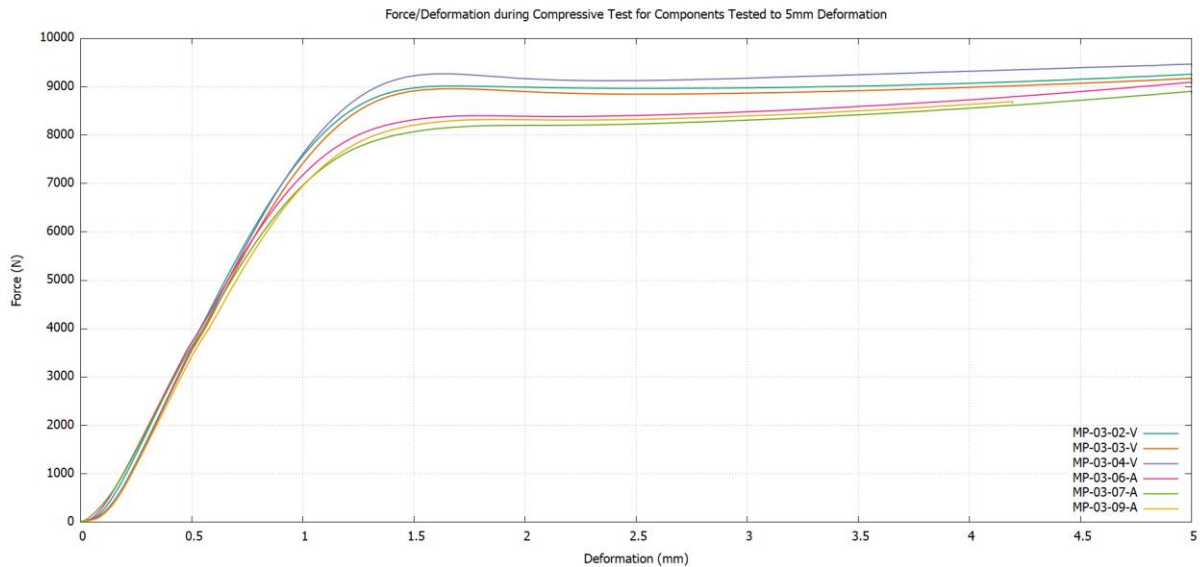


Figure 77: Force/deformation of components tested to 5mm compressive deformation

For most of the components the force decreased slightly after yield before increasing again. The reason the force increases after yield is because the effective cross-sectional area of the component increases as it deforms under compression.

The numerical results of the compressive testing are presented below in Table 22. Table 22 shows the force at yield, the yield stress and the displacement at yield for each MP-03 component. The force at yield was determined by taking the maximum force recorded before a deformation of 2 mm. 2mm was chosen as the cut-off as all components had yielded before this displacement. The use of a cut-off to determine the maximum force, and therefore the force at yield was required because the force began rising again after yield. This meant that the force when the test was terminated was often the highest force recorded, causing the recording computer to incorrectly label this force as the force at yield. Table 22 also includes the yield stress that was calculated by dividing the force at yield by the component cross-sectional area (calculated using data from Table 14) and the deformation at yield which was recorded at the while determining the force at yield. Table 22 also includes the average values of each parameter for the atmosphere and vacuum sub-sets.

Component ID	Force at Yield (N)	Yield Stress (MPa)	Deformation at Yield (mm)
MP-03-01-V	9363.4	72.65	1.65
MP-03-02-V	9017.0	71.18	1.66
MP-03-03-V	8961.1	71.19	1.66
MP-03-04-V	9269.6	72.60	1.64
MP-03-05-V	9063.5	71.10	1.64
Vacuum Average	9134.9	71.74	1.65
MP-03-06-A	8402.4	65.40	1.77
MP-03-07-A	8203.1	63.95	2.00
MP-03-08-A	8101.0	63.75	1.99
MP-03-09-A	8324.1	64.89	1.84
MP-03-10-A	8326.4	64.50	1.91
Atmosphere Average	8271.4	64.50	1.90

Table 22: Compressive testing results

Looking at the yield stress in Table 22 it is very clear there is a large difference between the atmosphere and vacuum sub-sets which have average yield stresses of 64.50 MPa and 71.74 MPa respectively. The vacuum components have a yield stress almost 10% larger than the atmosphere components. Comparing the yield stress with a t-test yields the expected result, a value of 3.15×10^{-7} , showing beyond a doubt that there is a statistical difference in yield stress. It is hypothesized that this difference is due to the theory formulated in the Section 8.2.3 in which the polycarbonate threads weld together more readily due to the fact they remain hotter, for longer, in the vacuum environment.

The deformation at yield also seems to show a large difference with the average deformation at yield for the vacuum components being 1.65 mm versus the average 1.90 mm for the atmosphere components. The t-test comparing these sub-sets returned a value of 0.0005 showing that there is a significant difference.

The MP-03 compressive components were also qualitatively analyzed. The first thing that was observed was that yield occurred in the top half of every compressive component. This can be seen below in Figure 78 which shows MP-03-03-V and MP-03-06-A after compressive testing. The bulging caused by the plastic deformation at and after yield is localized in the top half of the components. The plastic deformation is localized to the top half of the component for all other MP-03 as well. It is possible that the bottom half of the component has a larger diameter than the top half. During the FFF process the layers remain hot, and potentially malleable, as further layers are printed. The mass of these further layers then compresses the bottom layers causing them to bulge, creating a larger diameter. This is a common issue in 3D printing and is commonly referred to as “elephant foot”. It may be useful to carry out a dimensional study to determine if components with the MP-03 geometry do have a larger diameter near the bottom and to determine if there is any difference between components fabricated in atmosphere and vacuum.

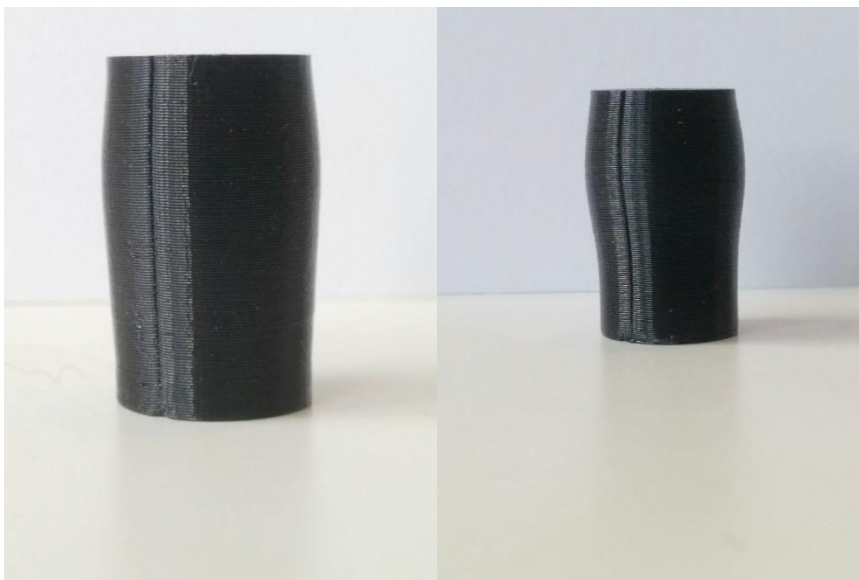


Figure 78: MP-03-03-V and MP-03-06-A after compressive testing

Figure 79 below shows MP-03-01-V and MP-03-10-A after compressive testing. These components were compressively tested to a deformation of 20 mm and look very different from those tested to a deformation of 5 mm. The components are visibly ruptured at several locations along the circumference. The rupture of the components was discussed above and can be seen as sudden decreases in force at high deformation in Figure 75. Interesting to note is that the vacuum

compressive components did not rupture at the seam discussed as a defect in the MP-03 components in Section 7.3.5. The seam can still be seen on MP-03-01-V in Figure 79. The seam could not be seen of the atmosphere components tested until 20 mm of deformation, so the component may or may not have ruptured at the seam.



Figure 79: MP-03-01-V and MP-03-10-A after compressive testing

In conclusions the components printed in vacuum have a significantly higher compressive strength at yield than components printed in atmosphere. The vacuum components also have significantly lower deformation at yield, indicating they are stiffer. Qualitatively there is no difference between components fabricated in atmosphere and vacuum.

9 Conclusions and Recommendations

In this final section the work done will be summarized and final conclusions will be drawn. These conclusions will be used to answer the research questions and research sub-questions. After the research questions have been addressed any remaining questions will be identified as opportunities for further research. Any other opportunities for future research in the area of FFF in an on-orbit environment will also be identified and discussed. Following this a rough “road-map” will be presented with the aim to show the next steps in moving from the research presented in this report towards the final goal of implementing FFF on-orbit for the purpose of manufacturing structural components for space systems.

9.1 Conclusions

There are several important conclusions that can be drawn from the thesis work however to gain better context of these conclusions the research question will first be reiterated. The top level research question was formulated in Section 1.2.1 as *“Can Fused Filament Fabrication (FFF) be carried out in a vacuum environment representative of Low Earth Orbit (LEO) and fabricate polymer-based components that are representative of components used for space systems?”*

This is a very difficult question to answer on its own, so it was broken down into three sub-questions in Section 1.2.2. These questions were: can an FFF printer can function in a simulated on-orbit environment, can FFF be used to accurately fabricate structural components in a simulated on-orbit environment and what are the mechanical properties of components fabricated using FFF in a simulated on-orbit environment. These three questions are the key questions that need to be answered before a definite answer to the top-level research question can be determined. The conclusions drawn from the research therefore are intended to answer these three questions sequentially with the answers to each sub-question being analyzed to determine an answer to the top-level research question.

The first research sub-question was formulated as *“Can an FFF printer function in an environment representative of the on-orbit environment?”* This is an important question as if a printer cannot carry out the FFF process in a simulated on-orbit environment, FFF cannot be implemented in a real environment. It was found that an FFF printer, with minimal modifications, can survive and function in an simulated on-orbit environment. The standard servo motors functioned normally and did not overheat in the vacuum environment of 1000 Pa even though they are not rated for use in a vacuum environment. The oil-less bearings used in the test printer also performed nominally allowing the three axes to move in vacuum as they did in atmosphere. The filament feed system functioned nominally in the vacuum environment with no unexpected behaviour observed. The printhead and buildplate heaters functioned normally with modified PID constants showing that PID control is adequate for regulating the printhead and buildplate temperature in a vacuum environment. It is possible that a dedicated cooling system may be required to regulate the relevant temperature on-orbit as the radiative cooling may not be adequate. The FFF printer was able to successfully print polycarbonate components, except for components with very small cross-sectional areas. In conclusion it was found that an FFF printer can survive in a vacuum environment of 1000 Pa and successfully carry out the FFF process on components with a cross-sectional area above a certain threshold.

The second research sub-question was “Can an FFF printer accurately fabricate components in a vacuum environment representative of the on-orbit environment?” This was investigated by measuring the dimensions and masses of three sets of components and performing a qualitative

analysis. The first conclusion that was drawn was that there is no qualitative difference between components fabricated in atmosphere and vacuum. There was no appreciable difference in the number, severity or type of defects between the atmosphere and vacuum components. Also, there was no appreciable difference in the overall quality and finish of the components. Quantitatively there were several important things to note, the first of is that several measured dimensions had statistically significant differences between the atmosphere and vacuum components. In general, the vacuum components had larger widths and lengths and shorter heights than the equivalent atmosphere components. It is important to note that there was no significant difference in volume between any sub-sets of components and only one instance of a significant difference in mass meaning the different dimensions are likely only cause by deformation, not by material loss through outgassing. Although there were significantly different dimensions the variation of the dimensions of the vacuum components was small and could be easily accommodated for with offsets in the CAD geometry as is standard for components fabricated with FFF. This means that there is no practical difference, quantitatively or qualitatively, between components printed in atmosphere and vacuum. In conclusion the FFF process can be used in a vacuum environment to fabricate components that are dimensionally accurate and have the proper mass. This is assuming the appropriate dimensional offsets have been identified and implemented in the CAD geometry for the specific processing conditions.

The third and final research sub-question was *“How do the mechanical properties of FFF polymer-based components change when fabricated in a vacuum environment representative of the on-orbit environment?”* It was found that there was no difference in flexural behaviour between components fabricated in atmosphere and vacuum. In the tensile test the components printed in vacuum exhibited significantly higher ultimate tensile strength, approximately 5% higher than the ultimate tensile strength of components fabricated in atmosphere. The vacuum fabricated components also had much larger extension at fracture in the tensile test indicating that they are less brittle. In the compressive test the vacuum components had a significantly higher compressive yield strength. The compressive yield strength was approximately 10% higher for the vacuum components when compared with the components fabricated in atmosphere. In conclusion it was found that components fabricated in a vacuum environment have better tensile and compressive behaviour than the equivalent components fabricated in atmosphere.

In conclusion FFF can be carried out in a vacuum environment representative of Low Earth Orbit (LEO) to fabricate polycarbonate components that are representative of components used for space systems. The commercially available FFF printer was able to survive and function in a vacuum environment showing that there are no fundamental issues with the FFF process that would preclude it from being used on-orbit. Components with accurate dimensions, although different from the dimensions of those fabricated in atmosphere, were fabricated showing that components can be reliably fabricated in an on-orbit environment. The material properties of polycarbonate fabricated using FFF in vacuum were determined and found to be greater than the equivalent properties when fabricated in atmosphere, allowing for structural components to be accurately designed to withstand the loading conditions. As all three of these criteria were met FFF could theoretically be implemented on-orbit.

9.2 Recommendations

In the following section recommendations for further research are presented. These recommendations may be made due to limitations in the scope of the thesis research, continuations of the research or related to the findings of the research. A short, preliminary “road-map” of the research required for the implementation of FFF on-orbit.

9.2.1 Future Research

The first area for future research is to fabricate test components, for the same or similar testing, in a vacuum environment with a much lower pressure. Although the pressure used, 1000 Pa is only 1% of atmospheric pressure it still allows for a small amount of convective cooling as discussed in Section 5.2.1. This pressure is still several orders of magnitude higher than the pressure at LEO ($\sim 10^{-3}$ Pa) [20]. It is expected that the results observed in this research will be exaggerated by even lower pressures. It is also possible that phenomena which were not observed in this thesis research, due to the relatively high pressure, will manifest in a lower pressure environment. The exact parameters of the FFF implementation, such as dimensional offsets and required level of cooling, will also need to be determined prior to any real-life implementation which will therefore require testing in a lower pressure environment.

Testing of the FFF process in a vacuum environment with different materials is also an opportunity for future research. Testing needs to be done on a wide variety of polymers to determine if the behaviours observed during this research is exclusive to PC or if it is transferable to other polymers. Testing is particularly required with high strength engineering polymers such as PEEK and PEI as these are the materials most likely to be used on-orbit. These materials also have extreme processing conditions and present a worst-case scenario with regards to thermal control.

The geometries fabricated in vacuum that were thoroughly analyzed in this research were very simple. Further research could look into how fabrication of more complex geometries is carried out. This could include convex or concave surfaces, holes for fasteners, standoffs. Investigation of functional components, such as trusses or antenna should also be investigated with these components being geometrically optimized for fabrication with FFF.

The clogging issue discussed in Section 5.3.1 is also worthy of future research. Although this issue was solved by swapping the printhead to the PEEK rated printhead with better hot/cold section isolation it is not known exactly what caused this issue or how it can be best solved. As a clogged nozzle would be a serious problem in a real implementation of FFF on-orbit further research is needed to determine the cause and design solutions to prevent clogging from occurring. This would likely involve both physical testing in a vacuum environment and a complete thermal model.

The cooling of components with small cross-sectional areas was problematic throughout the research and further research needs to be done to determine what geometries can be printed accurately. Novel methods of cooling the top layer of the component as it is fabricated, such as conductive cooling via a cool plate suspended from the printhead, could be investigated.

Once the basics of the FFF process are better understood in a vacuum environment the entire FFF process would need to be optimized for an on-orbit implementation. This would include, but is not limited to, design of a custom printer, material selection and storage and processing parameters. These would have to be considered in a high level, systems manner to determine the mission concept, requirements and goals.

Other testing that would be useful would be combined testing in a vacuum and microgravity environment. This would provide the most accurate picture of the on-orbit environment and would validate the assumption that if FFF can be shown to work in vacuum and microgravity separately then it can function in a combined environment. This testing would be extremely difficult due to the difficulty in creating the test conditions.

9.2.2 Roadmap to Implementation On-Orbit

Figure 80 below shows a rough roadmap from the current state of the art to an FFF printer that could feasibly be used on-orbit. It mainly follows the recommendations for future research. The first main step is to print in PEEK as PEEK is much more likely to be used on-orbit than PC. Once PEEK usage in an on-orbit environment has been established research can be done into printing more complex component with PEEK in a higher vacuum environment. This could also include varying thermal environments. At the same time studies need to be done to determine the causes and effects of the clogging of the printhead and the poor printing of components with small cross-sectional areas. Once the causes are established solutions need to be determined as these problems cannot arise in a real implementation of FFF on-orbit.

After these steps have been accomplished design can be carried out for a custom FFF printer which is optimized to print in the on-orbit environment. This printer will likely not be based on existing commercial printers and will incorporate the lessons learned from previous research into FFF printing on-orbit. Once this printed is constructed it will need to be extensively tested. After appropriate testing it could be used to carry out FFF on-orbit. As FFF in an on-orbit environment is at such an early stage it is difficult to predict what problems may arise and what needs to be done to bring this technology to market. This roadmap is therefore a very preliminary look at the future of the technology.

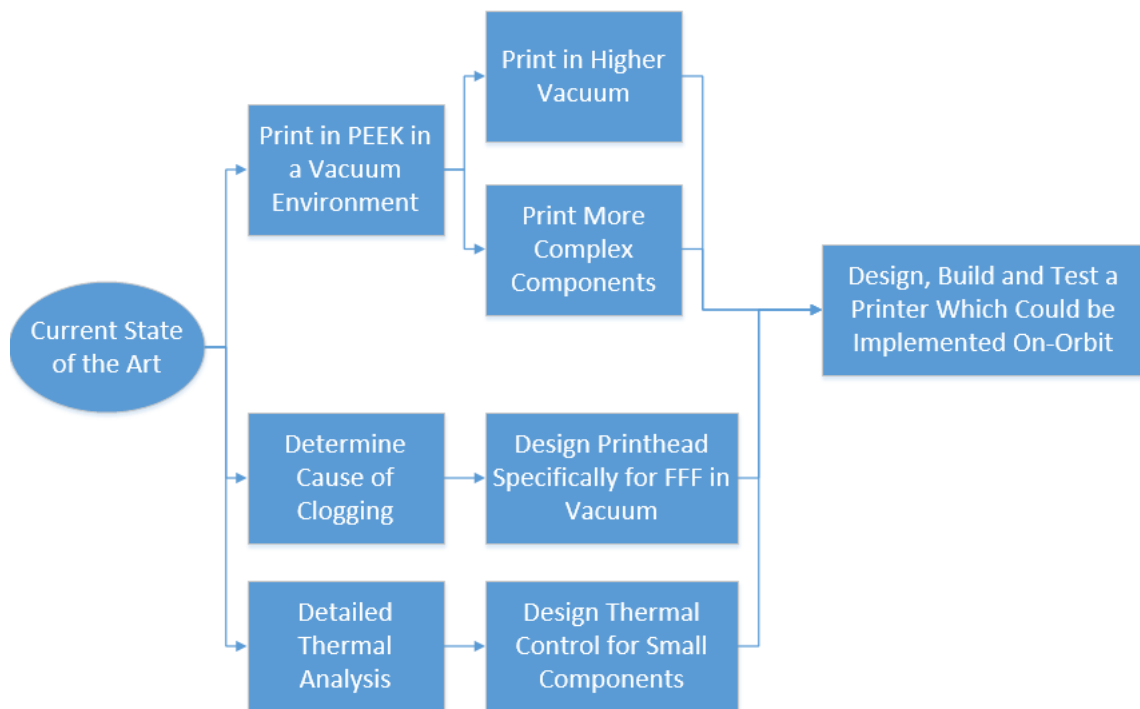


Figure 80: A roadmap to a feasible FFF printer for use on-orbit

Bibliography

- [1] R. P. Hoyt *et al.*, “SpiderFab: An architecture for self-fabricating space systems,” *AIAA Sp. 2013 Conf. Expo.*, pp. 1–17, 2013.
- [2] Made in Space, “Extended Structures Additive Manufacturing Machine (ESAMM).” [Online]. Available: <http://www.madeinspace.us/projects/esamm/>. [Accessed: 04-Apr-2017].
- [3] Made in Space, “Archinaut.” [Online]. Available: <http://madeinspace.us/archinaut/>. [Accessed: 18-Apr-2017].
- [4] Magna Parva Ltd, “In-Space Manufacturing of Very Large Structures.” [Online]. Available: <https://inspacemanufacturing.com>. [Accessed: 18-Apr-2017].
- [5] M. L. Wilson, I. O Macconochie, and G. S. Johnson, “Potential for On-Orbit Manufacture of Large Space Structures Using the Pultrusion Process,” *NASA Tech. Memo.*, pp. 1–16, 1987.
- [6] M. M. Johnston, M. J. Werkheiser, K. G. Cooper, M. P. Snyder, and J. E. Edmunson, “3D Printing In Zero-G ISS Technology Demonstration,” vol. 94035.
- [7] Q. A. Bean, K. G. Cooper, J. E. Edmunson, M. M. Johnston, and M. J. Werkheiser, “International Space Station (ISS) 3D Printer Performance and Material Characterization Methodology.”
- [8] G. Musso *et al.*, “Portable on Orbit Printer 3D: 1st European Additive Manufacturing Machine on International Space Station,” *Adv. Phys. Ergon. Hum. Factors*, vol. 489, pp. 643–655, 2016.
- [9] T. J. Prater *et al.*, “Summary Report on Phase I Results from the 3D Printing in Zero G Technology Demonstration Mission, Volume I,” vol. I, no. July, 2016.
- [10] eoPortal Directory, “ISS Utilization: 3D Print (3D Printing in Zero-G Technology Demonstration).” [Online]. Available: <https://directory.eoportal.org/web/eoportal/satellite-missions/i/iss-3d-print#mission-status>. [Accessed: 13-Jun-2017].
- [11] Made in Space, “Additive Manufacturing Facility (AMF) User Guide,” 2016.
- [12] I. Gibson and D. Rosen, *Additive Manufacturing Technologies*, 2nd ed. Springer.
- [13] Builder 3D Printers B.V., “Builder Premium Medium Red.” [Online]. Available: <http://builder3dprinters.com/product/builder-premium-medium-red/>. [Accessed: 02-Jan-2018].
- [14] Ultimaker, “Ultimaker Original+.” [Online]. Available: <https://ultimaker.com/en/products/ultimaker-original>. [Accessed: 02-Jan-2018].
- [15] Fabbaloo, “Bowden or Direct? A Primer on Extruder Styles.” [Online]. Available: <http://www.fabbaloo.com/blog/2015/11/11/bowden-or-direct-a-primer-on-extruder-styles>. [Accessed: 02-Jan-2018].
- [16] Ultimaker, “Ultimaker 3 Specification Sheet,” p. 2.
- [17] M. Molitch-Hou, “3D Printing Filaments: What’s the Deal with ULTEM and PEEK?” 2017. [Online]. Available: http://www.engineering.com/3DPrinting/3DPrintingArticles/ArticleID/14465/3D-Printing-Filaments-Whats-the-Deal-with-ULTEM-and-PEEK.aspx?e_src=relart. [Accessed: 04-Aug-2017].
- [18] National Aeronautics and Space Administration, “What Is Microgravity?,” 2012. [Online].

- Available: <https://www.nasa.gov/audience/forstudents/5-8/features/nasa-knows/what-is-microgravity-58.html>. [Accessed: 21-Aug-2017].
- [19] National Physical Laboratory, "What do 'high vacuum' and 'low vacuum' mean? (FAQ - Pressure)," 2010. [Online]. Available: [http://www.npl.co.uk/reference/faqs/what-do-high-vacuum-and-low-vacuum-mean-\(faq-pressure\)](http://www.npl.co.uk/reference/faqs/what-do-high-vacuum-and-low-vacuum-mean-(faq-pressure)). [Accessed: 28-Jul-2017].
- [20] G. Horneck, "Space Environment," in *Encyclopedia of Astrobiology*, M. Gargaud, R. Amils, J. C. Quintanilla, H. J. (Jim) Cleaves, W. M. Irvine, D. L. Pinti, and M. Viso, Eds. Berlin, Heidelberg: Springer Berlin Heidelberg, 2011, p. 1543.
- [21] E. Grossman and I. Gouzman, "Space environment effects on polymers in low earth orbit," *Nucl. Instruments Methods Phys. Res. Sect. B Beam Interact. with Mater. Atoms*, vol. 208, no. 1–4, pp. 48–57, 2003.
- [22] J. L. de Segovia, "Physics of outgassing," *Cern Eur. Organ. Nucl. ...*, pp. 99–110, 1999.
- [23] J. R. Wertz and W. Larson, *B3 - Space Mission Analysis and Design*. 1999.
- [24] J.-H. Han and C.-G. Kim, "Low earth orbit space environment simulation and its effects on graphite/epoxy composites," *Compos. Struct.*, vol. 72, no. 2, pp. 218–226, 2006.
- [25] J. L. Barth, "Space and atmospheric environments: From low earth orbits to deep space," *Eur. Sp. Agency, (Special Publ. ESA SP, no. 540, pp. 17–30, 2003.*
- [26] R. Skomorohov, C. Welch, and A. Hein, "In-orbit Spacecraft Manufacturing: Near-Term Business Cases," *Researchgate.Net*, no. October, 2016.
- [27] K. Short and D. Van Buren, "Printable spacecraft: Flexible electronic platforms for NASA missions," *Pasadena, Calif. Calif. Inst. ...*, no. September, 2012.
- [28] W. Notardonato, W. Johnson, A. Swanger, and W. Mcquade, "In-Space Propellant Production Using Water," pp. 1–11, 2012.
- [29] European Space Agency (ESA), "Building the International Space Station." [Online]. Available: http://www.esa.int/Our_Activities/Human_Spaceflight/International_Space_Station/Building_the_International_Space_Station3. [Accessed: 13-Jun-2017].
- [30] D. M. Harland, "Space station," *Encyclopedia Britannica*. 1998.
- [31] R. Rembala and C. Ower, "Robotic assembly and maintenance of future space stations based on the ISS mission operations experience," *Acta Astronaut.*, vol. 65, no. 7–8, pp. 912–920, 2009.
- [32] European Cooperation for Space Standardization, "Space product assurance: Thermal vacuum outgassing test for the screening of space materials," no. November, pp. 1–45, 2008.
- [33] European Space Agency (ESA), "Outgassing Data." [Online]. Available: http://esmat.esa.int/Services/outgassing_data/outgassing_data.html. [Accessed: 08-Aug-2017].
- [34] ECSS, "Space product assurance: Data for selection of space materials and processes (ECSS-Q-70-71A rev. 1)," no. June, pp. 1–36, 1999.
- [35] J. Straub, "Initial Work on the Characterization of Additive Manufacturing (3D Printing) Using Software Image Analysis," *Machines*, vol. 3, no. 2, pp. 55–71, 2015.
- [36] J. Straub, "Characterization of 3D Printing Output Using an Optical Sensing System," *Dimens. Opt. Metrol. Insp. Pract. Appl. Iv*, vol. 9489, pp. 1–9, 2015.

- [37] M. Napoli and J. J. Dunn, "R3DO: A Plastic Recycling System For Creating 3D Printer Feedstock On-Orbit.," *Propos. # 14-1 H10.01-9308 response to NASA SBIR 2014 Solicitation*, pp. 3–6, 2014.
- [38] Thermo Fisher Scientific, "Thermo Scientific Heraeus® Heating and Drying Ovens," p. 16, 2007.
- [39] vacuubrand, "Technology for Vacuum Systems Instructions for use." pp. 1–17, 2009.
- [40] Ultimaker, "Ultimaker 2+ Specification Sheet."
- [41] Makerbot, "The All-New Makerbot Replicator+." [Online]. Available: <https://www.makerbot.com/replicator/>. [Accessed: 09-Jan-2018].
- [42] Ultimaker, "Ultimaker products." [Online]. Available: <https://ultimaker.com/en/products>. [Accessed: 05-Jan-2018].
- [43] European Space Agency (ESA), "3D Printing CubeSat Bodies for Cheaper, Faster Missions," 2017. [Online]. Available: http://www.esa.int/Our_Activities/Space_Engineering_Technology/3D_printing_CubeSat_bodies_for_cheaper_faster_missions. [Accessed: 13-Jun-2017].
- [44] B. Grim, M. Kamstra, A. Ewing, C. Nogales, J. Griffin, and S. Parke, "MakerSat : A CubeSat Designed for In-Space Assembly," no. 208.
- [45] Ö. Soykasap, "Deployment analysis of a self-deployable composite boom," *Compos. Struct.*, vol. 89, no. 3, pp. 374–381, 2009.
- [46] J. M. Gardner, C. J. Stelter, E. A. Yashin, and E. J. Siochi, "High Temperature Thermoplastic Additive Manufacturing Using Low-Cost, Open-Source Hardware," no. October, 2016.
- [47] 3D4Makers, "Best Practices in 3D Printing PEEK FDM Filament," 2017. [Online]. Available: <https://www.3d4makers.com/blogs/news/best-practices-in-3d-printing-peek-fdm-filament>. [Accessed: 04-Aug-2017].
- [48] 3DXTech, "Ultem™ 9085 3D Filament." [Online]. Available: <https://www.3dxtech.com/ultem-9085-3d-printing-filament/>. [Accessed: 05-Jan-2018].
- [49] National Aeronautics and Space Administration, "Outgassing Data for Advanced Search and Report." [Online]. Available: https://outgassing.nasa.gov/cgi/uncgi/search/search_html_ad.sh. [Accessed: 05-Jan-2018].
- [50] Boedeker, "Outgassing of Engineering Plastics In High-Vacuum Applications." [Online]. Available: <http://www.boedeker.com/outgas.htm>. [Accessed: 05-Jan-2018].
- [51] Ultimaker, "How to print with Ultimaker PLA." [Online]. Available: <https://ultimaker.com/en/resources/22225-how-to-print-with-ultimaker-pla>. [Accessed: 05-Jan-2018].
- [52] Ultimaker, "How to print with Ultimaker ABS." [Online]. Available: <https://ultimaker.com/en/resources/22226-how-to-print-with-ultimaker-abs>. [Accessed: 05-Jan-2018].
- [53] Ultimaker, "How to print with Ultimaker PC." [Online]. Available: <https://ultimaker.com/en/resources/22231-how-to-print-with-ultimaker-pc>. [Accessed: 05-Jan-2018].
- [54] Ultimaker, "How to print with Ultimaker Nylon." [Online]. Available:

- <https://ultimaker.com/en/resources/22233-how-to-print-with-ultimaker-nylon>. [Accessed: 05-Jan-2018].
- [55] P. Azimi, D. Zhao, C. Pouzet, N. E. Crain, and B. Stephens, "Emissions of Ultrafine Particles and Volatile Organic Compounds from Commercially Available Desktop Three-Dimensional Printers with Multiple Filaments," *Environ. Sci. Technol.*, vol. 50, no. 3, pp. 1260–1268, 2016.
- [56] D. A. N. Zhao *et al.*, "Emissions of ultrafine particles and volatile organic compounds from commercially available desktop 3D printers with ... Emissions of Ultra fi ne Particles and Volatile Organic Compounds from Commercially Available Desktop Three-Dimensional Printers with," *Environ. Sci. Technol.*, no. January, pp. 1–30, 2016.
- [57] B. Stephens, P. Azimi, Z. El Orch, and T. Ramos, "Ultrafine particle emissions from desktop 3D printers," *Atmos. Environ.*, vol. 79, pp. 334–339, 2013.
- [58] Demaco, "Posi-Trap Specifications," no. 978. .
- [59] Graver Technologies, "Filters for Vacuum Pumps," no. 2.
- [60] Terra Universal, "FS209E and ISO Cleanroom Standards." [Online]. Available: <https://www.terrauniversal.com/cleanrooms/iso-classification-cleanroom-standards.php>. [Accessed: 01-Dec-2017].
- [61] United States Environmental Protection Agency, "Particulate Matter (PM2.5) Trends." [Online]. Available: <https://www.epa.gov/air-trends/particulate-matter-pm25-trends>. [Accessed: 04-Dec-2017].
- [62] European Commission, "Air Quality Standards," 2017. [Online]. Available: <http://ec.europa.eu/environment/air/quality/standards.htm>. [Accessed: 04-Dec-2017].
- [63] United States Environmental Protection Agency, "NAAQS Table." [Online]. Available: <https://www.epa.gov/criteria-air-pollutants/naaqs-table>. [Accessed: 04-Dec-2017].
- [64] National Aeronautics and Space Administration, "Outgassing Materials Advanced Search Results." [Online]. Available: https://outgassing.nasa.gov/cgi/uncgi/search/search_ad.sh. [Accessed: 07-Jan-2018].
- [65] RepRap, "G-code." [Online]. Available: <http://reprap.org/wiki/G-code>. [Accessed: 07-Feb-2018].
- [66] Yun Li, Kiam Heong Ang, and G. C. Y. Chong, "PID control system analysis and design," *IEEE Control Syst. Mag.*, vol. 26, no. 1, pp. 32–41, 2006.
- [67] "High Torque Hybrid Stepping Motor Specifications."
- [68] Ultimaker, "Technical Data Sheet PC." pp. 1–3.
- [69] ASTM International, "Standard Test Methods for Flexural Properties of Unreinforced and Reinforced Plastics and Electrical Insulating Materials," pp. 1–12, 2017.
- [70] ASTM International, "Standard Test Method for Tensile Properties of Plastics," *ASTM Int.*, vol. 8, pp. 46–58, 2003.
- [71] ASTM International, "Standard Test Method for Compressive Properties of Rigid Plastics," *ASTM Int.*, vol. i, pp. 1–8, 2008.

Appendices

Appendix A – vacuubrand MD-1 Specifications

This information was sourced from [39]

Type		MD 1	MD 1 VARIO-SP
Maximum pumping speed (ISO 21360)	cfm (m ³ /h)	0.7 / 0.8 ^(a) (1.2 / 1.4 ^(a))	1.1 (2400 rpm) (1.8)
Ultimate vacuum (absolute)	Torr (mbar)	1.1 (1.5)	< 0.75 (700 rpm) (< 1.0)
Maximum permissible inlet pressure (absolute)	psi (bar)	16 (1.1)	
Maximum permissible outlet pressure (absolute)	psi (bar)	16 (1.1)	
Maximum pressure difference between inlet and outlet	psi (bar)	16 (1.1)	
Permissible ambient temperature storage / operation	°F (°C)	14 to 140 / 50 to 104 (-10 to +60 / +10 to +40)	
Permissible relative atmospheric moisture during operation (no condensation)	%	30 to 85	
Maximum permissible installation altitude above mean sea level	ft (m)	6500 (2000)	
Rated motor power	hp (kW)	0.11 (0.08)	0.09 (0.064)
No-load speed	rpm	1500 / 1800 ^(a)	0 - 2400 ^(b)
Maximum permissible range of supply voltage (±10%) Attention: Observe specifications of rating plate!		100-120 V~ 50/60 Hz; 200-230 V~ 50/60 Hz; 120V~ 60 Hz	24 V DC safe extra low voltage (SELV) ^(c)
Maximum rated current at: 100-120 V~ 50/60 Hz 200-230 V~ 50/60 Hz 120 V~ 60 Hz 24 V DC	A A A A	1.6 / 1.7 0.8 / 0.85 1.7 -	- - 7
Motor protection		thermal cutout, manual reset ^(d) ; MD 1 C/US: additional fuse 2.5AT	current limitation (temperature sensor on the circuit board)
Degree of protection IEC 529		IP 42 ^(e)	IP 20
Inlet		hose nozzle for tubing I.D. 1/4" (6 mm) G 1/8"	

Specifications

Printer and printing properties

Technology	Fused Deposition Modeling (FDM)
Print head	Swappable nozzle
Build volume	223 x 223 x 205 mm
Filament diameter	2.85 mm
Layer resolution	0.25 mm nozzle: 150 to 60 micron 0.40 mm nozzle: 200 to 20 micron 0.60 mm nozzle: 400 to 20 micron 0.80 mm nozzle: 600 to 20 micron
XYZ accuracy	12.5, 12.5, 5 micron
Print head travel speed	30 to 300 mm/s
Build speed	0.25 mm nozzle: up to 8 mm ³ /s 0.40 mm nozzle: up to 16 mm ³ /s 0.60 mm nozzle: up to 23 mm ³ /s 0.80 mm nozzle: up to 24 mm ³ /s
Build plate	Heated glass build plate
Build plate temperature	50 to 100 °C
Build plate leveling	Assisted leveling process
Supported materials	PLA, ABS, CPE, CPE+, PC, Nylon, TPU 95A
Nozzle diameter	Included are 0.25, 0.4, 0.6 and 0.8 mm nozzles
Nozzle temperature	180 to 260 °C
Nozzle heat up time	~ 1 minute
Build plate heat up time	< 4 minutes
Operating sound	50 dBA
Connectivity	Standalone 3D printing from SD card (included)

Physical dimensions

Dimensions	342 x 357 x 388 mm
Dimensions (with bowden tube and spool holder)	342 x 493 x 588 mm
Nett weight	11,3 kg
Shipping weight	18,5 kg
Shipping box dimensions	390 x 400 x 565 mm

Power requirements

Input	100 - 240V 4A, 50-60Hz 221 W max.
Output	24 V DC, 9.2 A

Ambient conditions

Operating ambient temperature	15 - 32 °C
Nonoperating temperature	See material specifications for optimal conditions 0 - 32 °C

Appendix C – Connector Pinouts

This table specifies the pinouts for the four Dsub connectors which were used to pass signals to and from the printer through the vacuum chamber. The four connectors are specified by their: Connector number, the colour of tape used to label the connector during the thesis work, the plug for the connector on the interior of the vacuum chamber and the colour code of the wire bundle on the inside of the vacuum chamber that carried the signals for that connector. Each connector lists: the pin number according to the Dsub connector data sheet, the printer function assigned to that pin, the designator as printed on the PCB and the colour of the wire that terminates on the PCB.

Connector 1	Blue tape	Bottommost	Red VC wiring
Pin Number	Function	Designator on Main PCB	Wire Colour
1	Z stepper motor	Z	Red
2	Z stepper motor	Z	Blue
3	Z stepper motor	Z	Black
4	Z stepper motor	Z	Green
5	LED Power	LED PWM	Red
6	X stepper motor	X	Red
7	X stepper motor	X	Blue
8	X stepper motor	X	Black
9	X stepper motor	X	Green
Connector 2	Red tape	Second from bottom	Black VC wiring
Pin Number	Function	Designator on Main PCB	Wire Colour
1	LED Ground	LED PWM	Black
2	Z-switch	Z-STOP	Black
3	Filament feed stepper motor	E1	Teal
4	Filament feed stepper motor	E1	Red
5	Buildplate heater A-1	HEATED BED	Grey
6	Z-switch	Z-STOP	Black
7	Filament feed stepper motor	E1	Black
8	Filament feed stepper motor	E1	Green

9	Buildplate heater A-2	HEATED BED	Grey
Connector 3	Brown tape	Third from bottom	Blue VC wiring (Be sure to use a converter on the blue wiring due to miswiring of the vacuum chamber wiring)
Pin Number	Function	Designator on Main PCB	Wire Colour
1	Buildplate heater B-1	HEATED BED	Grey
2	Buildplate thermistor A	TEMP 3	Black
3	Y stepper motor	Y	Black
4	Y stepper motor	Y	Green
5	Unused	Unused	Unused
6	Buildplate heater B-2	HEATED BED	Grey
7	Buildplate thermistor B	TEMP 3	Black
8	Y stepper motor	Y	Blue
9	Y stepper motor	Y	Red
Connector 4	Grey tape	Topmost	Yellow VC wiring
Pin Number	Function	Designator on Main PCB	Wire Colour
1	Unused	Unused	Unused
2	Printhead thermistor A	TEMP 1	Beige
3	Y-switch	Y-STOP	Red
4	X-switch	X-STOP	Blue
5	Printhead heater A	HEATER 1	Beige
6	Printhead thermistor B	TEMP 1	Beige
7	Y-switch	Y-STOP	Red
8	X-switch	X-STOP	Blue
9	Printhead heater B	HEATER 1	Beige

Appendix D – MATLAB Script for Servo Cooling

```
% Servo motor heat loss
% Marshall Quinn 4513002

close all
clc

%% Constants
sigma=5.67e-8; %W/m^2K^4 Stefan Boltzmann constant
T_inf=298; %Room temperature (25 C) assumes wall of vacuum chamber
is regulated to room temp
T_servo=290+273;
h_low=5; %(W/m^2K) assuming natural convection with air
h_high=35;

l=42.3*1e-6; %length of NEMA 17 servo (m)
w=42.3*1e-6; %width of NEMA 17 servo (m)
h=38*1e-6; %height of NEMA 17 servo (m)

epsilon=0.875; %emissivity (engineering tool box, black lacquer on
iron)

%A_servo=2*1e-6*(l*w+l*h+w*h);

%% Max Atmo Temp and Internal Power Generation
long_volume_T=readtable('atmo_long_volume_print_y1_x2_e3.txt');
long_volume_A=table2array(long_volume_T);
T_max_y=max(long_volume_A(:,2));
T_max_x=max(long_volume_A(:,3));
T_max=max(T_max_x, T_max_y)+273;

%Q_in=Q_out
Q_rad_total=4*epsilon*sigma*l*h*(T_max^4-
T_inf^4)+2*epsilon*sigma*l*w*(T_max^4-T_inf^4);
Q_conv_total_low=4*h_low*l*h*(T_max-T_inf)+2*h_low*l*w*(T_max-
T_inf);
Q_conv_total_high=4*h_high*l*h*(T_max-T_inf)+2*h_high*l*w*(T_max-
T_inf);
Q_in_low=Q_rad_total+Q_conv_total_low;
Q_in_high=Q_rad_total+Q_conv_total_high;

T_vac_low=(Q_in_low/(2*sigma*epsilon*(2*l*h+l*w))+T_inf^4)^(1/4)-273
T_vac_high=(Q_in_high/(2*sigma*epsilon*(2*l*h+l*w))+T_inf^4)^(1/4)-
273

%% Actual Vacuum Temp
long_volume_T_vac=readtable('vac_long_volume_y1_x2_z3_e4.txt');
long_volume_A_vac=table2array(long_volume_T_vac);
T_max_y_vac=max(long_volume_A_vac(:,2));
T_max_x_vac=max(long_volume_A_vac(:,3));
T_max_vac=max(T_max_x_vac, T_max_y_vac)
```

Appendix E – MATLAB Script for FFF Thread Cooling

```

close all
clc

%Marshall Quinn 4513002
%Cooling Time of Printed Components
%Based on 1-45 of viewfactor pdf from AE4S20
%Assumes rectangular prism shape
%Assumes placed on central front/back axis of plate

%% Variables
T_plate=110+273; %Temperature of buildplate
T_inf=25+273; %Temperature of surroundings
T_comp=260+273; %Temperature of the component at printing

w=120; %Width of component
h=3.2; %Height of component
d=12.7; %Depth of component

w_p=200; %Width of plate
d_p=200; %Depth of plate

A_tb=w*d; %Area of top/bottom
A_ss=w*h; %Area of sides (long)
A_ee=d*h; %Area of ends (short)

sigma=5.67e-8; %Stefan boltzmann

%% Conductive Transfer from Plate to Bottom

%% Transfer from Top to Surroundings
Q_tb=sigma*A_tb*(T_comp^4-T_inf^4);

%% Transfer from Sides to Plate and Surroundings
%View factor of rectangles sharing an edge (1-39) view factor pdf
%Assumes theta=90 deg (plate and faces are perpendicular)

%View Factor of Sides to Plate
N_s=h / ((w_p+w)/2);
L_s=((d_p-d)/2)/((w_p+w)/2);

Fs_p=(1/(pi*L_s))*(L_s*atan(1/L_s)+N_s*atan(1/N_s)-
sqrt(N_s^2+L_s^2)*atan(1/sqrt(N_s^2+L_s^2))+0.25*log(((1+L_s^2)*(1+N_s^2)/(1+N_s^2+L_s^2))*(L_s^2*(1+N_s^2+L_s^2)/((1+L_s^2)*(L_s^2+N_s^2))))^(L_s^2*(N_s^2*(1+N_s^2+L_s^2)/((1+N_s^2)*(L_s^2+N_s^2))))^(N_s^2)));

N_so=h / ((w_p-w)/2);
L_so=((d_p-d)/2)/((w_p-w)/2);

Fso_p=(1/(pi*L_so))*(L_so*atan(1/L_so)+N_so*atan(1/N_so)-
sqrt(N_so^2+L_so^2)*atan(1/sqrt(N_so^2+L_so^2))+0.25*log(((1+L_so^2)*(1+N_so^2)/(1+N_so^2+L_so^2))*(L_so^2*(1+N_so^2+L_so^2)/((1+L_so^2)*(L_so^2+N_so^2))))^(L_so^2*(N_so^2*(1+N_so^2+L_so^2)/((1+N_so^2)*(L_so^2+N_so^2))))^(N_so^2)));

```

```

*(L_so^2+N_so^2))^(L_so^2)*(N_so^2*(1+N_so^2+L_so^2)/((1+N_so^2)*(L
_so^2+N_so^2))^(N_so^2));

%View Factor Summarizer
A_so=h*((w_p-w)/2);
A_st=A_so+A_ss;

Fs_p_total=(A_st*Fs_p-A_so*Fso_p)/(A_ss)
%Fs_p_total=(1/(2*A3))*(A13*F13_24+A35*F35_46-A1*F1_2-A5*F5_6);

%% Transfer from Ends to Plate and Surroundings
%View factor of rectangles sharing an edge (1-39) view factor pdf
%Assumes theta=90 deg (plate and faces are perpendicular)

N_e=h / ((d_p+d)/2);
L_e=((w_p-w)/2)/((d_p+d)/2);

Fe_p=(1/(pi*L_e))*(L_e*atan(1/L_e)+N_e*atan(1/N_e)-
sqrt(N_e^2+L_e^2)*atan(1/sqrt(N_e^2+L_e^2))+0.25*log(((1+L_e^2)*(1+N
_e^2)/(1+N_e^2+L_e^2))*(L_e^2*(1+N_e^2+L_e^2)/((1+L_e^2)*(L_e^2+N_e^
2))))^(L_e^2)*(N_e^2*(1+N_e^2+L_e^2)/((1+N_e^2)*(L_e^2+N_e^2))^(N_e^
2)));

N_eo=h / ((d_p-d)/2);
L_eo=((w_p-w)/2)/((d_p-d)/2);

Feo_p=(1/(pi*L_eo))*(L_eo*atan(1/L_eo)+N_eo*atan(1/N_eo)-
sqrt(N_eo^2+L_eo^2)*atan(1/sqrt(N_eo^2+L_eo^2))+0.25*log(((1+L_eo^2)
*(1+N_eo^2)/(1+N_eo^2+L_eo^2))*(L_eo^2*(1+N_eo^2+L_eo^2)/((1+L_eo^2)
*(L_eo^2+N_eo^2))))^(L_eo^2)*(N_eo^2*(1+N_eo^2+L_eo^2)/((1+N_eo^2)*(L
_eo^2+N_eo^2))^(N_eo^2)));

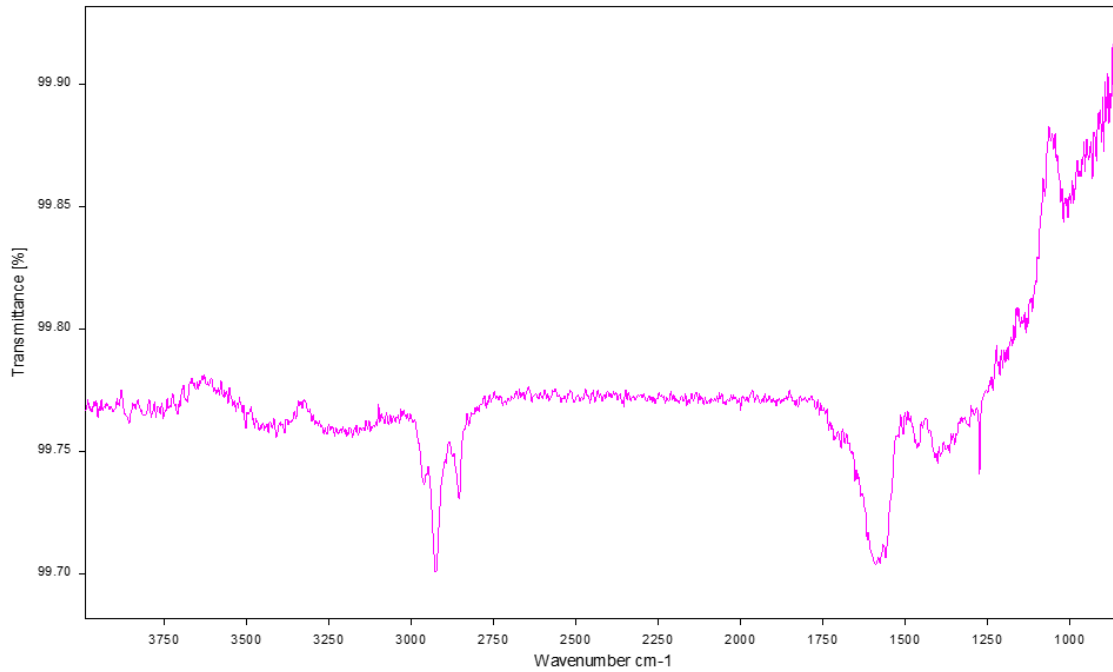
%View Factor eummarizer
A_eo=h*((d_p-d)/2);
A_et=A_eo+A_ee;

Fe_p_total=(A_et*Fe_p-A_eo*Feo_p)/(A_ee)
%Fs_p_total=(1/(2*A3))*(A13*F13_24+A35*F35_46-A1*F1_2-A5*F5_6);

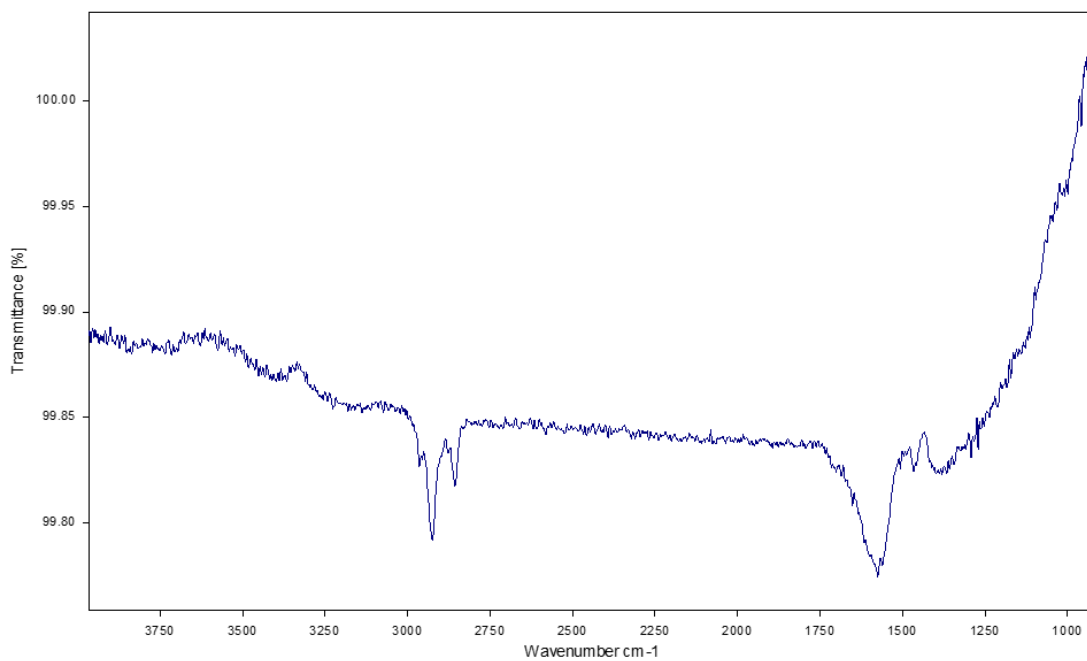
```

Appendix F – FTIR Analysis of Outgassing Windows

These are the two FTIR spectra used in the outgassing investigation. The first spectrum, in pink, is from window #169 and is from the test where the window was exposed to the vacuum environment with the printer fabricating a component. The second spectrum, in navy, is from window #170 where the window was exposed to the vacuum environment with the printer powered on but not printing.



Sample: Contamination during 3D printing, win #169	Technique: Transmission Cal File: Di281.0	Instrument: VERTEX 70v
--	---	------------------------



Sample: Contamination during 3D printing, win #170	Technique: Transmission Cal File: Di281.1	Instrument: VERTEX 70v
--	---	------------------------

Appendix G– “Solid No Brim” Cura Profile

This is a screenshot of the “Solid No Brim” Cura profile that was used for the slicing and gcode generation of all MP series components. It shows the values used all important Cura parameters. Parameters not displayed were left in their default settings. Cura 3.1.0 was used to generate the gcode for all MP series components.

Ultimaker 2+

Material: Black PC

Nozzle: 0.4 mm

[Check compatibility](#)

Print Setup Recommended Custom

Profile: Solid No Brim - 0.2mm

Search...

Quality

Layer Height		0.2	mm
Initial Layer Height		0.27	mm
Line Width		0.35	mm

Gradual Infill Steps		0	
<i>Infill Before Walls</i>		<input type="checkbox"/>	
Minimum Infill Area		0	mm ²
 Material			▼
Enable Retraction		<input checked="" type="checkbox"/>	
 Speed			▼
Print Speed		45	mm/s
Infill Speed		45	mm/s
Outer Wall Speed		20	mm/s
Inner Wall Speed		30	mm/s
 Shell			▼
Wall Thickness		1.2	mm
Top/Bottom Thickness		0.8	mm
Top Thickness		0.8	mm
Bottom Thickness		0.8	mm
Top/Bottom Pattern		Lines	▼
Outer Before Inner Walls		<input type="checkbox"/>	
Initial Layer Horizontal Expansion		0	mm
 Infill			▼
<i>Infill Density</i>		100	%
Infill Pattern		Lines	▼
Infill Line Directions		[]	
Infill Overlap Percentage		5	%

Top/Bottom Speed		20.0	mm/s
Travel Speed		120	mm/s
 Travel			▼
Combing Mode		All	▼
Avoid Printed Parts When Traveling		<input checked="" type="checkbox"/>	
Travel Avoid Distance		0.6562	mm
Layer Start X		0.0	mm
Layer Start Y		0.0	mm
Z Hop When Retracted		<input type="checkbox"/>	
 Cooling			▼
<i>Enable Print Cooling</i>		<input type="checkbox"/>	
 Support			▼
<i>Generate Support</i>		<input type="checkbox"/>	
 Build Plate Adhesion			▼
<i>Build Plate Adhesion Type</i>		None	▼
 Special Modes			▼
Print Sequence		All at Once	▼
Spiralize Outer Contour		<input type="checkbox"/>	